REMOVAL OF POLLUTANTS OF DIFFERENT TYPES FROM MODEL SOLUTIONS AND SEWAGES
- STATIC AND DYNAMIC TESTS

Zbigniew HUBICKI, Marek MAJDAN, Dorota KOŁODYŃSKA, Monika WAWRZKIEWICZ, Anna WOŁOWICZ, Agnieszka GŁĄDYSZ-PŁASKA, Magdalena MAKARSKA-BIAŁOKOZ, Grzegorz WÓJCIK, Justyna BĄK, Marzena GĘCA, Agnieszka LIPKE
DEPARTMENT OF INORGANIC CHEMISTRY

Nowadays the issues concerning technology and environmental protection are of great interest for numerous scientific centers all over the word. They are connected first of all with the synthesis of a large group of inorganic, hybrid inorganic-organic and inorganic-inorganic sorbents of defined physicochemical parameters and definite application. Their omplementary character is confirmed by many literature reports indicating the possibility of using synthesized materials in the environmental aspects – removal of some impurities from aqueous solutions by adsorption [1]. Such a situation is found in the case of inorganic oxide materials of both nanooxides and multi-component systems [2]. These materials are very interesting with respect to their structure and physicochemical properties determined during their synthesis.

Of a numerous group of their synthesis methods used for preparation of the above mentioned oxides, there should be mentioned precipitation process, sol-gel method, hydro- or solvo-thermal one. Each of them has advantages and disadvantages and allows to obtain quite different usable properties of final products which point out to potential areas of their application. Regardless of the way synthesis is conducted, it is also possible to control physicochemical parameters of products by their combination with other oxide component, organic agent or biopolymer. Such combination result in the synthesis of quite new hybrid material having advantages of both components in its structure. Possibility of combining inorganic material e.g. Fe_3O_4 or TiO_2 with organic or bioorganic compounds results from accessibility of characteristic functional groups on their surface. Alginate, cellulose and chitosan are biopolymers which can be used as carriers for controlled drug release, membranes with regulated permeability, sensor devices and artificial muscles. Their sorption ability towards heavy metal ions and dyes was also proved as for individual biopolymersc as well as in composites. Therefore the alginate modification of nanosized TiO_2-SiO_2 composite is a very simple and cheap method preventing aggregation of their particles and improving sorption properties.

Sodium alginate (ALG) consists of sequences of M (M-blocks) and G (G-blocks) residues to form MG sequences (MG-blocks). Chelation of metal cations, such as Ca(II), by carboxylate groups of MG-blocks causes the cross-linking of alginates.

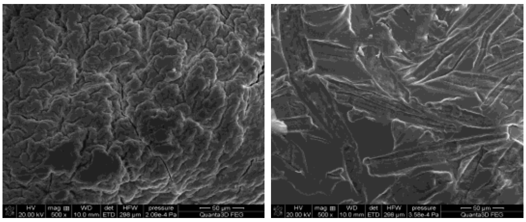

Fig.1. SEM-EDX analysis of ST20-ALG and ST20-ALG-Cu

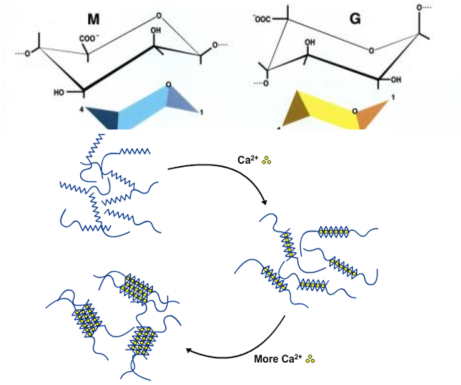

This type of sorbents is not well-known and some basic rules of kinetics and adsorption of heavy metal ions especially when accompanied by the photoreduction from aqueous solutions have not been fully understood. In the case of organic-inorganic composites, oxide particles can improve thermal properties, self-sustaining capability to work under different conditions, better hydrophobic interactions with polymers and specific properties such as chemical binding capability for a variety of compounds. During the studies it was found that with the increasing contact time the adsorption capacity (q_t) as well as sorption percentage (%S) increase initially and then reach the equilibrium. After 60 minutes, adsorption of Cu(II) and Zn(II) ions reaches 80% and then achieves plateau of 99% after 240 min. The quick sorption of Pb(II) on ST20 can suggest domination by the chemical sorption. The kinetics of Cu(II), Zn(II), Cd(II) and Pb(II) on ST20 and ST20-ALG was determined using pseudo first order, pseudo second order, intraparticle diffusion and Elovich models using the batch mode. Analogous studies were made in the column mode.

Also a new mesoporous silica-alumina oxide (97% SiO_2, 3% Al_2O_3) synthesized by pyrogenic method was proposed as a sorbent for acid (C.I. Acid Orange 7), reactive (C.I. Reactive Black 5) and direct (C.I. Direct Blue 71) dyes as well as for heavy metal (Co(II), Cu(II), Ni(II), Zn(II)) ions removal from the aqueous solutions and wastewaters. The kinetic and equilibrium studies were performed. An equilibrium time of 1 min and >240 min was required for the adsorption of heavy metal ions and dyes onto mixed oxide, respectively. The experimental data were better fitted to the Freundlich equation than to the Langmuir one. The potentiometric titrations indicated that dyes and heavy metal ions adsorption influence the structure of electrical double layer at the mixed oxide - liquid interface which was evidenced by changes in the solid surface charge density. The results showed that these materials could be used as effective adsorbents especially for heavy metal ions removal from aqueous and industrial wastewaters.

References:

[1] W. Zhao, Y. Chen, W. Zhang, J. Wang, C. Hu, W. He, *Canad. J. Chem. Eng.*, **94** (2016) 2289.

[2] S.G. Chung, J.C. Ryu, M.K. Song, B. An, S.B. Kim, S.H. Lee, J.W. Choi, *J. Hazard. Mater.*, **267** (2014) 161.

STUDIES OF ELECTRODE PROCESSES AND PRECONCENTRATION OF TRACE ELEMENTS AND BIOLOGICALLY ACTIVE COMPOUNDS AND ITS EXPLOITATION FOR ANALYTICAL PURPOSES

Mieczysław KOROLCZUK, Małgorzata GRABARCZYK,
Iwona GĘCA, Mateusz OCHAB
DEPARTMENT OF ANALYTICAL CHEMISTRY
AND INSTRUMENTAL ANALYSIS

The purpose of the studies was the application of chloranilic acid as a complexing agent for ultra-trace determination of germanium ions in water samples. Various parameters affecting the height and shape of the adsorptive stripping peak were examined in order to obtain the optimum conditions for germanium (IV) determination. The effect of the supporting electrolyte, concentration of chloranilic acid, potential and time of accumulation on the peak current were examined.

The preliminary measurements were performed for solutions containing a constant concentration of Ge(IV) and chloranilic acid equal to 1×10^{-8} mol L^{-1} and 5×10^{-3} mol L^{-1}, respectively, and the following supporting electrolyte with a concentration of 0.1 mol L^{-1}: HNO_3, $HClO_4$, HCl, CH_3COOH and acetate buffer in the pH range from 3.0 to 5.3. It was observed that of all the examined acids an extreme signal was obtained in HNO_3 while with the increase of pH the signal of germanium drastically decreased.

The chloranilic acid used as a complexing agent for Ge(IV) is indispensable to obtain a voltammetric signal of germanium and its concentration has a great impact on the peak current. To choose the optimum quantity of chloranilic acid in the sample, the effect of its concentration on the peak current was studied in the range from 1×10^{-6} mol L^{-1} to 5×10^{-3} mol L^{-1}. The peak of germanium appeared at a concentration of chloranilic acid equal to 1×10^{-5} mol L^{-1} and increased with the increasing concentration of the complexing agent. However, a concentration higher than 5×10^{-4} mol L^{-1} did not cause significant changes in the peak height, so it was adopted as the optimum concentration for further experiments.

The influence of the accumulation potential on the voltammetric peak current was examined over the potential range from 0.2 V to -0.5 V, using a solution containing 1×10^{-8} mol L^{-1} of Ge(IV), 5×10^{-4} mol L^{-1} of chloranilic acid and 0.1 mol L^{-1} of HNO_3. The peak current increased with the changing potential from -0.5 to -0.1 V and then in the range from -0.1 to 0.2 V the peak current slightly decreased. That is why the potential of -0.1 V at which the germanium signal reached a maximum was selected as an optimum accumulation potential in the proposed method.

The effect of preconcentration time on the voltammetric response of germanium in the range from 10 to 60 s was also studied. As can be seen, a linear increase of the stripping peak current with the accumulation time of 30 s was observed.

Analytical characterization was performed using the optimum conditions which were selected as described above, that is 0.1 mol L HNO_3 as the supporting electrolyte, 5×10^{-4} mol L^{-1} chloranilic acid as a complexing agent, -0.1 V accumulation potential and 30 s accumulation time. In such conditions the calibration graph for Ge(IV) was linear in the range from 5×10^{-10} to 2×10^{-7} mol L^{-1} and obeyed the equation $y = 15.75x + 2.76$, where y and x are the peak current (nanoamper) and Ge(IV) the concentration (nanomol per liter), respectively. The linear correlation coefficient was $r = 0.998$. The relative standard deviation from five determinations of germanium at a concentration of 1×10^{-9} mol L^{-1} was 4.4 %. The detection limit estimated from three times the standard deviation at low Ge(IV) concentration and an accumulation time of 30 s was about 1.67×10^{-10} mol L^{-1}.

Ryszard DOBROWOLSKI, Joanna DOBRZYŃSKA
DEPARTMENT OF ANALYTICAL CHEMISTRY
AND INSTRUMENTAL ANALYSIS

Platinum is noble metal characterized by low reactivity, resistance to corrosion and high temperature. In view of numerous applications, significant amount of platinum is emitted into the environment. The main source of platinum emission are car converters. Due to harmful effects of platinum compounds the level of pollution has to be controlled. A low concentration of platinum in environmental samples is the main reason of analyte preconcentration before its determination. Platinum ions can be preconcentrated by using of solid phase extraction.

Among the wide range of sorbents used for analytical purposes silica based mesoporous materials seem to be attractive due to their mechanical and chemical stability, as well as possibility of simple modification of surface properties. Particularly, mesoporous silica material SBA-15, which consists of parallel cylindrical pores with axes arranged in a hexagonal unit cell and possess large surface area, high pore volume and thick pore walls, can be used as a support for synthesis of organic–inorganic hybrids. Thanks to functional organic groups organic-inorganic hybrids exhibit high adsorption affinity towards different organic molecules and inorganic ions. Unfortunately, adsorption selectivity with respect to particular ions, in presence of competitor ions, is usually limited.

The application of ion-imprinted organic–inorganic hybrids leads to improvement of the adsorption selectivity. The monomers containing functional groups form a complex with the imprinted ion which is incorporated into just formed structure. Then ions imprinted in the sorbent structure are removed thus generating a specific bonding sites. In the present work, Pt(II)-imprinted thiocyanato-functionalized SBA-15 and analogous material without imprinting were synthesized and compared as sorbents of Pt(II) ions. The basic parameters affecting the adsorption of platinum ions onto Pt(II)-imprinted modified SBA-15 such as contact time and pH of the solution were studied and optimized.

The Pt(II) ion imprinted thiocyanato-functionalized SBA-15 was obtained by using of sol-gel one-pot route synthesis procedure. Firstly, 2 g of P123 was dissolved in 72 ml of 1.6 mol/L HCl under vigorous stirring at 40°C. After 8 h 0.4 g of potassium tetrachloroplatinate(II), 18 mmol TEOS and 2 mmol TCTES were added to this solution. The resulting mixture was stirred at 40°C for 24 h and aged at 100°C for next 48 h. The obtained solids were thoroughly washed with deionized water, filtered and dried at 100°C. Pluronic123 was removed by three-time extraction with acidified ethanol (99.8%) at 78°C. Finally the template Pt(II) ions were removed from the material using 0.5 mol/L thiourea in 5% HCl, until Pt was not detected in the leaching solution, which was monitored by GF AAS. For comparison, the non-imprinted material was also prepared and treated under identical conditions without adding Pt(II) ions. The ion imprinted and non-ion imprinted sorbents were named as Pt(II)TCTES and TCTES, respectively.

Adsorption/desorption experiments were carried out in static way. The effect of pH on the adsorption of Pt(II) ions was studied in the range between 0.5 an 7.0 for the adsorption system containing 5 mg of solid and 5 mL of 100 mg/L Pt(II) solution. As presented in Fig.1 in the case of ion imprinted materials adsorption is higher than 40% in whole studied pH range. The adsorption of Pt(II) on TCTES is very low when pH is lower than 3. The changes of adsorption for varied pH values may be the result of formation of various hydroxide–chloride complexes of Pt(II) and competitive sorption of HCl_2^- and Cl^- ions.

The time required for adsorption of metal ions is an important factor for any sorbent. The relations presented in Fig.2 show that adsorption equilibrium for the Pt(II)TCTES and TCTES is achieved after 5 and 72 h, respectively. Rapid reaching of equilibrium is caused by the existence of imprinted sites in the pore wall framework of the Pt(II)TCTES and the absence of steric hindrance, which simplifies contact of Pt(II) ions with adsorption centres.

Based on the analysis of the adsorption isotherms the maximum static adsorption capacity of Pt(II) was set at 76.4 and 42.4 mg/g for Pt(II)TCTES and TCTES, respectively. The influence of nitrates and chlorides on Pt(II) adsorption ability on the Pt(II)TCTES and TCTES was investigated. It was stated that nitrates at concentrations up to 1 mol/L do not hinder adsorption of Pt(II) in studied adsorption systems. Contrary to nitrates, the presence of chlorides at level of 0.1 mol/L significantly decreases adsorption of Pt(II). It was found that the desorption of platinum from Pt(II)TCTES by using HCl and HNO_3 was 0.5 and 42%, respectively. The highest desorption (92 %) was reached by using 1 mol/L thiourea as an eluent. Due to incomplete desorption the slurry sampling graphite furnace atomic absorption spectrometry was chosen for determination of platinum in environmental samples after its enrichment onto Pt(II)TCTES.

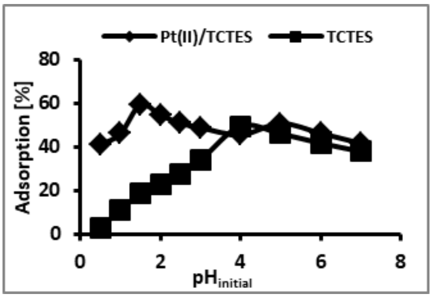

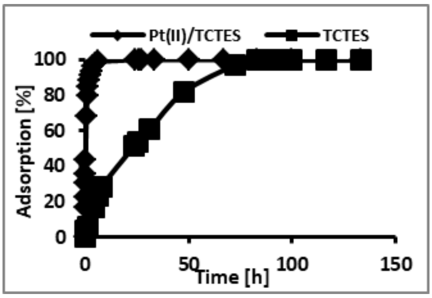

Fig.1. Influence of pH on the adsorption Pt(II) onto Pt(II)TCTES and TCTES; m = 0.0 g, V = 5 mL, $t_{Pt(II)TCTES}$ = 24h, t_{TCTES} = 72 h, T 25ºC, c_{Pt}=100 mg/L

Fig.2. Adsorption kinetics of Pt(II) onto Pt(II)TCTES and TCTES; m=0.005 mg, V=5 mL, c_{Pt}=100 mg/L, pH =1.5.

Jolanta NIESZPOREK, Dorota GUGAŁA-FEKNER, Dorota SIEŃKO
DEPARTMENT OF ANALYTICAL CHEMISTRY
AND INSTRUMENTAL ANALYSIS

Using experimental data obtained from differential capacity measurements of the double layer, zero charge potential and surface tension at this potential the adsorptive properties of adenosine in acetate buffer at different pH were determined. The decrease in the value observed in the differential capacity curves (Fig.1) indicates clear adenosine adsorption on the electrode surface. However, adenosine undergoes desorption at more negative potentials. In the area of more negative potentials, occurs a characteristic "hump" whose height increases with an increase in adenosine concentration. The orientation of the adenosine molecule with the aromatic ring on the electrode surface is indicated by the shift of E_z towards more negative potentials in both supporting electrolytes.

The possibility of determining parameters E_{max} and σ_{max} indicate the physical nature of adenosine adsorption, which must be associated with the fact that the adsorbed adenosine particles exhibit vertical or diagonal orientation. (Fig.2.)

The inhibitory effect of adenosine on Zn^{2+} ions electroreduction occurring at the lowest concentration in the acetate buffer pH 4 results from blocking of the electrode surface by its flatly adsorbed molecules. Such arrangement of molecules of an organic compound on the surface of mercury hinders depolariser ions from accessing the electrode, thus decelerating the speed of the electrode process. However, the presence of the progresive amount of adenosine in the buffer solution with pH 4 causes a change in the orientation of molecules of this compound on mercury to diagonal or perpendicular, conducive to the occurrence of the electrode process. An increase in adenosine concentration is also conducive to Zn^{2+} ions electroreduction kinetics in the buffer with pH 6. The catalytic properties of adenosine can be explained with unstable active complexes between Zn^{2+} ions and the adenosine molecule being formed on the electrode surface. Such a complex is a kind of a bridge facilitating an exchange of.

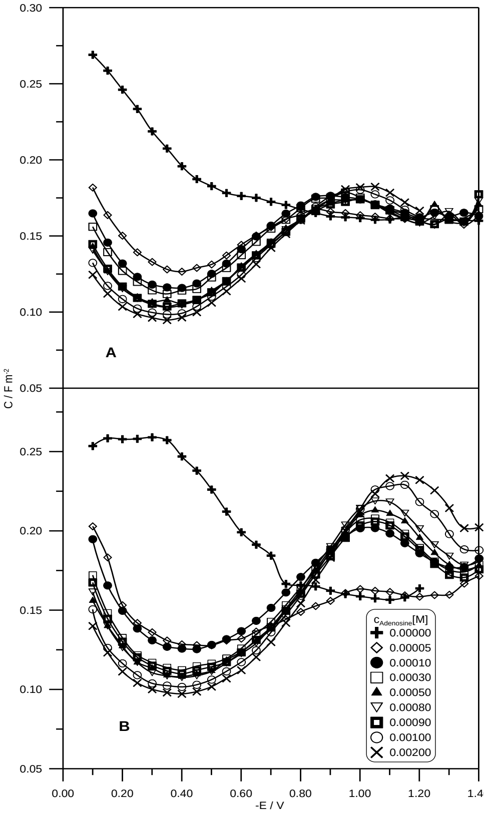

Fig. 1. Curves of the differential volume for the double layer extrapolated to zero frequency for various adenosine concentrations listed in the legend in acetate buffer pH 4 (A) and pH 6 (B).

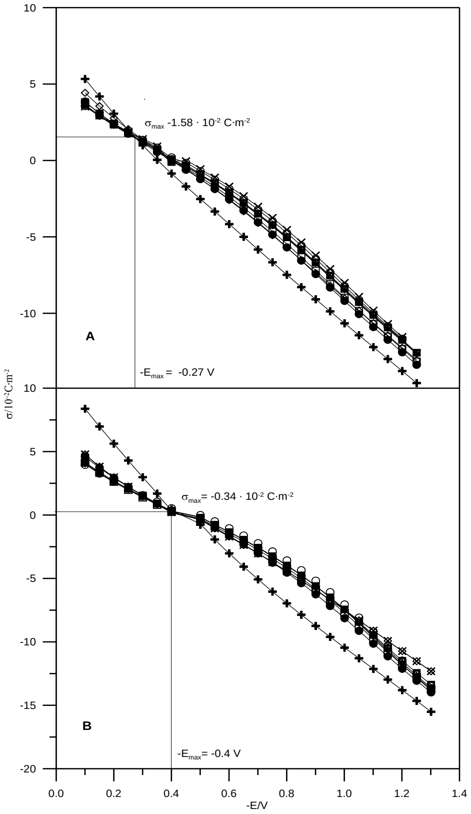

Fig. 2. Correlation between the electrode surface charge and its potential for various adenosine concentrations in in acetate buffer pH 4 (A) and pH 6 (B).

The electroreduction of Zn^{2+} ions in diluted $NaClO_4$ solutions on a mercury electrode is catalyzed also by metimazole. This action can be explained by the formation of an unstable active complex on the surface of the electrode constituting the Hg-metimazol-Zn^{2+} bridge facilitating the exchange of charge in the analyzed electrode process. The accelerating effect of metimazole increases with the increase in the concentration of the supporting electrolyte, which in turn is probably associated with a change in the hydration of both the depolarizer and the mercury surface.

Cecylia WARDAK, Joanna LENIK
DEPARTAMENT OF ANALYTICAL CHEMISTRY
AND INSTRUMENTAL ANALYSIS

Nanostructured materials, including nanotubes, nanofibers, nanorods, nanowires, nanoparticles, nanocpomposites and other nanomaterials have attracted considerable research interest in the last years in both scientific research and industrial applications [1,2]. They are characterized by unique physical and chemical properties, such as large surface area, high reactivity, good conductivity and good electrocatalytic activity which make them suitable for construction a variety of chemical sensors and biosensors. Ion-selective electrodes are an important class of potentiometric sensors which can be used for directly determining various inorganic and organic analytes in medical, environmental and industrial samples [3,4]. Polymeric membrane ion-selective electrodes with internal solid contact (SC ISEs) turned out to be reliable potentiometric-sensing devices with special advantages including simple construction, small size, low cost of production, and mechanical stability. Solid contact ISEs are good from the practical point of view because they can have various shapes and sizes as well as can work in any position. Total elimination of the internal filling provides such important advantage as possibility of miniaturization and microfabrication of ISEs. Furthermore the detection limit of solid contact electrodes could be extended to the subnanomolar range due to the elimination of transmembrane ion fluxes.

The aim of this work was developed of solid contact Pb- ISE based carbon nanofibers (CNFs). Carbon nanofibers and other carbon nanomaterials are suitable to acts as an ion-to-electron transducer due to their high electronic conductivity and large redox capacitance. Moreover their hydrofobicity prevents the formation of interfacial water layer between an ion-selective membrane and electric contact. Solid contact ISEs based on carbon nanomaterials possess high potential stability and reproducibility and exhibited resistance to light, redox interferences and presence of gases such as CO_2 or O_2 [5].

In the present work single-piece lead selective electrodes with membranes doped carbon nanofibers were constructed and studied. The CNFs were directly dispersed in the polymeric membrane. The optimal composition of the lead ion-selective membrane was as follows (% wt.): 33% PVC, 32.5 % BBPA (bis(1-butylpenthyl) adipate, 32.5 NPOE (2-nitrophenyl octyl ether), 1% carbon nabofibers and 1% ionophore (tetr-butylcalix [4] arene-tetracis (N,N-dimethylthio-acetamide).

A glassy carbon disk was used as internal reference electrode. Before the electrode preparation the glassy carbon electrode was polished with 0.3 μm Al_2O_3 powder and well rinsed with water and THF. The membrane components (CNFs, PVC, plasticizer, and lead ionophore (IV)) were weighed and thoroughly mixed, sonicated and deaerated. Then the mixture was applied on a glassy carbon (GC) electrode and gelated at 90 ◦C for 10 min. For comparison purpose another solid con-tact electrode so called coated disc electrode having the same construction and containing no CNFs in the membrane were constructed and studied. Electrochemical properties of tested electrodes were studied by potentiometry and electrochemical impedance spectroscopy.

The potentiometric response of studied lead electrodes was determined in the lead nitrate solutions of the concentration $1x10^{-1}$-$1x10^{-8}$ mol L^{-1}. Electrochemical impedance spectroscopy (EIS) measurements were performed in 0.01 M $Pb(NO_3)_2$ by using an AUTOLAB electrochemical analyzer. The impedance spectra were recorded at open circuit potential with an amplitude 0.1 V and in the frequency range 5 kHz-1 MHz. On the basis of obtained results analytical parameters of studied electrodes were determined. They were listed in Table.

Table 1. Comparison of analytical parameters of lead solid contact electrodes

Parametr	Electrode GC/(CNFs)Pb^{2+}-ISM	Electrode GC/Pb^{2+}-ISM
Characteristic slope mV/pa	31,1	31,2
Detection limit, mol L^{-1}	$1,6\times10^{-8}$	$2,5\times10^{-7}$
Measuring range, mol L^{-1}	$1,0\times10^{-7}$-$1,0\times10^{-2}$	$1,0\times10^{-6}$-
Response time, s	≤7	≤25
Rezistance, kΩ	18,9	246
Potential drift, μV/h	19,2	322

As it can be seen in Table 1 electrode containing CNFs as additional membrane component exhibited better analytical parameters than electrode having conventional membrane composition. Presence of carbon nanofiber in the ion-selective membrane cause a decrease membrane resistance and facilitates the ion to electron transduction processes at the interface between inner electrode and membrane and in that Pb-SCISe exhibits lower detection limit, wider measuring range and shorter response time.

Summing up, the research has shown successful usage of carbon nanofibers in the polymeric membrane of solid contact lead-sensitive electrode. The proposed electrode is characterized by good analytical parameters: low detection limit $1.6x10^{-8}$ mol L^{-1}, wide measuring range 10^{-2} – $1.0x10^{-7}$ mol L^{-1}, the slope characteristic 31.1 mV/decade, short response time and high potential stability.

References:

[1] T. Yin, W. Qin, *Trends Anal. Chem.*, **51** (2013) 79.
[2] I. Makra, R.E. Gyurcsányi, *Electrochem. Commun.*, **43** (2014) 55.
[3] J. Bobacka, A. Ivaska, A. Lewenstam, *Chem. Rev.*, **108** (2008) 329.
[4] E. Bakker, E. Pretsch, *Trends Anal. Chem.*, **20** (2001) 11.
[5] C. Wardak, *Sensors Actuators, B Chem.*, **209** (2015) 131.

Agnieszka NOSAL - WIERCIŃSKA
DEPARTMENT OF ANALYTICAL CHEMISTRY
AND INSTRUMENTAL ANALYSIS

Determination of Bi(III) ions in weak complexing solutions is extremely difficult and sometimes literally impossible. The cap-pair effect [1] was proved to raise possibilities of determination of Bi(III) ions in weak complexing solutions [1].

The hydrolysis of the aqua ion $Bi(H_2O)_9^{+3}$ limits the pH range within which the process of Bi(III) ion electroreduction may be studied [2]. Changes in chloric(VII) acid to sodium chlorate(VII) concentration ratios in the supporting electrolyte affect the structure of bismuth aqua ions and change the protonation of amino acid molecules, thus influencing a variety of interactions [2,3].

In previous publication we found that the presence of homocysteine and the protonation of the catalysing substance have effects on the rate of the multi-step process of Bi(III) electroreduction in chlorates(VII) with varying water activity [3].

In biological systems, a great part of homocysteine transforms into an oxidised form – homocystine (HCY). The reaction consists in the formation of disulphide bridges between two homocysteine molecules [1]. Homocystine is a close cystine analogue. It is not a component of proteins but participates in important biological functions. It is excreted in urine as a result of homocystinuria [4].

The effects of homocystine protonation on the kinetics and the mechanism of multi-step process of Bi(III) electroreduction in chlorates(VII) with varying water activity has been studied. The methodology of the study is based on electrochemical methods. The highest catalytic activity of homocystine was stated in 2 $mol \cdot dm^{-3}$ chlorates(VII) for the greatest amount of sodium chlorate(VII). The mechanism of the catalytic effect of HCY is associated with formation of active Bi – $Hg(SR)_2$ complexes which facilitate the electrode process. Active complexes of Bi(III) ions with catalysing substance are created when the hydration sphere of Bi(III) ions is partially degraded, and thus close to the external Helmholtz plane [4].

References:

[1] A. Nosal – Wiercińska, *Electroanalysis*, **26** (2014) 1013.

[2] A. Nosal – Wiercińska, M. Grochowski, M. Wiśniewska, K. Tyszczuk – Rotko, S. Skrzypek, M. Brycht, D. Guziejewski, *Electrocatalysis*, **6** (2015) 315.

[3] M. Grochowski, A. Nosal – Wiercińska, M. Wiśniewska, A. Szabelska, B. Gołębiowska, *Electrochim. Acta,* **207** (2016) 48.

[4] M. Grochowski, A. Nosal – Wiercińska, *J. Electroanal. Chem.*, **788** (2017) 198.

Katarzyna TYSZCZUK-ROTKO
DEPARTMENT OF ANALYTICAL CHEMISTRY
AND INSTRUMENTAL ANALYSIS

The aim of the study was to show a new application of polysiloxanes modified with metal for voltammetric determinations. So far, we have demonstrated the advantages of simultaneous modification of the glassy carbon electrode surface with organosilica thin film and electrochemically deposited lead nanoparticles in respect to Hg(II) and Bi(III) determination [1, 2]. As we demonstrated, the use of lead nanoparticles as modifier of thiol-functionalized polysiloxane film caused a 5-fold and 2-fold increase in Hg(II) and Bi(III) signals, respectively.

The possibility of application of other metals (copper, bismuth, antimony, gold, silver) as modifiers of the working electrode surface covered with polysiloxane film was checked. The best results were obtained for electrochemically deposited copper particles, which caused a ca. 2-fold increase in the Hg(II) signal. However, the observed enhancement was lower than that at the electrode modified by lead particles. The other metals were eliminated as possible modifiers of electrode surfaces covered with polysiloxane film due to the decrease in the Hg(II) peak current or its enhancement caused by overlapping of the metallic modifier and mercury oxidation signals.

Furthermore, studies were carried out to show the applicability of the functionalized polysiloxane modified with lead nanoparticles. A glassy carbon electrode covered with thiol-functionalized polysiloxane film modified by electrodeposited lead nanoparticles was used for determination of Ag(I) by square-wave anodic stripping voltammetry. Under optimized conditions, the voltammetric signal was proportional to the Ag(I) concentration in the range of 0.0093 to 1.85 nmol L^{-1} with excellent limits of detection and quantification of 1.2 pmol L^{-1} and 4.1 pmol L^{-1} after 90 s of accumulation on the electrode surface covered with thiol-functionalized polysiloxane film, respectively. The proposed method was applied for determination of Ag(I) in river water samples collected from Bystrzyca and Vistula without mineralization and a total silver concentration in commercially available silver-containing products.

References:

[1] K. Tyszczuk-Rotko, I. Sadok, M. Barczak, *Microporous and Mesoporous Materials*, **230** (2016) 109.
[2] K. Tyszczuk-Rotko, I. Sadok, M. Barczak, M. Jabłońska-Czapla, *Electrochimica Acta*, **208** (2016) 102.

STUDIES OF INTERIAL PHENOMENA AT DIFFERENT INTERFACES INCLUDING THE SYSTEMS WITH SURFACTANTS AND BIOSURFACTANTS

THERMODYNAMIC STUDY OF QUERCETIN AND RUTIN MIXTURES WITH ALCOHOLS

Katarzyna SZYMCZYK, Anna TARABA, Joanna KRAWCZYK,
Anna ZDZIENNICKA, Bronisław JAŃCZUK
DEPARTMENT OF INTERFACIAL PHENOMENA

Flavonoids are a large subclass of natural polyphenols widely distributed in plants. They are accumulated in almost all plant organs. Some of them are responsible for colours of fruit (mainly in the skin), veins of leaves, petals of flowers [1]. Numerous flavonoids were extensively studied for their various biological activities and beneficial effects on human health. Flavonoids such as quercetin (3,3′,4′,5,7-pentahydroxyflavone) and its glycoside, rutin are potent antioxidants. Quercetin was often chosen as an active main because it is considered the most powerful antioxidant, and the most widely distributed in nature. Moreover, it has already been used for its anti-inflammatory and anti-tumour activities as well as for cellular protective properties in brain, liver, kidney and colon diseases [2,3].

However, in spite of exhibiting a wide range of pharmacological properties, quercetin and other flavonoids present two obstacles to their pharmaceutical use. The first problem is poor solubility in aqueous media and the other is the sensitivity of flavonoids to oxidative degradation, resulting in poor stability in the aqueous aerobic environment [4]. Lauro et al. found the solubility at room temperature to be cq = 7.7 mg/L [5]. The poor solubility can be increased by organic solvents, ionic liquids, supercritical water or supercritical carbon dioxide in combination with ethanol [6]. Ethanol is one of the best solvents for quercetin however, the stability of quercetin in ethanol and in water at higher temperatures is limited. For rutin isolation the methanol, methanol/water and buffered methanol/water mixtures are the most frequently employed extractants [7]. However, to determine proper solvents and to design an optimized production process, the interactions between a given flavonoid and solvent at the bulk phase and at different interfaces should be known. The solvents affect greatly the molecular properties such as bond length, polarizability, electron distribution, dipole moments, relative stabilities of different conformers and spectroscopic parameters. This in turn would influence the intramolecular or intermolecular interactions and the anti-oxidative effects of the molecule [8]. Thus the purpose of the presented studies was to determine the thermodynamic parameters of adsorption at the water-air interface that is the standard free enthalpy (ΔG^0_{ads}), enthalpy (ΔH^0_{ads}) and entropy (ΔS^0_{ads}) of adsorption as well as the infinite dilution activity coefficient (γ^{∞}) of water-alcohol solutions of quercetin and rutin. For this purpose the surface tension of water-methanol (MeOH), water-ethanol (EtOH) and water-propanol (PrOH) solutions of quercetin and rutin (C = 4x10^{-5} and 10^{-4}M) in the wide range of alcohol concentration (Cp = 0-80%) was measured at T = 293, 303 and 313 K.

From the obtained measurements and calculations it proved that for the studied solutions all the values of ΔG^{0}_{ads} are negative and for a given flavonoid concentration decrease with the increasing T. Also the smallest values of ΔG^{0}_{ads} are observed for PrOH. It is interesting that in the case of water-EtOH solutions the efficiency to adsorb EtOH at the water-air interface is higher for the rutin solution at C = 4x10^{-5} M than those for quercetin. The positive values of ΔS^{0}_{ads} indicate that all studied systems become more random after adsorption. In addition, the values of ΔH^{0}_{ads} for all solutions calculated on the basis of standard free enthalpy of adsorption as well as Gamboa and Olea equation [9] for π = 20 and 30 mN/m are negative and indicate that bond making predominates in the adsorption process. It is interesting that for PrOH all the γ^{∞} values calculated using the method proposed by Gracia-Fadrique et al. [10] are larger than 1 which, according to the Motomura's model [11], indicates that the interactions between the molecules of flavonoids and solvents, that is water and alcohols in the studied mixtures are considerably larger than those between the single molecules. Also for PrOH the values of γ^{∞} for quercetin are higher than those for rutin which means that in practical applications the mixture of quercetin and propanol at small concentrations should possess the best surface active properties.

References:

[1] P. Walstra, Physical chemistry of foods, Marcel Decker, New York, NY, 2003.

[2] T. Hatahet , M. Morille, A. Hommoss, C. Dorandeu, R.H. Müller, S. Bégu, *Eur. J. Pharm. Biopharm.*, **102** (2016) 51.

[3] X. Qu, D. Qi, F. Dong, B. Wang, R. Guo, M. Luo, R. Yao, *Brain Res.*, **1553** (2014) 31.

[4] D.P. Makris, J.T. Rossiter, *J. Agric. Food Chem.*, **48** (2000) 3830.

[5] M.R. Lauro, M.L. Torre, L. Maggi, F. De Simone, U. Conte, R.P. Aquino, *Drug Dev. Ind. Pharm.*, **28** (2002) 371.

[6] A. Chafer, T. Fornari, A. Berna, R.P. Stateva, *J. Supercrit. Fluids*, **32** (2004) 89.

[7] A.L. Dawidowicz, K. Bernacik, R. Typek, *Food Anal. Methods.*, **9** (2016) 213.

[8] Y-Z Zheng, Y. Zhou, Q. Lian, D-F Chen, R. Guo, C-L. Xiong, X-J. Xu, Z-N. Zhang, Z-J. Huang, *Dyes and Pigments*, **141** (2017) 179.

[9] C. Gamboa, A.F. Olea, *Colloids Surf. A.*, **278** (2006) 241.

[10] J. Luiz Lópes-Cervantes, J. Gracia-Fadrique, E. Calvo, A. Amigo, *Fluid Phase Equilib.*, **356** (2013) 193.

[11] K. Motomura, N. Ando, H. Matsuki, M.M. Aratono, *J. Colloid Interface Sci.*, **139** (1990) 188.

STUDIES OF INTERIAL PHENOMENA AT DIFFERENT INTERFACES INCLUDING THE SYSTEMS WITH SURFACTANTS AND BIOSURFACTANTS

PLASMA PROCESS FOR PMMA LAYER DEPOSITION ON THE GLASS SURFACE

Diana RYMUSZKA, Konrad TERPIŁOWSKI, Lucyna HOŁYSZ,
Aleksandra SZCZEŚ, Emil CHIBOWSKI, Małgorzata JURAK,
Agnieszka Ewa WIĄCEK, Julita WŁOSOWSKA
DEPARTMENT OF INTERFACIAL PHENOMENA

Plasma modification leads to changes in material properties which include biological, chemical, mechanical, optical or electrical ones [1]. The major advantages of plasma modification include the simplicity and the lack of products formed during the plasma process [2]. The use of plasma technology provides ability to change the surface properties of all types of polymers and glass independent of their structure and reactivity. Furthermore, this technology is environmentally friendly, which is very important aspect nowadays [3]. There are four basic types of applications of plasma surface modification: cleaning, coating, etching and activation. Coating involves layer deposition on the support which results in improvement of such surface properties as adhesion or printability. The coating process is widely used in the case of all industrial materials, glass, metals and ceramics.

The aim of the study was deposition of poly(methyl mathacrylate) (PMMA) layers on the glass surface. Three systems were investigated. The first one included deposition of the PMMA layers by solution spreading on the untreated glass surface (glass/PMMA–UT) and the second on the glass surface treated by air plasma (glass-PT/PMMA–ST). The third type of the created polymer layer was deposited-analogously by spreading of PMMA solution on the untreated glass support (glass/PMMA) which next was treated by air, nitrogen and argon plasmas (glass/PMMA–PT). On the PMMA layers contact angles were measured for water, formamide and diiodomethane using the sessile drop method.The surface free energy was determined applying two different theoretical approaches: the contact angle hysteresis (CAH) [4] and the Lifshitz-van der Waals/acid-base (LWAB) [5] models. Furthermore, the topography of the surfaces was reflected in the 3D images obtained using optical profilometer (not presented in this report). For the systems in the case of which glass surface was modified before PMMA layer deposition (ST) no significant changes in wettability were observed in comparison to the UT systems. For all types used for contact angle measurements liquid changes were small and they can be treated as deviation. It can be assumed that modification of glass surface by air, nitrogen and argon plasma does not affect significantly on the hydrophilic-hydrophobic properties of PMMA layer.

Greater changes in wettability were observed for the systems where PMMA layer was treated by plasma (glass/PMMA–PT). The water contact angles for the layers deposited by nitrogen and argon plasmas were lower than for the UT system. On the other hand, higher values of water contact angles were observed for PT modified by air plasma which can be explained by the increase of oxygen content introduced during the plasma process which resulted in creation of polar functional groups.

Surface free energy calculated from both CAH and LWAB approaches has similar values indicating that chosen approaches are comparable. The biggest changes in the surface free energy were observed for the PT layers deposited by argon plasma being approximately 7 mJ/m^2 higher than surface free energy calculated for UT.

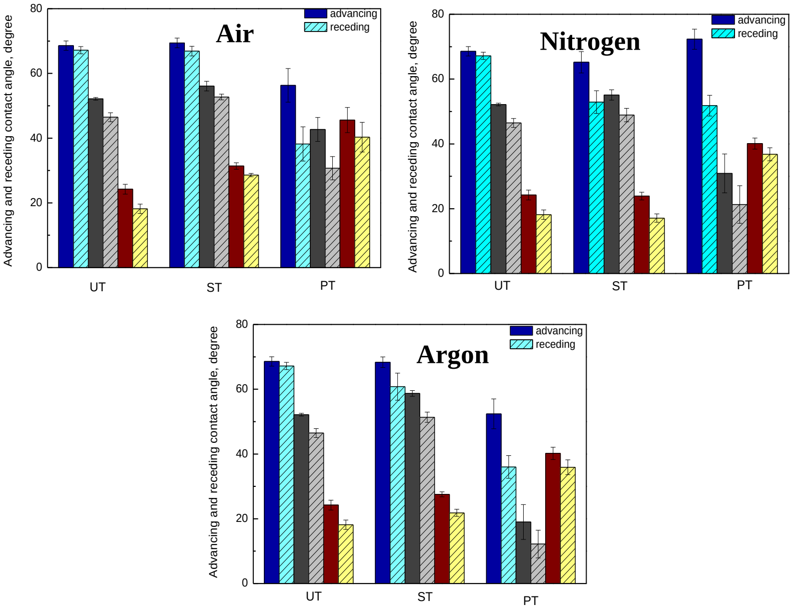

Fig. 1. Advancing and receding contact angles of water (blue), formamide (grey) and diiodomethane (brown) measured on the PMMA layers deposited on the glass surface.

High influence of plasma on the topography is observed for PT layers, which is confirmed by higher differences in values of roughness parameters in comparison to the UT systems for all types of plasma. Glass surface modification has also influence on topography of the PMMA layers but it is not as large as for the layers deposited by plasma.

References:

[1] P.K. Chu, J.Y. Chen, L.P. Wang and N. Huang, *Mat. Sci. Engineer.*, **R 36** (2002) 143–206.

[2] A.Reznickova Z. Kolska, V. Hnatowicz, P. Stopka and V. Svorcik, *Nuclear Inst. Meth. Phys. Res. B*, **269** (2011) 83–88.

[3] F. Huang, Q. Wei, X.Wang and W. Xu, *Polym. Test.*, **25** (2006) 22–27.

[4] E. Chibowski, *Adv. Colloid Interface Sci.*, **103** (2003) 149–172.

[5] C.J. van Oss, R.J. Good and M.K. Chaudhury, *Langmuir*, **4** (1988) 884–91.

CHROMATOGRAPHIC AND SPECTROSCOPIC PROCEDURES IN ANALYSIS OF ORGANIC, BIOACTIVE COMPOUNDS

Andrzej L. DAWIDOWICZ, Irena CHOMA, Jadwiga SKUBISZEWSKA-ZIĘBA, Dorota WIANOWSKA, Barbara CHARMAS, Rafał TYPEK, Michał DYBOWSKI, Piotr BOROWSKI, Małgorzata OLSZOWY, Katarzyna BERNACIK
DEPARTAMENT OF CHROMATOGRAPHIC METHODS

Transformation of chlorogenic acids during the coffee beans roasting process. Chlorogen acid (5-CQA) (ester of caffeic with quinic acid) is a naturally occurring phenolic compound widely distributed in plants. Coffee beans are most frequently mentioned as a plant product remarkably rich in 5-CQA. This acid is an important biosynthetic intermediate, e.g., in lignin biosynthesis, and plays an important role in the plant's response to stress. It is claimed to have antiviral, antibacterial, antifungal and antioxidant activity combined with relatively low toxicity and side effects. As an antioxidant, it may contribute to the prevention of type 2 diabetes mellitus and cardiovascular diseases. In vivo studies on animal subjects have demonstrated that the administration of 5-CQA lessens the hyperglycemic peak resulting from glycogenolysis brought about by administering glucagon, a hyperglycemiant hormone. Other studies also confirmed its reduction of glucose levels in blood and an increase in the intrahepatic concentration of glucose-6-phosphate and of glucagon. The reports concerning the neuroprotective efficacy of coffee prove that chlorogenic acid might be largely responsible for the inhibition of H_2O_2-induced apoptotic neuronal death. As results from the literature show, coffee supplemented with chlorogen acid reduces body mass and body fat faster than instant coffee. Potential uses of 5-CQA are also suggested in pharmaceuticals, foodstuffs, feed additives and cosmetics. All these findings are responsible for the growing interest in the natural occurrence of 5-CQA and its properties [1]

Coffee beans extract is one of the most popular beverages all over the world. Only a small percentage of coffee consumers drink coffee extracts made of green coffee beans. Most of them prepare their coffee beverages from roasted and ground coffee beans or from instant coffee, i.e., from the coffee form which has been obtained in the high temperature process. As results from [2] show, the process of coffee roasting results in the decrease of chlorogenic acids concentration in the beans as a significant percent of CQAs present in green coffee beans is degraded into volatile components. 4 % of CQAs stays maximal in coffee beans after roasting process.

According to [1], the heating of 5-CQA in the temperature range of 100–200 °C in the presence of steam or in the form of water solution causes chlorogen acid isomerization and transformation.

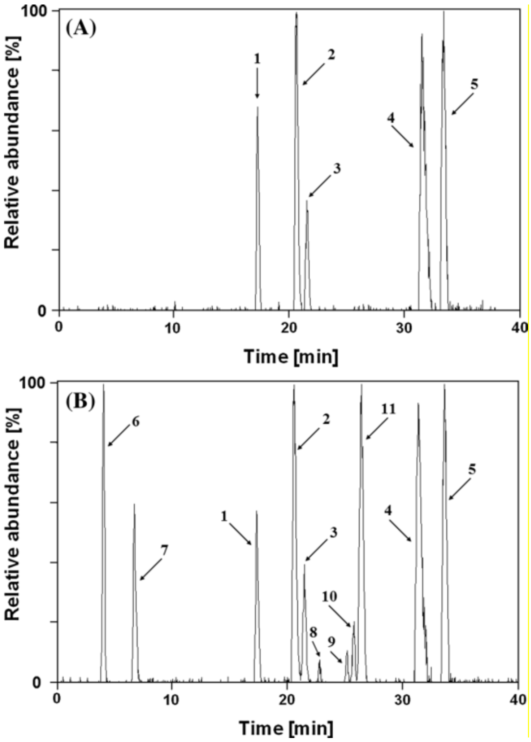

Fig. 1 Exemplary chromatograms (SIM function) of water extract from green coffee beans (A) and roasted coffee beans (B)

The reports prove that 5-CQA not only isomerizes to 3- and 4-CQA, but also undergoes other transformations such as esterification and reaction with water (hydrolysis and/or addition of water molecule to the double bond). As green coffee beans contain some amount of water, it seems worth examining whether the presence of water in them causes the chlorogenic acids transformation during roasting. The question is valid because plant materials have a complex matrix, and there are a lot of other components, besides water, that can affect the CQAs transformation process.

As results from the presented results, the roasting process of green coffee beans not only leads to the degradation of CQA isomers to volatile components, but also causes their transformation to quinic acid and its epimer (both CQAs degradation product) and to four 3-Caffeoylquinic acid-1,5-lactones (3-Caffeoylquinic acid-1,5-lactone, epimer 3-caffeoylquinic acid-1,5-lactone, 4-Caffeoylquinic acid-1,5-lactone and epimer 4-caffeoylquinic acid-1,5-lactone) - the dehydration products of CQAs. Besides these transformations, the change of the ratio between the amounts of CQA isomers and dicaffeoylquinic acid (diCQA) isomers is observed in coffee beans during their roasting. These changes can be explained by the different thermal stabilities of the individual isomers, yet mutual transformations of CQA and diCQA isomers cannot be excluded. It is worth mentioning that the increase of water content above its standard level in initial coffee beans slows down only the changes occurring during the roasting process.

Antifungal Activity of Chelidonium majus Extracts - Antagonistic Action of Chelerythrine and Sanguinarine Against Botrytis cinerea. *Chelidonium majus* L., commonly known as greater celandine, is a herbaceous perennial plant of the family *Papaveraceae*, that is native to Europe and Asia but has spread throughout the world. The main constituents of this plant are alkaloids such as benzophenanthridines (e.g. chelidonine, chelerythrine and sanguinarine) and protoberberines (e.g. coptisine and berberine). These compounds are toxic in moderate doses. Yet when they are used in the correct dosage, they exhibit numerous biological properties, including choleretic, colagogue, spasmolytic, antitumour, antiinflammatory, antibacterial, antiviral and fungicidal effects, both *in vitro* and *in vivo*.

Botrytis cinerea is an airborne plant pathogen with a necrotrophic lifestyle that affects many plant species worldwide. This fungus causes the grey mould in vegetables, ornamentals and fruits, that is responsible for great damage in crops in the field or after the harvest period. In addition, *B. cinerea* is not indifferent to humans since it can cause a respiratory allergic reaction in predisposed individuals. In view of this, many attempts were undertaken to develop fungicidal agents inhibiting effectively the growth of this fungus.

There are many fungicides for *B. cinerea* control, most of them are the synthetic agents. Yet due to the genetic plasticity of this fungus at present many of these agents are ineffective. Therefore new fungicides are constantly being looked for, particularly among therapeutic plants and compounds isolated from them as they are considered to be non-toxic to mammals and non-target organisms. They also are regarded to be safer for the environment, which is important taking into account the negative environmental impact of the majority of synthetic fungicides.

The report presents the results of research work on the similarities and differences in the antifungal properties of the *Ch. majus* extracts and the sanguinarine and chelerythrine solutions of the same concentrations as those in the plant extracts. In the experiments the effect of different extraction conditions *i.e.* maceration or extraction in the Soxhlet apparatus using chloroform, ethyl acetate, acetone or methanol as extractants on the antifungal activity of the *Ch. majus* extracts against *B. cinerea* was tested *in vitro.*

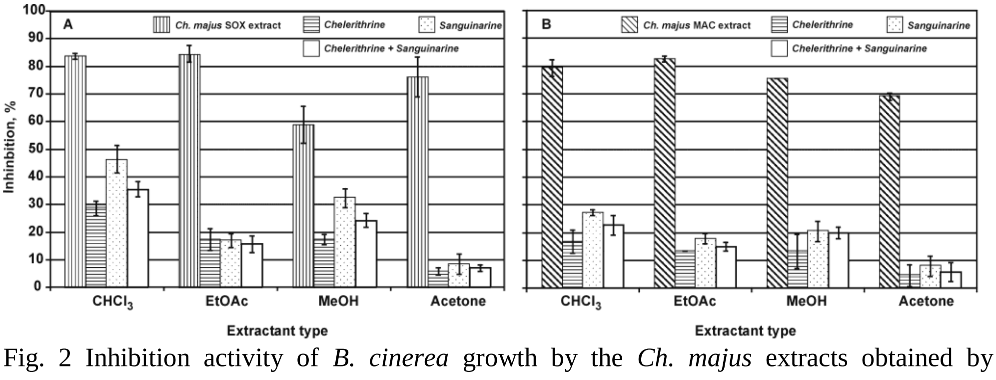

Fig. 2 Inhibition activity of *B. cinerea* growth by the *Ch. majus* extracts obtained by isolation in the Soxhlet apparatus (A) and maceration (B) using different extractants (chloroform, ethyl acetate, methanol or acetone) and chelerythrine/sanguinarine standard solutions alone and their mixtures

Comparing the presented results (Fig. 2), it can be seen that the *Ch. majus* L. extracts inhibit the growth of *B. cinerea* very effectively. The inhibiting activity of the extracts is highly affected by the type of the applied extractant and extraction method. The highest inhibiting activity is exhibited by the extracts obtained in the Soxhlet apparatus using chloroform.

Owing to the comparison of the antifungal properties of the extracts with the activity of chelerythrine/sanguinarine alone and a mixture of these alkaloids applied at the same concentration as those in the corresponding extracts, it has been demonstrated for the first time that the extracts activity is significantly greater and it does not always reflect the quantity of alkaloids in them. It has been proved that in the mixture the antifungal activity of chelerythrine and sanguinarine is antagonistic in the concentration dependent way. Based on the presented data it is not clear, however, whether the observed greater antifungal activity of the extracts is a result of enhancing the antifungal properties by the other alkaloids, though they are present at very low concentration levels, or by other compounds. In order to resolve the problem of synergistic action of the *Ch. majus* extracts components explicitly and/or to indicate the extracts components enhancing their antifungal properties, another series of experiments is required. However, this task is very complicated taking into account how very complex mixtures are the extracts and that the synergistic action can depend on the ratio of individual compounds in the extracts.

TLC-Direct Bioautography as a Method for Evaluation of Antibacterial Properties of Thymus vulgaris L. and Salvia officinalis L. Essential Oils of Different Origin. Thyme (*Thymus vulgaris* L.) and sage (*Salvia officinalis* L.) are popular perennial plants from the Lamiaceae family. The aromatic leaves of thyme and sage are basic herbs used in cooking. They are also popular medicinal plants well-known for their anti-inflammatory, antibacterial, antifungal, and antioxidant properties [3]. Thyme and sage essential oils (EOs) are widely applied in aromatherapy and cosmetology. The composition and biological properties of *T. vulgaris* and *S. officinalis* are well described in the literature [4]. Thin-layer chromatography – direct bioautography (TLC–DB) is a method used in evaluation of biological activities of plants and their constituents [5-7]. TLC-DB is a hyphenation of TLC with a biological assay performed directly on a chromatographic plate. The developed TLC plate is immersed in a bacterial suspension and left for incubation. Bacteria grow directly on a surface of a TLC plate except spots of antibacterial substances. Then, the plate is visualized by spraying with tetrazolium salt which is converted by bacteria into the purple formazan. Finally, pale inhibition zones are observed against the purple surface of the plate. In this way antimicrobial properties can be assigned to individual components. Thus, TLC-DB can be used for screening chromatographic and antibacterial properties of plants and their constituents in parallel. It can be also used for evaluation of a total activity of a whole sample in a so-called dot-blot bioautography. In that TLC-DB variant samples are spotted on a surface of a TLC plate and the bioautography step is performed without a development of a plate [5].

The dot-blot bioautography was used to evaluate antibacterial properties of *T. vulgaris* L. and *S. officinalis* L. essential oils produced by three different Polish manufactures. The whole samples were applied at three concentrations on thin-layer chromatography (TLC) plates which were then subjected to bioautography against *Bacillus subtilis*. The samples of the highest activity were found. Then, they were separated using TLC and once more subjected to bioautography against *B. subtilis.*

In parallel, derivatization with anisaldehyde – sulphuric acid reagent was performed to visualize the EOs components (Fig. 3). As was proved, only the EOs of *T. vulgaris* L. possessed strong antibacterial properties for which mostly thymol and carvacrol were responsible. Their contents were calculated using TLC-UV densitometry. The highest contents were found in the essential oils of the highest total antibacterial activity revealed in the dot-blot test. It means that a dot-blot test can be used for simple and fast evaluation of antibacterial properties of essential oils [8].

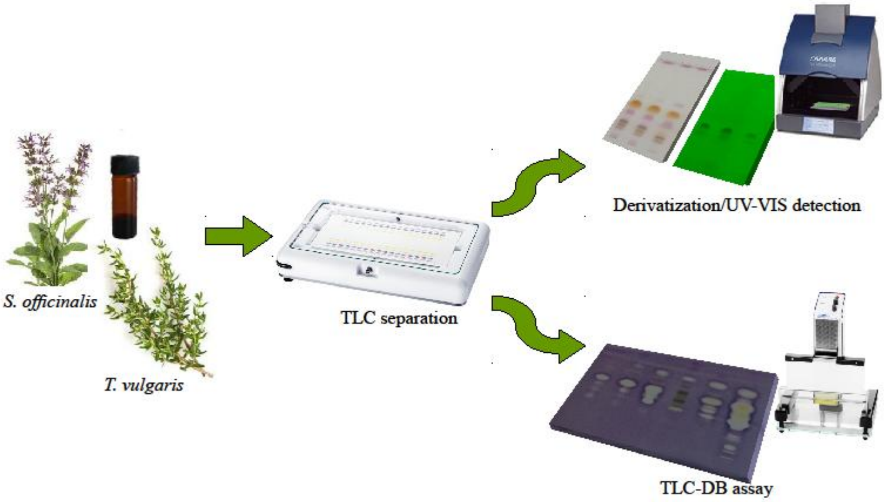

Fig. 3 The scheme of TLC-DB of *T. vulgaris* and *S. officinalis* essential oils.

Influence of mechanochemical treatment on thermal and structural properties of silica-collagen and hydroxyapatite-collagen composites. In bone tissue engineering collagen and hydroxyapatite (HAp), have enormous potential as biomaterials because of their accessibility, biocompatibility, the ability to connect with other materials, ease of processing, assimilation in the body and much more. Bone belongs to the tissue family with a complex structure organized hierarchically. This tissue consists of 70-80% w/w of mineral part (mainly hydroxyapatite) and 20-30% w/w of other components (mainly collagen).

One of the main challenges to bone tissue engineering is to develop scaffolds with optimal mechanical, functional and architectural properties to create the favorable conditions for cell colonization and organization, which can ensure the integration of the scaffold with the host tissue. In tissue engineering there is a wide range of proposals for obtaining such collagen and hydroxyapatite based scaffolds, and also with other additives such as metals, fibers (carbon, glass, polymers), etc.

The aim of this work was to study the use of mechanochemical processing (MChT) to produce the collagen-hydroxyapatite and collagen-silica composites of 30/70 w/w ratio. Mechanochemical processes (MChT) were carried out in a planetary mill (Pulverisette 7, FRITSCH, Germany) at different rotations of milling (200 and 400 rpm) and various periods of time (30, 60 and 120 min). Pressure and

temperature parameters created during milling were recorded using EASY GTM software (FRITCH, Germany). The obtained composites were analyzed using low-temperature nitrogen adsorption/desorption and thermal analysis (TG-DTA).

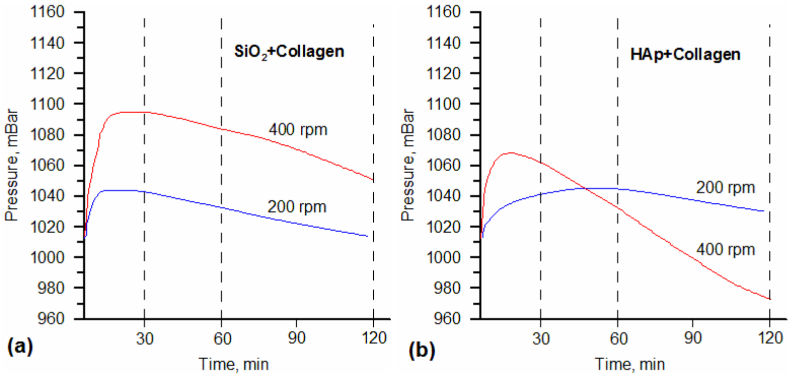

Fig. 4. Values of pressure created during MChT depending on time.

Analyzing the course of curves presented in Fig. 4 we can see that at 200 rpm, the pressure at the beginning increases and with the extension of the MChT time decreases. However for the HAp+Collagen system (Fig. 4b), it decreases only to a small extent but, for SiO_2+Collagen one (Fig. 4a), a significant pressure drop can be seen along with the treatment time. What is interesting, however, is the observed increase in pressure, and then a decisive decrease for samples with collagen treated mechanochemically at 400 rpm. Particularly noteworthy is the curve for HAp+Collagen (Fig. 4b) which, with an extension of time up to 120 minutes, drops to a pressure below the initial level. The course of the observed dependence of pressure as a function of time for samples with collagen may suggest the formation of stable SiO_2-Collagen and Hap-Collagen biocomposites.

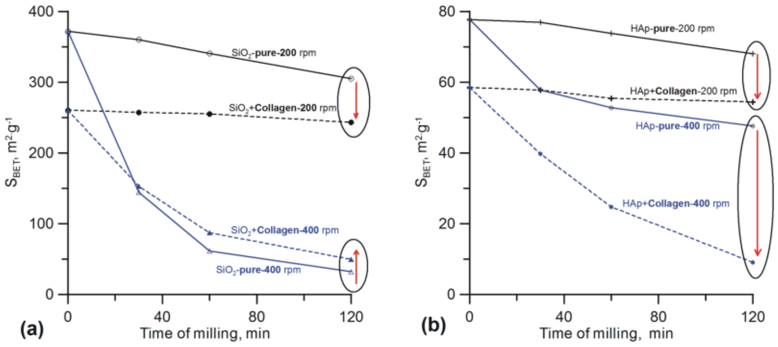

Fig. 5 Dependencies of the specific surface area (S_{BET}) values in relation to the MChT treatment time.

From the comparison of relationships presented in Fig. 5 it follows that at 200 rpm, S_{BET} values for systems with collagen are lower than those for modified pure SiO_2 and HAp. However, what is interesting, in case of SiO_2-Collagen systems modified at 400 rpm, these samples have higher S_{BET} values compared to this parameter for pure SiO_2 MChT treated. On the basis of this it can be assumed that in this case a new spatial structure is created. However, such relationship is not observed for HAp-Collagen systems. The observed trends are marked with red.

The results of TG and DTA show that for all samples up to 200 ^{o}C, endothermic peaks associated with the evaporation of physically adsorbed water are visible. For pure SiO_2 and HAp, they are also visible at higher temperature ranges. In contrast, for the pure collagen sample, could be observed two exothermic peaks in the 200-400 ^{o}C range (DTAmax≈300 ^{o}C) and 400-800 ^{o}C (DTAmax≈580 ^{o}C) associated with condensation and combustion processes correspondingly.

In mineral-collagen composites the collagen degradation temperature is lower for about 100 ^{o}C and its range is narrower compared to that for pure collagen. This maybe the prove of good connection of both components, mineral and protein in prepared SiO_2-Collagen and HAp-Collagen biocomposites.

Very interesting and promising results were obtained encouraging further research in this direction [9].

Thermal and structural studies of modified silicas and Ti/Si composites for their use as biological active agent carriers. Porous silica gels are widely applied in numerous fields of modern science and technology as adsorbents, catalyst carriers, polymer fillers and chromatographic column packings. They can be used also as drugs and biological active component carriers. Such extended applications result from mechanical and thermal resistance, developed specific surface area as well as defined structure of pores. A wide range of possible applications of such materials requires preparation of new ones of different surface characteristics.

Such objectives can be achieved by applying hydrothermal treatment [10] of initial material or matrix doping using different metals or oxides, e.g. TiO_2 [11].

Hydrothermal modification (HTT) is one of the most frequently used and the most effective methods for adjusting textural and structural parameters of the adsorbents and catalysts surfaces. Under different HTT conditions (sources of energy: microwave reactor or steel autoclave, atmosphere of water vapour or liquid water), tetrahedral structure of water changes, hydrogen bonds disrupt, and as a result, the physicochemical parameters of water change. Consequently, its capacity of dissolution of solids increases. Due to such modification there are changes, among others, in specific surface area, size and structure of pores as well as chemical character of solids surface [10].

Complex oxides, especially those based on silica as the mineral matrix, play a significant role in the adsorption and catalytic processes. TiO_2–SiO_2 complex oxides (TS) are very frequently applied. Incorporation of the transition metals (in the form of elements, ions or oxides, particularly titanium) into the silica gel structure can induce changes in the porous structure of complex oxides and leads to creation of additional, specific catalytic properties. These materials are considered as a substitute for pure TiO_2, due to the superior mechanical strength and thermal stability of such highly dispersive composites [11].

The aim of the presented studies was the application of differential scanning calorimetry (cryoporometry, DSC) and thermogravimetry (TG), especially taking into account thermal analysis performed under quasi-isothermal conditions (Q-TG), for characterization of the structural and thermal properties of silicas and composite materials.

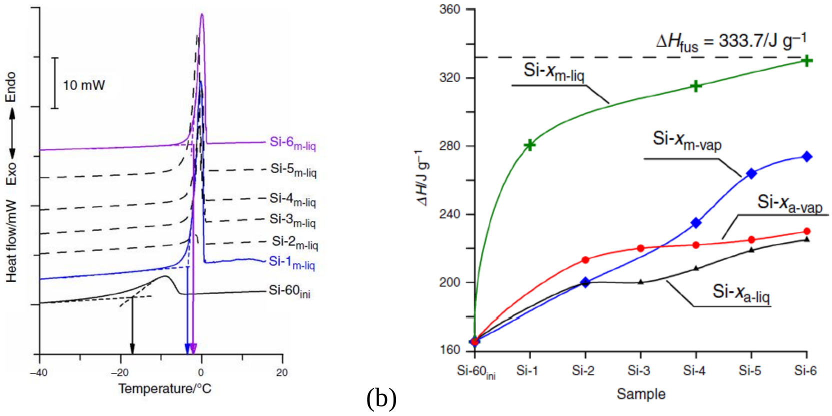

a) (b)

Fig. 6. The exemplary DSC curves of ice melting in the pores of the modified silica gels series Si-$x_{m\text{-}liq}$ (a) and the changes of phase transition enthalpy (ΔH) determined from the DSC curves of ice melting confined in the pores of the analyzed silicas (b).

These methods can provide useful information about the structure, temperature and interfacial behavior of liquids confined in solids pores which is essential for solids use as carriers of biologically active substances.

Calorimetric studies were carried out using a differential scanning calorimeter (DSC PYRIS Diamond, Perkin-Elmer, USA). The DSC data obtained from melting of ice confined in the pores of HTT silicas were used for determination of sizes of water clusters bound in/to the pore walls. It was shown that HTT causes intensive changes of silica material surface. Size and character of changes depend on both the kind of system and the source of energy. Strong interactions of water molecules confined in the silica of differentiated porosity resulted in lowering of ice melting points (Fig. 6a) and changes of the enthalpy of phase transition of ice melting confined in the pores (Fig. 6b) [10].

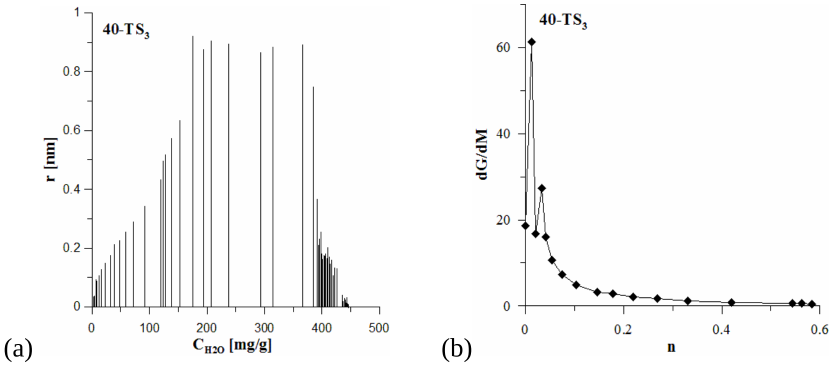

Fig. 7. Dependence of the effective radius of the evaporating drop on the concentration of adsorbed water (a) and dG/dM under the conditions of slight surface filling with adsorbed water (b) for the chosen complex oxide TS-40_3 (dG/dM indicates the change of the surface free energy during water evaporation from the surface).

The DSC investigations of titania-silica composites showed the reduction of freezing–melting temperatures of the water confined in the pores. The extent of these changes depends largely on the type of the initial silica gel and quantity of the TiO_2 layers. Moreover, there was a significant change in the melting enthalpy (ΔH) of ice confined in the pores. It is caused by strong interactions of the liquid with the pores surface due to surface hydrophilicity.

Following the Q-TG analysis, the TiO_2 deposition can block the surface hydroxyl groups. Therefore polarity of the surface and force of interactions with H_2O molecules change. This is evidenced by the analysis of shape of dG/dM and the effective radius of the evaporating drop depending on the adsorbed water concentration. The exemplary dependences are shown in Fig. 7.

The vibrational corrections to NMR shielding

Nuclei within a molecule remain in constant motion due to the molecular vibrations, which always take place regardless of temperature of the sample. It is well known that magnetic shielding is dependent on the electron density around the nuclei. It is thus not surprising that any change in the position of the nucleus, which results in, *inter alia*, the change in the nuclear potential, changes the electron density and, as a consequence, changes the magnetic shielding. Therefore it is necessary to include such effects in the calculations to obtain accurate results.

The basic equation for the so-called vibrational correction to the magnetic shielding constant σ reads [12,13]

$$\Delta\sigma = \frac{1}{4}\sum_{K}^{3N-6}\frac{1}{\omega_K}\left[\left(\frac{d^2\sigma}{dQ_K^2}\right)_e - \frac{1}{\omega_K}\left(\frac{d\sigma}{dQ_K}\right)_e\sum_{L}^{3N-6}\frac{F_{e,KLL}}{\omega_L}\right] \tag{1}$$

where ω denotes the harmonic frequency, Q – the normal coordinate, F – the cubic force constant. Indices K and L refer to normal modes of vibrations, and subscript e indicates that the value is to be computed at the equilibrium geometry. The terms are named 2nd and 1st order term with respect to shielding, respectively.

In principle, the first- and second-order derivatives of the magnetic shielding constant, as well as the third-order derivatives of the energy (cubic force constants) can be computed analytically. However, typical quantum chemistry (QC) packages, like PQS we are using, do not have implementations of the relevant routines. What remains to be done is programming of the routines for numerical differentiation. The above-mentioned derivatives can be first obtained in the Cartesian coordinates, and then transformed to normal coordinate representation after solving the vibrational problem.

Thus, a general home-made program was written. The first- and the second-order derivatives of the NMR shielding constants with respect to the nuclear Cartesian coordinates can be calculated by the numerical differentiation of the shielding constants. The third-order energy derivatives can be also calculated numerically as the second derivatives of the energy gradient. This procedure requires $18N^2+1$ single-points shielding constants calculations, and $18N^2–12N+5$ single-point gradient calculations (without taking advantage of the molecular symmetry). In both cases the Cartesian step can be set to, say, 0.05 a.u. Then, the vibrational problem can solved based on the quadratic force constants **H** routinely computed by all QC packages, and the transformation matrix **L** from normal (**Q**) to Cartesian (**ρ**) coordinates (**ρ**=**LQ**) can be found. The **L** matrix can be used in the transformation procedure, and the vibrational corrections can be calculated according to the above-mentioned equation.

The program consists of the following modules:

1. preparation of the input files for numerical differentiation of the magnetic shielding constants and the energy gradient. The procedure requires the Cartesian coordinates of nuclei at equilibrium geometry. Then, by applying the Cartesian steps of the assumed length the positions of nuclei are changed accordingly and input files are generated;
2. run of all the necessary single-point calculations and collection of the data (the energy first-order derivatives and the shielding constants) in a separate file for subsequent numerical differentiation. This is accomplished with the aid of the Linux script;
3. numerical differentiation of the energy gradient and the magnetic shielding constants. In this way the third-order energy $\boldsymbol{E}_c'''$derivatives as well as the first- and the second-order derivatives of the shielding constants, $\boldsymbol{\sigma}_c'$ (a row vector) and $\boldsymbol{\sigma}_c''$ (a square matrix), respectively, over the Cartesian displacements of the nuclei (as indicated by the subscript *c*) are computed according to the well-known formulas (see, e.g., [14]);
4. solution of the vibrational problem for to obtain the **L** transformation matrix ($\mathbf{HL}=\mathbf{ML}\boldsymbol{\omega}^2$);
5. transformation of the Cartesian derivatives into the normal coordinate representation. The following formulas were used:

$$\boldsymbol{\sigma}_Q' = \boldsymbol{\sigma}_c'\mathbf{L} \text{ and } \boldsymbol{\sigma}_Q'' = \mathbf{L}^{\mathrm{T}}\boldsymbol{\sigma}_c''\mathbf{L}, \tag{2}$$

with a similar (though somewhat more complex) expression for the third-order energy derivatives. The subscript Q indicates that the relevant tensors are expressed in normal coordinate representation;

6. calculation of the vibrational correction to the magnetic shielding constant according to equation 1.

With this implementation more accurate calculations of the chemical shifts are now possible.

References:

[1] A.L. Dawidowicz, R. Typek, *J. Agric. Food Chem.*, **58** (2010) 12578–12584.
[2] J.K. Moon, T. Shibamoto, *J Agric. Food Chem.*, **58** (2010) 5465–5470.
[3] W.C. Evans, *Pharmacognosy,* Saunders, London, 2000.
[4] G. Horváth et al., *J. Essent. Oil Research,* **18** (2006) 315−317.
[5] I.M. Choma and W. Jesionek, Effects-Directed Biological Detection: Bioautography in Instrumental Thin-Layer Chromatography, ed. C. Pool, Elsevier, Amsterdam, 2015, pp. 279-312.
[6] I.M. Choma and E.M. Grzelak, *J. Chromatogr. A,* **1218** (2011) 2684−2691.
[7] A. Marston, *J. Chromatogr. A,* **1218** (2011) 2676−2683.
[8] W. Jesionek, B. Majer-Dziedzic and I.M. Choma, *J. Liq. Chromatogr. & Rel. Technol*, **40** (2107) 292-296.
[9] J. Skubiszewska-Zięba, E. Skwarek, B. Charmas, N. Zając, V.V. Sydorchuk, Influence of mechanochemical treatment on thermal and structural properties of silica-collagen and hydroxyapatite-collagen composites. Part I. International Conference NANO-2017, 23 - 26 August 2017, Chernivtsi, Ukraine.
[10] B. Charmas, J. Skubiszewska-Zięba, *Journal of Thermal Analysis and Calorimetry,* **129** (2017) 23-32.
[11] B. Charmas, J. Skubiszewska-Zięba, H. Waniak-Nowicka, *Adsorption Science & Technology,* **35 (7-8)** (2017) 706-713.
[12] T.A. Ruden, K. Ruud, in: Calculation of NMR and EPR Parameters. Theory and Applications, M. Kaupp, M. Bühl, V.G. Malkin (Edytors), Wiley, Weinheim, 2004 (chapt. 10, p. 153).
[13] M. Dračínský, J. Kaminský, P. Bouř, *J. Chem. Phys.*, **130** (2009) 094106.
[14] L. Råde, B. Westergren, Mathematics Handbook for Science and Engineering, Brikhäuser B, Lund 1995.

STUDY OF LONG-TERM STABILITY OF NATIVE AND FUNCTIONALIZED MESOPOROUS SBA-15 MATERIALS

Mariusz BARCZAK, Andrzej DĄBROWSKI, Mateusz DRACH,
Leszek ŁAJTAR, Jolanta NARKIEWICZ-MICHAŁEK,
Damian NIECKARZ, Krzysztof NIESZPOREK,
Przemysław PODKOŚCIELNY, Paweł SZABELSKI,
Krzysztof WOLIŃSKI
DEPARTMENT OF THEORETICAL CHEMISTRY

SBA-15 mesoporous silica material are actually one of the most popular sorbents for many molecules [1-3]. Their synthesis is usually carried out via controlled hydrolysis and condensation of tetraethoxysilane under strong acidic conditions in the presence of amphiphilic block copolymer followed by its removal by extraction or calcination. The resulting materials possess many advantages such as easy one-step synthesis, tunable pores size, thick pore walls, high specific surface area, and good textural properties [4-6]. These properties make them useful in many fields such as adsorption [7], catalytic processes [8], medicine [9] or separation [10]

In majority of applications the stability of mesoporous matrixes is a crucial factor. Usually considered stabilities are "processing-oriented" short-time (hours, days) stabilities including thermal [11], hydrothermal [12], mechanical [13], chemical [14]. All of them are very important during the direct processing of the mesoporous silicas in above mentioned applications. However, from the point of view of potential applications very important is also storage (shelf) long-term stability which reflects changes occurring upon long time (months and years) of the sample. Although a sample is not exposed directly to the harsh conditions (humidity, light, elevated temperatures, mechanical stress, etc.) it still undergoes structural and chemical changes defining its usefulness after given time.

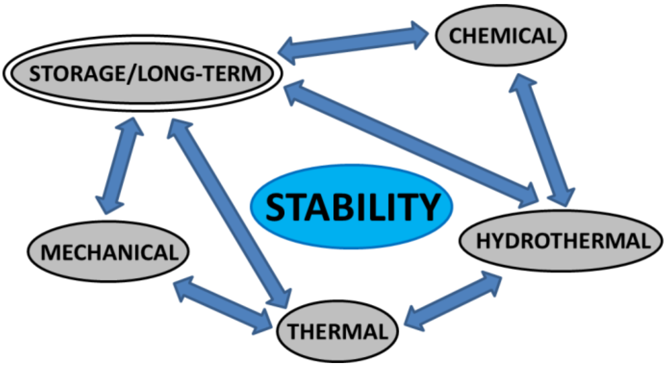

Fig. 1. Schematic relationship between different types of stability of M41S mesoporous silica materials

To investigate the effect of prolonged time on the changes into porous structure, nitrogen sorption isotherms were measured for four different samples:

pure-silica (A1), amine (L2 and L4) and thiol (A3) functionalized which were synthesized and characterized by us previously [15,16]. The changes in porous structure after four years (samples L2 and L4) and two years (samples A1 and A3) are summarized in Table 1.

Table 1. Parameters of porous structure calculated from nitrogen adsorption/desorption isotherms

Sample	Description	initial			after four years		
		S_{BET} [m^2g^{-1}]	V_t [cm^3]	d_{BJH} [nm]	S_{BET} [m^2g^{-1}]	V_t [cm^3]	d_{BJH} [nm]
A1	Pristine (TEOS 20)	857	1.28	5.3	754	1.18	7.5
L2	TEOS:ATES (18:2)	838	1.43	6.7	436	0.82	6.1
L4	TEOS:TMPD (18:2)	738	1.30	6.5	346	0.67	5.9
A3	TEOS: MPMS (18:2)	607	0.76	3.5	562	0.62	4.3

As it can be seen, the structural parameters change upon long time periods what testifies that the SBA-15 silica samples are not so stable upon storage. Interestingly for the amino-functionalized silicas L2 and L4 pore sizes decreases while for the pristine and thiol functionalized silicas A1 and A3 – increases. The significant specific surface area decreases are observed for all the samples. For all the samples but A0 there are also significant decreases in pore volumes. Amine-functionalized samples are particularly susceptible for long-time degradation, due to the presence of highly hydrophilic (thus susceptible for humidity) amine groups.

References:

[1] D. Y. Zhao, et al., *Science*, **279** (1998) 548.
[2] D. Y. Zhao, et al., *J. Am. Chem. Soc.*, **120** (1998) 6024.
[3] C. G. Goltner, S. Henke, M. C. Weissenberger, M. Antonietti, *Angew. Chem. Int. Ed.*, **37** (1998) 613.
[4] M. Kruk, M. Jaroniec, C.H. Ko, R. Ryoo, *Chem. Mater.*, **12** (2000) 1961-1968.
[5] F. Zhang et al., *J. Phys. Chem. B*, **109** (2005) 8273.
[6] R.M. Grudzien, B.E. Grabicka, D.J. Knobloch, M. Jaroniec, *Colloids & Surf. A: Physicochem. Eng. Aspects*, **291** (2006) 139.
[7] M. Badaničová, V. Zeleňák, *Monatsh. Chem.*, **141** (2010) 677.
[8] R.M. Rioux, H. Song, J.D. Hoefelmeyer, P. Yang, G.A. Somorjai, *J. Phys. Chem. B*, **109** (2005) 2192.
[9] S. Wang, *Micropor. Mesopor. Mater.*, **117** (2009) 1.
[10] R. Brady, B. Woonton, M. L. Gee A. J. O'Connor, *Innov. Food Sci. Emerg. Technol.*, **9** (2008) 243–248.
[11] P. Shah, V. Ramaswamy, *Micropor. Mesopor. Mater.*, **114** (2008) 270.
[12] E.B. Celer et al., *J. Mater. Chem.*, **16** (2006) 2824.
[13] S. Chytil, L. Haugland, E.A. Blekkan, *Micropor. Mesopor. Mater.*, **111** (2008) 134.
[14] A. Galarneau et al., *J. Phys. Chem. C*, **111** (2007) 8268.
[15] R. Dobrowolski, et al., *Coll. Surf. A Physicochem. Asp.*, **435** (2013) 63.
[16] M. Barczak, et al., *Mat. Chem. Phys.*, **181** (2016) 126.

PREPARATION AND INVESTIGATION OF CATALYTIC SYSTEMS IN THE REACTIONS INVOLVING CARBON OXIDES, HYDROCARBONS AND THEIR OXYGEN CONNECTIONS

Tadeusz BOROWIECKI, Marcin CICHY, Wojciech GAC,
Magdalena GRELUK, Andrzej MACHOCKI,
Sylwia PASIECZNA-PATKOWSKA, Marek ROTKO,
Janusz RYCZKOWSKI, Grzegorz SŁOWIK, Witold ZAWADZKI
DEPARTMENT OF CHEMICAL TECHNOLOGY

Catalytic materials for the process of removal (oxidation) of soot from Diesel exhaust gases

Investigations associated with the search of a highly active and selective catalytic material for the process of soot oxidation from diesel exhaust gases were continued. It is very important issue because the emission of soot into the atmosphere is highly undesirable. Diesel soot is strongly toxic for living organisms and contributes to the greenhouse effect.

Cobalt-cerium catalysts containing different amounts of potassium were tested. Cobalt-cerium precursors were prepared by a co-precipitation method and calcined at 400^{o}C. The suitable amounts of potassium were introduced by the impregnation method. Their catalytic properties (activity and selectivity) were measured in the "tight contact" using model soot (Printex U) and the reaction mixture containing 10 vol.% of O_2 and inert gases (argon and helium). The studies were conducted in a quartz reactor filled with 50 mg of the catalyst-soot mixture (45 mg of catalyst and 5 mg of soot) and 450 mg of finely ground quartz. The effects of soot oxidation during the temperature-programmed experiment (ramp rate was 10^{o}C/min) were analyzed by a mass spectrometer.

Cobalt-cerium-potassium catalysts permit to decrease the temperature of soot oxidation but their activity and selectivity (contrary to expectation) is worse than cobalt-cerium catalysts. This state of affair is probably the result of the presence of the not-fully decomposed potassium precursor (KNO_3) on the catalyst surface. The presence of significant amounts of potassium nitrate was confirmed by the XRD analysis. Further studies will be conducted.

Glycerol steam reforming

Calcium hydroxyapatite (HAp) supported cobalt and cobalt-cerium catalysts were examined for hydrogen production in glycerol steam reforming. The catalysts were synthesized by incipient wetness impregnation method and characterized through X-ray diffraction, adsorption-desorption isotherms of N_2 and temperature-programmed reduction of H_2. Catalytic properties were examined in terms of glycerol conversion, selectivity toward hydrogen and C containing products in temperature range of 650 – 800 °C. The effect of active metal reduction and residence time (thereby flow feed rate) was analysed. It was found that the growth of residence time increased the hydrogen selectivity in the whole temperatures range whereas the catalyst reduction, before the catalytic process, decreased the hydrogen selectivity at temperatures lower than 750 °C. The cerium addition improved the catalytic behaviour for hydrogen production via glycerol steam reforming. Cerium oxide supressed the sintering of cobalt particles and as a result Co-Ce/HAp ensured higher stability and H_2 selectivity than Co/HAp. Under reaction conditions investigated in this study, the highest selectivity toward hydrogen at 650 °C was obtained for 7.5Co-Ce/HAp catalyst.

Methanol steam reforming

Steam reforming of methanol (SRM) is one of the most efficient low-temperature hydrogen production methods. The reaction product mixture containing mainly H_2 and CO_2 can be easily handled and utilized in the fuel cell systems for electricity production. Steam reforming of methanol was studied over carbon supported Pd-Zn catalysts with different Pd/Zn stoichiometry. The catalysts were studied by means of various physicochemical methods, including X-ray diffraction, temperature-programmed reduction and chemisorption of H_2. It has been observed that structural and surface properties of the catalysts were related to Pd/Zn ratio. The increase of ZnO content in the catalysts led to formation of intermetallic compound Zn-Pd.

Steam reforming of methanol was carried out in a fixed bed flow reactor under atmospheric pressure. It was found that activity and selectivity of the catalysts were strongly affected by the Pd/Zn ratio. Moderate activity and high CO selectivity was observed for low zinc containing catalysts. The increase of ZnO content in the catalysts led to of activity enhancement and limited CO selectivity.

Bioethanol

Bioethanol is a cheap and valuable product, which can be used for synthesis of important chemicals and energy carriers, such as hydrogen or gasoline. The aim of the studies was elucidation of the role of acidity in selected zeolites on the mechanism of transformation of ethanol to hydrocarbons and deactivation phenomena. A series of zeolites of different SiO_2/Al_2O_3 ratio were investigated by temperature-programmed methods and in-situ diffuse reflectance infrared Fourier transform spectroscopy (DRIFTS). It was stated that acidity zeolites plays crucial role in the way of ethanol conversion to suitable products and deactivation phenomena due to the formation of carbon deposits.

OPTIMIZATION OF MUNICIPAL WASTE MANAGEMENT SYSTEMS INCLUDING METHODS FOR MECHANICAL-BIOLOGICAL TREATMENT OF THE WASTE

Adam LESIUK
DEPARTMENT OF CHEMICAL TECHNOLOGY

Municipal waste management system in Poland from 2013 was built on the waste management plants. The waste management plants must be implemented by the technology based on mechanical-biological treatment (MBP) of municipal waste [1, 2]. Number of waste management plants in Poland using the MBP is over 120 installations, in the Lubelskie region 15 [3].

According to the law, only waste that has been processed (recovery processes, including recycling, fermentation or composting may be directed) can be admitted to the storage [4]. The result is a so called waste stream, so called secondary raw materials, which should be directed to recovery. The mass of the municipal waste stream (glass, plastics, metals, paper) led to recovery also depends on the morphological composition of waste.

One of the most important problems in the waste management system is the lack of current research in the field of municipal waste management, including research on the morphological composition of waste and the physical and chemical properties of waste, in individual region [2].

The study of the balance of collected waste in Radzyń Podlaski over three years (2014-2016) which are processed at the Waste Management Plant in Adamki near Radzyń Podlaski (Fig. 1. and Table 1).

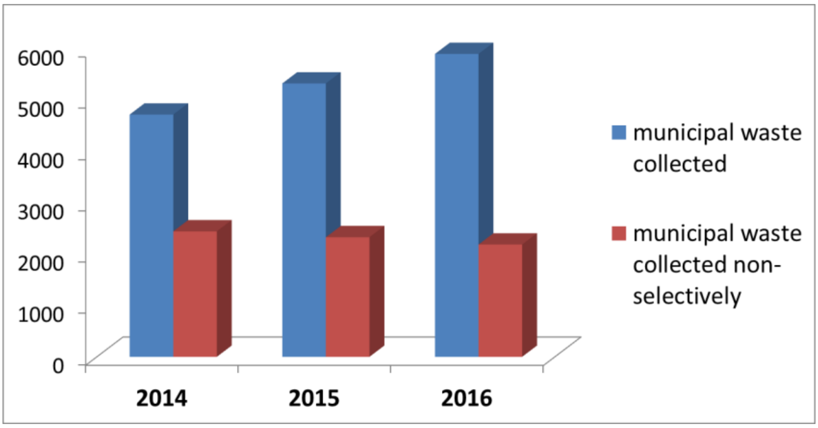

Fig.1. Mass (tons per year) of collected municipal waste in 2014 -2016 in Radzyń Podlaski.

Table 1. Unit indicator of waste accumulation per capita in years 2014 – 2016 [5-7].

Specification	**unit indicator of waste accumulation per capita (kg/year)**		
	2014	**2015**	**2016**
Poland	269	283	303
Lubelskie region	178	179	196
Radzyń Podlaski	293	333	371

The chart and table 1 show that the mass of waste generated and the unit accumulation rate from year to year is systematically growing. These increases are much higher than in the Lubelskie Voivodeship or the Polish average.

The following Table 2 shows results research (1 year) share of secondary raw materials in municipal mixed waste generated in Radzyń Podlaski and Lublin.

Table 2. Share of secondary raw materials in municipal mixed waste generated in the Radzyń Podlaski and Lublin.

Component	Share of secondary raw materials of municipal mixed waste (%)	
	Radzyń Podlaski	Lublin
paper	5.9	5.8
plastics	14.6	11.3
glass	6.4	6.2
metals	2.0	1.2
sum	**28.9**	**24.5**

The research shows that the share of secondary raw materials in mixed waste collected in Radzyń Podlaski is higher than in Lublin and amounts to around 30% of collected waste (632 tonnes in 2016). It is a large amount of raw materials and it is necessary to make changes in the waste management system that will increase the mass of waste collected selectively.

References:

[1] Ustawa z dnia 14 grudnia 2012 r. o odpadach (Dz.U. 2013 poz. 21).
[2] Krajowy Plan Gospodarki Odpadami 2022, Warszawa 2016.
[3] Plan Gospodarki Odpadami dla województwa lubelskiego 2022, Lublin 2016.
[4] Ustawa odpadach z 14 grudnia 2012 roku (Dz.U. 2013 poz. 21)
[5] GUS, Informacje i opracowania statystyczne, Ochrona środowiska 2015,
[6] GUS, Informacje i opracowania statystyczne, Ochrona środowiska 2016
[7] GUS, Informacje i opracowania statystyczne, Ochrona środowiska 2017

INVESTIGATION OF ADSORPTION OF INORGANIC AND ORGANIC SUBSTANCES IN MICELLAR, OXIDE AND ENVIRONMENTAL DISPERSE SYSTEMS

Andrzej KOMOSA, Stanisław CHIBOWSKI, Elżbieta GRZĄDKA,
Władysław JANUSZ, Adam W. MARCZEWSKI, Jolanta ORZEŁ,
Iwona OSTOLSKA, Małgorzata PASZKIEWICZ, Jacek PATKOWSKI,
Marek RESZKA, Ewa SKWAREK, Marta SZYMULA, Teresa URBAN,
Małgorzata WIŚNIEWSKA
DEPARTMENT OF RADIOCHEMISTRY AND COLLOID CHEMISTRY

A plant named saw sedge (*Cladium mariscus* L. Pohl) can be treated as a source of nano silica particles. This is an herbaceous plant belonging to sedge family (*Cyperaceae*). It grows up to 2.5m height and forms a bulrush at wetland areas. In Lublin region the saw sedge occurs on large areas of carbonaceous wetlands at Chełm town vicinity. Although the saw sedge is involved in a species protection (since 2004), for normal growing an annually mowing of leafy parts, connecting with removing of this material, is necessary. However, up till now the removing material has not found any utilization.

Ground stalks and leaves of dried saw sedge were used as a studied material. FTIR analyses were done using Nicolet 8700A (Thermo Scientific) spectrophotometer equipped with attenuated total reflectance (ATR) accessory with a single bounce diamond crystal. For a bulk elemental analysis ED-XRF Epsilon 5 (Panalytical) was applied.

The X-ray fluorescence study has shown that the saw sedge contained 2.6% Si (5.7% SiO_2) and a small amount of such elements as: 1.1% Ca, 1.1% K, 0.6% Cl and 0.1% S (Fig.1). Microscopic data, using the SEM Quanta 3D FEG-(Fei) scanning microscope with EDAX system for mapping of elements by an X-ray fluorescence method have shown that silica was distributed on a cellulose background as microspheres of about 10µm of diameter.

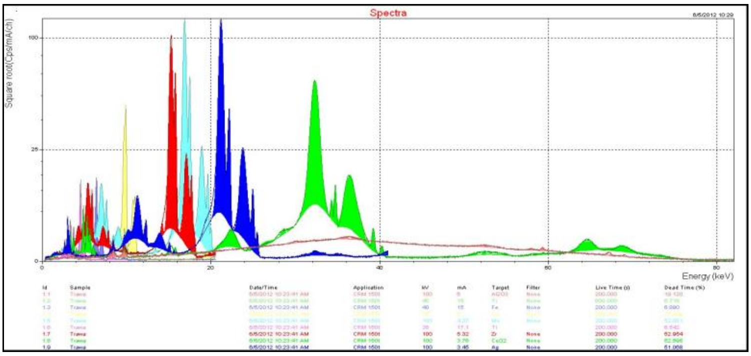

Fig. 1. ED-XRF spectra of a dry saw sedge sample obtained with Ti, Ge and Zr targets.

To concentrate the silica a leaching method with a mixture of HNO_3 and H_2SO_4 was applied; next dry ashing at 400°C and 600°C was performed. Acid leaching of the material resulted in partial separation of silica crystals of 10 µm diameter but also numerous aggregates of 50-100 µm dimension appeared. After thermal sample treatment in 400°C, followed by nitric acid leaching, organic matter was not removed completely but in 600°C it was. Determined specific surface of this latter material was rather large of 54.8 m^2/g (by nitrogen adsorption according to BET isotherm). The above treatment led to concentrate of silica in the sample. It was shown also by potentiometric titration that the pHpzc of the sample after thermal treatment followed by nitric acid leaching was equal to 3.53. This value was confirmed by a zeta potential study: isoelectric point laid at pH=3, what fits in with literature value for silica.

Analyses using the X-ray diffraction method of dry saw sedge sample showed only small contribution of crystalline silica in amorphous matter.

FTIR-ATR spectra of a dry saw sedge revealed a presence of cellulose (bands of 1630; 1430; 1320; 1200; 1160 cm^{-1}) and silica (1100; 1050; 720; 670; 470 cm^{-1}), as it is seen of Fig.2. However, after thermal treatment, the bands which were characteristic for silica (1049 and 1114.7 cm^{-1}) were seen on the spectrum (Fig.3).

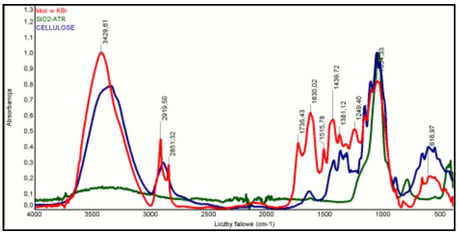

Fig. 2. FTIR-ATR spectra of a dry saw sedge sample (red) and, for comparison, cellulose (blue) and silica (green) spectra taken from the spectrometer database.

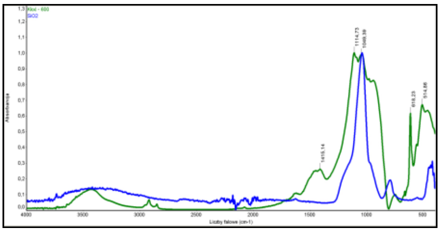

Fig. 3. FTIR-ATR spectra of ashed saw sedge followed by acid leaching in comparison with pure silica (green line - saw sedge sample, blue line - silica standard).

A large amount of a saw sedge windrow was obtain every year and should be utilized. This material can be treated as a source of silica of spherical nano particles. As silica is bound with a cellulose matter it is possible to apply it as a fuel or, taking into account a high specific surface area, as an efficient adsorbent as well.

Acknowledgement

Authors wish to thank Zofia Komosa and Marta Kulpa for their help in sample treatment and measurements.

SYNTHESIS AND CHARACTERIZATION OF d- AND f-ELECTRON METAL COMPLEXES AND NOVEL N/O/S DONOR LIGANDS

Agata BARTYZEL, Beata CRISTÓVÃO, Wiesława FERENC, Halina GŁUCHOWSKA, Renata ŁYSZCZEK, Liliana MAZUR, Agnieszka OSTASZ, Dariusz OSYPIUK, Iwona RUSINEK,
Justyna SIENKIEWICZ-GROMIUK
DEPARTMENT OF GENERAL AND COORDINATION CHEMISTRY

The design and synthesis of coordination compounds are currently of great interest due to their potential applications in a wide variety of fields such as magnetism, medicine, optoelectronic materials, molecular separation, and so on. We have synthesized novel complexes of d- and f-block elements with different bridging and chelating O/N/S ligands. The obtained complexes were characterized by methods: X-ray single crystal and powder diffraction techniques, photoluminescence, CHN, TG-DSC, TG-FTIR, FT-IR, Raman, UV-VIS, XANES, XPS, biological, magnetic studies as well as quantum chemical calculations.

The heterotrinuclear $Cu^{II}_2Ln^{III}$ complexes with the *N,N'*-bis(2,3-dihydroxybenzylidene)-1,3-diamino-2,2-dimethylpropane) were obtained. The compounds crystallize in the monoclinic space group $P2_1/n$. In the crystals of the complexes the central Ln^{III} ion is surrounded by two CuH_2hamp units, so that Ln^{III} and Cu^{II} ions are linked by phenoxido bridging groups. The compounds are stable at room temperature and their decomposition processes proceed in the similar way. The temperature dependence of the magnetic susceptibility and the field-dependent magnetization indicated that the interaction between Cu^{II} and Ln^{III} ions is ferro- or antiferromagnetic. The mono- and dinuclear Cu(II) complexes were synthesised during reactions of *N,N'*-bis(5-bromo-3-methoxysalicylidene)-1,3-diamino-2-propanol with Cu(II) acetate. They are stable at room temperature. In the mononuclear complex the Cu(II) ion occupies the smaller N_2O_2 cavity of the ligand whereas in the crystal of the dinuclear one the completely deprotonated Schiff base coordinates with central atoms through two imine nitrogen atoms, a pair of phenolic oxygen atoms and an oxygen atom of deprotonated hydroxyl group. Cu(II) ions with LK=5 and LK=4 are connected via an oxygen atom derived from the aliphatic part of the N,O-donor ligand and the bridging carboxylate group of the acetate ion.

The new bis *o*-hydroxy N_2O_3-donor Schiff base was synthesised. The 2,2'-((2-hydroxypropane-1,3-diyl)bis(nitrilophenylmethylidyne))diphenol occurs as the phenol-imine/zwitterionic form. The phenol-imine/keto-amine tautomeric equilibria were also investigated in solution in the polar protic and aprotic solvents. The effect of polar protic solvents on synthesis of Ni^{II} complexes with the Schiff base was studied. This allowed to obtain four different nickel(II) complexes. The use of equimolar quantities of substrates leads to formation of mononuclear complexes ($[Ni(C_{29}H_{24}N_2O_3)]\cdot(CH_3OH)(H_2O)_{0.25}$ (methanol) and $[Ni(C_{29}H_{24}N_2O_3)]\cdot H_2O$ (ethanol)) where metal centres are coordinated *via* the N_2O_2-core of Schiff base ligand giving distorted square planar geometry. Increasing the concentration of metal ions with respect to the ligand allowed obtaining the tetranuclear $[Ni_4(C_{29}H_{24}N_2O_3)_2(CH_3COO)_2(CH_3OH)_{3.65}(H_2O)_{0.35}]\cdot(CH_3OH)_7$ (methanol) and hexanuclear $Ni_6(C_{29}H_{24}N_2O_3)_2(C_{16}H_{17}N_2O_2)_2(CH_3COO)_2]\cdot(C_2H_5OH)$ (ethanol) metal clusters In crystal obtained from methanol the Ni^{II} ions have octahedral geometry whereas in complex synthesised form ethanol the metal centres are four- and six-coordinate. It was also demonstrated that solvent molecules play a significant role in stabilization of the structure of the obtained nickel(II) complexes.

The 2,4-bromophenoxyacetates of selected transition metals form complexes with general formula $ML_2\cdot nH_2O$ or $ML_3\cdot nH_2O$ where: L = $C_8H_5Br_2O_3$, M(II)=Mn, Co, Ni, Cu and M(III)=Nd, n=1 for Nd(III) compound, n=2 for Mn(II), n=4 for Cu(II) and n=5 for Co(II) and Ni(II) complexes. The compounds crystallize in monoclinic systems. The carboxylate groups act as bidentate chelating or bridging agents. On heating in air, the analyzed compounds are decomposed in two, three or four steps. The enthalpy values of the dehydration process changed from 36.40 kJ/mol to 81.76 kJ/mol. The magnetic moments of compounds confirm the presented complexes to obey the Curie–Weiss law.

The 1,3-phenylenediacetic acid form with Gd(III), Dy(III), Er(III) and Lu(III) ions 3-D coordination polymers of the general formula $[Ln_2L_3(H_2O)]\cdot H_2O$. Lanthanide ions are bridged through bidentate-bridging and threedente bridging-chelating carboxylate groups from L^{2-} ligands. Water molecules appear in inner and outer coordination sphere. Compounds are thermally stable up to about 100°C and further heating lead to multi-step decomposition to the suitable oxides. Detailed investigations of dehydration process point out to reversibility of removal of water molecules and crystallinity of dehydrated forms of complexes. The series of lanthanide complexes with biphenyl-4,4'-dioxydicetic acid of the general formula $Ln_2L_3\cdot nDMF$ were obtained in solvothermal conditions with MW heating. They exhibit different thermal stability and different pathways of thermal decomposition. Europium and terbium complexes display photoluminescence properties.

The resonance forms and conformational behaviour of the series of new linear trisubstituted N^1-acylamidrazones have been investigated in the solid state and solution. The 1D- and 2D-NMR experiments, supported by theoretical calculations revealed that in solution all amidrazones exhibit conformational *syn*/*anti* isomerism that results from the hindered rotation around the amide bond. In the case of propenoic acid derivative the ROESY, HSQC, HMBC experiments proved a third equilibrium structure that corresponds to the planar *ylide* form. The SC XRD data confirmed that the compounds tend to exist as a *Z-anti* conformers of their hydrazone-amide tautomeric species in the solid state. The carboxyl-amide heterosynthon is favored provided that the carboxyl group is not involved in intramolecular hydrogen bonding. Interestingly, after replacement of the cyclic C^1-substituent by the smaller propanoic acid unit, which results in lower steric hindrance, both *syn* and *anti* conformers are available. Furthermore, in the former case both the neutral molecules and zwitterions are present in the same crystal. The unsolvated forms are stable in a wide range of temperatures, however, inclusion of the solvent molecules increases propensity to cyclization even at room temperature.

SYNTHESIS AND PROPERTIES OF POLYMERS

Barbara GAWDZIK, Andrzej BARTNICKI, Marta GROCHOWICZ,
Małgorzata MACIEJEWSKA, Janina NOWAK, Joanna OSYPIUK-TOMASIK, Beata PODKOŚCIELNA, Maciej PODGÓRSKI,
Andrzej PUSZKA, Magdalena ROGULSKA, Magdalena SOBIESIAK,
Łukasz SZAJNECKI, Marta WORZAKOWSKA
DEPARTMENT OF POLYMER CHEMISTRY

In the last few years there has been a growing interest in the methods of controlled radical polymerization that allows the synthesis of polymers with a defined molecular mass and a low dispersion of these mass. The molecular mass control of polymers is an important issue because final physical and mechanical properties of the polymer depend on the length of its chain. In order to control the length of the polymer chain, so-called chain transfer agents are used in polymerization process.

Thiols are well-defined chain transfer agents in the free radical polymerization for such ordinary monomers as styrene or methyl methacrylate. Thiols play a significant role among the chain transfer agents because of their efficiency in obtaining polymers of the desired molecular mass. Two important parameters that determine such use of thiols are weakness of the S–H bond and high reactivity of the thiol radicals [1-3]. The weakness of the S–H bond can be explained by the high reactivity of these compounds towards chain-carrying macroradicals, leading to high chain transfer constants, irrespectively of the used monomer. In turn, high reactivity of the thiol radicals is characterized by almost ideal chain transfer behavior of thiols, with a large decrease in the polymer molecular mass without a substantial change in the polymerization rate.

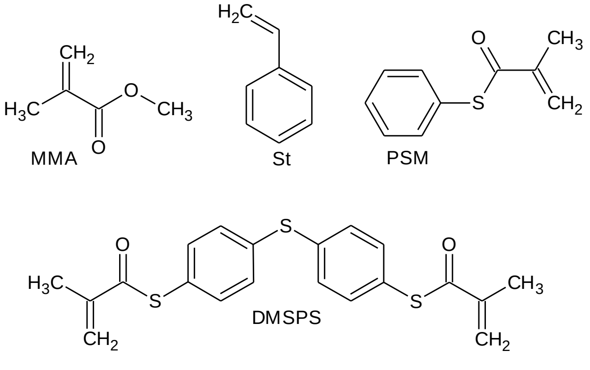

Fig. 1 Chemical structure of the monomers used in polymerization

This study presents the synthesis, structure and polymerization of S-phenyl 2-methylprop-2-enethioate (PSM). This compound was prepared in the reaction of thiophenol with methacryloyl chloride. The obtained PSM was purified on the chromatographic column. Chemical structure of the monomer was confirmed by spectroscopic methods (ATR–FTIR, GC–MS, ^{1}H and ^{13}C NMR).

Next bulk polymerization of PSM with styrene (St) or methyl methacrylate (MMA) was performed. In this way, linear copolymers were obtained. The number and mass average molar mass of the obtained copolymers were determined by gel permeation chromatography (GPC).

Additionally, crosslinked copolymers of the commercial monomer S,S'-thiodi-4,1-phenylene bis(thiomethacrylate) (DMSPS) under the same conditions were synthesized. The influence of thiol monomers on the physico-chemical properties of the obtained copolymers was determined. Thermal properties of the synthesized materials were investigated by means of DSC and TG/DTG [4-6].

DSC and TG/DTG measurements indicated that the obtained copolymers possess high thermal resistance; they are stable up to 220 ^{o}C. The thermal stability of the studied copolymers decreased with the increasing amount of PSM. The results of DSC analysis showed an endothermic effect in the range of 358-417 ^{o}C due to the total decomposition of PSM and DMSPS copolymers with methyl methacrylate and styrene. The glass transition temperature of styrene copolymers is about 90 ^{o}C, whereas for MMA-DMSPS copolymers T_g is about 115 ^{o}C and about 85 ^{o}C for MMA-PSM copolymers. GPC analysis showed that PSM *co*monomer influenced significantly the molecular mass of St-PSM and MMA-PSM copolymers. The average molecular mass (M_n, M_w) of the obtained copolymers decreased with the increasing amount of PSM comonomer.

Taking into account the chemical structure, thermal stability and molecular mass of synthesized PSM copolymers with St and MMA, and from the other hand the trends in POFs technology, it can be supposed that presented in this study PSM monomer can be used as a special additive for polymers used in optical fibres drawing.

References:

[1] A. Valdebenito, M.V. Encinas, *Polymer*., **46 (**2005) 10658.

[2] A. Valdebenito, M.V. Encinas, *J. Photochem. Photobiol. A: Chemistry*., **194** (2008) 206.

[3] T.Y. Lee, T.M. Roper, E.S. Jonsson, C.A. Guymon, C.E. Hoyle, *Macromolecules,* **37** (2004) 3606.

[4] B. Podkościelna, A. Lipke, M. Majdan, B. Gawdzik, A. Bartnicki, *J Therm. Anal. Calorim.*, **126** (2016) 161.

[5] B. Podkościelna, M. Sobiesiak, *J Therm. Anal. Calorim.*, **127** (2017) 625.

[6] K. Fila, M. Grochowicz, B. Podkościelna, *J. Therm. Anal. Calorim.,* DOI 10.1007/s10973-017-6833-z.

DIATOMITE AS AN ALTERNATIVE FOR TEOS SILICA SOURCES IN THE SBA-15 SYNTHESIS PROCESS

Stanisław PIKUS, Małgorzata SKIBIŃSKA, Aleksander PADEWSKI
DEPARTMENT OF CRYSTALLOGRAPHY

SBA-15 is a mesoporous silica materials with a hexagonal structure and a pore diameter between 5-15nm . It is characterized by high thermal stability and a large surface area in the range of 400-900 m^2 / g, that is way its has great application possibilities. The physicochemical properties of this material can be controlled by changing the conditions of the synthesis process, e.g. pH, mixing time, the temperature of the aging process, the addition of solvents, the reagents used. Typically SBA-15 is synthesized by the sol-gel method using tetraethylorthosilicate (TEOS) as a source of silica. However, due to the high processing costs of TEOS, was looking for new reagents which will be an alternative solution and can be used as a substitute.

The aim of this research was to use diatomite, containing 91% silica in the synthesis of SBA-15 material as an alternative to TEOS silica source. Diatomite is a sedimentary rock formed from the skeleton of single-celled diatoms. It is mainly made of amorphous hydrated silica. In addition, it contains macropores in its structure, which increase mass transfer, diffusion and therefore can improve the sorption capacity of the final synthesis products. However, it is primarily cheap and widely available material.

A classic synthesis of SBA-15 material was carried out using diatomite, in which the amount of TEOS was decreased and the amount of added diatomite was increased (see Table 1). This materials were characterized using the XRD method, nitrogen adsorption/desorption and SEM.

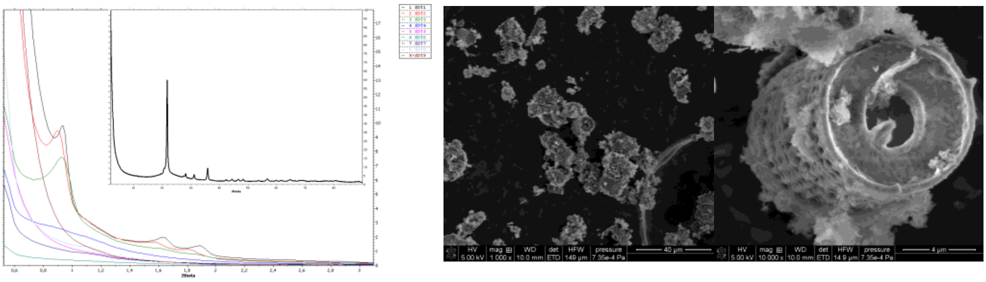

Fig. 1. a) X-ray diffraction patterns of SDT1-SDT9 samples b) SEM images of SDT3 sample.

Fig. 1 shows small-angle diffraction patterns. Only for the first three samples of SDT1-3 there were observed three peaks (110, 110, 200) characteristic for the ordered hexagonal structure of SBA-15, with a similar unit cell parameter circ.11nm. In other cases, where the amount of diatomite was already significant, the amount of TEOS was small and the amorphous material was obtained. In the wide-angle range, peaks from diatomite is noticeable in each of the samples but their intensity indicates that the part of the diatomite is used for the synthesis of SBA-15. Thus, the mineral did not completely decompose during the synthesis process and did not build into the structure of mesoporous silica. This is confirmed by SEM images, where the cylindrical structures characteristic for diatomite are visible.

Table 1 presents the structural parameters of the obtained materials. When the amount of diatomite increases, the total specific surface area of the materials decreases and is much lower than in the case of the classical SBA-15, also the micropore surface and the pore volume decrease. On the other hand, the pore size incerases, and it is the largest for the SDT6 sample, equals 19.1 nm. The changes are also noticeable in the case of the nitrogen adsorption/ desorption isotherm, where with the standard amount of TEOS we obtain a type IV isotherm with a wide hysteresis loop but when increasing the diatomite we have isothermal type II with less developed hysteresis loops.

Table 1. Textural properties of investigated composites.

SAmple	**Composotion of SBA-15-diatomite samples**			**S_{BET} (m^2/g)**	**S_{mic} (m^2/g)**	**Pore Volume**		**Pore Size distribution**
	TEOS [cm^3]	**Pluronic [g]**	**Diatomit [g]**			**Vt (cm^3/g)**	**V_{mic} (t-plot) (cm^3/g)**	**D_h [nm]**
SDT1	4.15	2	1.5	176	9.6	0.33	0.003	7.57
SDT2	3.65		2.0	119	5.2	0.34	0.001	11.54
SDT3	3.15		2.5	100	2.41	0.31	0.00004	12.43
SDT4	2.65		3.0	67	2.8	0.23	0.0007	13.75
SDT5	2.15		3.5	56	2.35	0.206	0.0005	14.79
SDT6	1.65		4.0	28	1.9	0.13	0.0006	19.1
SDT7	1.15		4.5	17	1.27	0.08	0.0004	18.57
SDT8	0.65		5.0	2.4	2.0	0.0089	0.0008	14.96
SDT9	0		5.5	1.65	0.34	0.004	0.0001	9.54

A certain amount of TEOS can be replaced by diatomite so as to obtain SBA-15 material with a typical hexagonal structure. However, a larger amount of diatomite prevents the synthesis of ordered SBA-15. As demonstrated by the studies, diatomite is not consumed completely in the SBA-15 synthesis process but some of it remains unchanged and provides a support for the synthesized hexagonal ordered porous material.

References:

[1] N. Rahmat, F. Hamzah, N. Sahiron, M. Mazlan, M. M. Zahari, IOP Conf. Series: Materials Science and Engineering, **133** (2016).

[2] W. Yu, L. Deng, P. Yuan, D. Liu, W. Yuan, P. Liu, H. Hem Z. Li, F. Chen, *Journal of Colloid and Interface Science,* **448** (2015) 545–552.

STRUCTURAL STUDIES OF NEW BIOLOGICALLY ACTIVE HETEROCYCLIC COMPOUNDS

Ilona B. MATEREK, Aleksandra SAWCZENKO, Anna E. KOZIOL
DEPARTMENT OF CRYSTALLOGRAPHY
Anna BIELENICA, Marta STRUGA
DEPARTMENT OF BIOCHEMISTRY, MEDICAL
UNIVERSITY OF WARSAW, WARSZAWA

Several series of new compouds containing the 1,3-disubstituted thiourea, 1,2,4-triazole, 1,3-thiazole, 1,3,4-thiadiazole, 1,3,4-oxadiazole, 1,3-thiazolidin-4-one, tetrazol-5-amine groups as pharmacophores have been synthesized at the Medical University of Warsaw [1–4]. The molecular structure of representative compounds has been determined by the X-ray crystallography.

1,3-Disubstituted thioureas have attracted an increasing attention due to their potential in medicinal chemistry. In past decades heterocyclic fragments such as the 1,2,4-triazole, 1,3,4-thiadiazole and 1,3,4-oxadiazole, and their derivatives were intensively investigated because of their biological activity. Fluconazole, efinaconazole, terconazole and fosfluconazole are used as antifungal agents, and their structures are based on the 1,2,4-triazole core. The 1,3,4-thiadiazole scaffold can be found in active substances like acetazolamide, methazolamide and megazol. Finally, the 1,3,4-oxadiazole arrangement is present in raltegravir and zibotentan. Among many heterocyclic compounds, these five-membered structures display unique spatial arrangements, which give possibilities to develop the synthetic pathways for microbiologically active compounds that can have potential therapeutic applications as new medicines. Among various heterocycles reported to date, thiazolidine, tetrazole and their derivatives have received much attention due to their various bioactivities. Molecules containing another five-membered ring, thiazolidinone, are associated mainly with antibacterial, antitubercular, antidiabetic and anticancer activities.

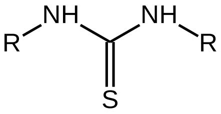

thiourea

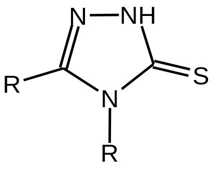

1,2,4-triazole

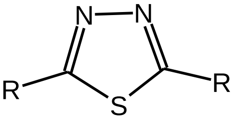

1,3,4-thiadiazole

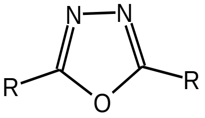

1,3,4-oxadiazole

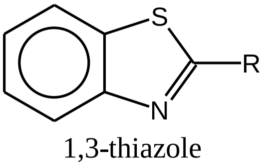

1,3-thiazole

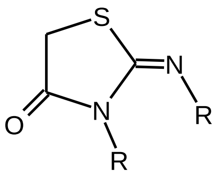

1,3-thiazolidin-4-one

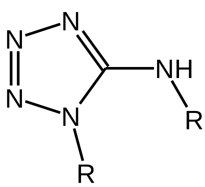

tetrazol-5-amine

A series of novel 1-(1-benzylpiperidin-4-yl)thiourea and 3-(furan-3-ylmethyl)thiourea [1] derivatives were synthesized and evaluated for their antimicrobial and cytotoxic activities. Results suggest that tested thioureas caused the cytotoxic effect in normal and cancer cells lines in dose dependent manner. The antiproliferative activity of two selected compounds against cells derived from human haematological tumours showed cytotoxicity against all tested cell lines.

The next work [3] showed that as compared to starting thiourea-based analogs, the transformation of the thioureidic fragment into the tetrazole ring reduced the cytotoxicity of compounds by 2–7 times. Similarly, the formation of the thiazolidin-4-one moiety resulted in 2–15 lower cytotoxicity. It is worth to note that the N-(4-nitrophenyl)tetrazo-1-yl derivative turned out to be cytotoxic for exponentially growing MT4 cells in the low micromolar range, being 3 times more potent than its parent thiourea.

The synthesis and the evaluation of new fifteen thiourea derivatives with 1,3-benzothiazole-2-yl moiety have been performed [4]. Among them was a group of seven biologically active showing cytotoxicity against human leukaemia/lymphoma-and solid tumour-derived cell lines, and antiviral activity against HIV-1 and representatives of ssRNA and dsDNA viruses.

Obtained results can provide some constructive data for further designing of novel family of potentially bioactive analogs.

References:

[1] A. Bielenica, K. Stępień, A. Sawczenko, T. Lis, A.E. Kozioł, S. Madeddu, D. Collu, F. Iuliano, A. Kośmider, M. Struga, *Letters in Drug Design & Discovery*, **14** (2017) 636– 646.

[2] D. Szulczyk, P. Tomaszewski, M. Jóźwiak, A. E. Kozioł, T. Lis, D. Collu, F. Juliano, M. Struga, *Molecules*, **22** (2017) 409.

[3] A. Bielenica, D. Szulczyk, W. Olejarz, S. Madeddu, G. Giliberti, I.B. Materek, A. E. Koziol, M. Struga, *Biomedicine & Pharmacotherapy*, **94** (2017) 804-812.

[4] A. Bielenica, G. Sanna, S. Madeddu, M. Struga, M. Jóźwiak, A.E. Kozioł, A. Sawczenko, I.B. Materek, A. Serra, G. Giliberti, *Chemical Biology and Drug Design*, (2017) 1-9, doi: 10.1111/cbdd.13009.

GEL SYNTHESIS AND STRUCTURE OF NOVEL BA(II) AND PB(II) COMPLEXES WITH CITRIC ACID

Anna E. KOZIOŁ
DEPARTMENT OF CRYSTALLOGRAPHY
Aleksandra DRZEWIECKA-ANTONIK
INSTITUTE OF PHYSICS, POLISH ACADEMY OF SCIENCES, WARSZAWA

Citric acid (H_3cit) is commonly occurring in nature tricarboxylic α-hydroxyl acid. It is one of the most essential metabolites present in all aerobic living organisms. Another important biological role is the stabilization of hydroxyapatite nanocrystals in bones. Citric acid is applied as food additive, component of pharmaceutics, detergents, chelating agents and others. Therefore the knowledge of coordination of citrate anions to heavy metal is crucial for health and environmental issues.

The studies [1] focused on citrate complexes with two important divalent metals of the sixth row, barium and lead. Ba(II) citrate is commonly used in biological and medical sciences as the adsorbent of calcium binding proteins. Pb(II) citrate is applied in electron microscopy for staining biological samples. The Ba(II) citrate structure is the first one reported in literature, while the Pb(II) complex it is the second structure synthesised without co-cations. The complexes were prepared in a silicic acid gel medium using the technique described by Henisch. The gelling mixture was prepared by adding a solution of sodium metasilicate to 1 M solution of H_3cit. The reagents - barium and lead nitrates – were poured over this medium and two new compounds $\{[5Ba^{2+}(cit^{3-})_2(Hcit^{2-})_2 \cdot 6H_2O] \cdot 2H_2O\}_n$ (**1**) and $\{[5.5Pb^{2+}(cit^{3-})_3\,(Hcit^{2-}) \cdot 5H_2O]\ 4.5H_2O\ \}_n$ (**2**) have been synthesized.

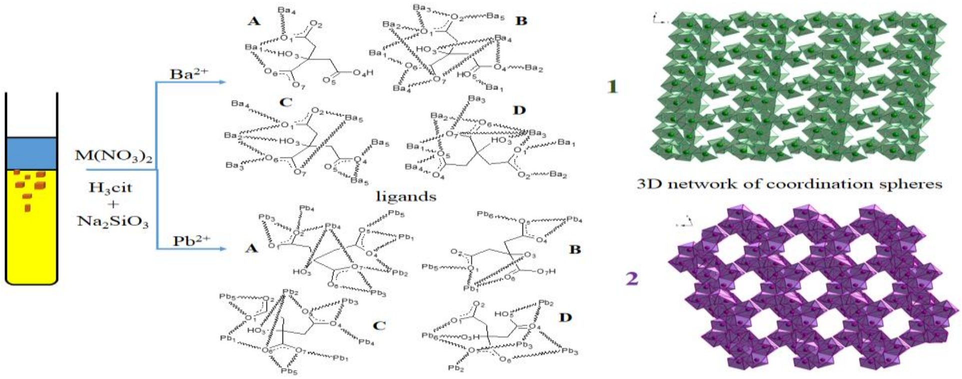

Both crystalline complexes form three-dimensional frameworks with two type of citrate anions having three and two deprotonated carboxylic groups. The cation coordination numbers vary from 6 to 11.

References:

[1] A. Drzewiecka-Antonik, A. E. Koziol, P. Rejmak, K. Lawniczak-Jablonska, L. Nittler, T. Lis, *Polyhedron,* **132** (2017) 1-11.

STANDARD AND MICROSTRUCTURED OPTICAL FIBERS WITH SHAPED DISPERSION FOR NEW LIGHT SOURCES

Krzysztof POTURAJ, Grzegorz WÓJCIK, Lidia CZYŻEWSKA,
Aleksander WALEWSKI, Janusz PĘDZISZ, Jarosław KOPEĆ,
Wiesław PODKOŚCIELNY, Małgorzata GIL, Paweł MERGO
LABORATORY OF OPTICAL FIBERS TECHNOLOGY

Thanks to the significant development of technology, optical fibers, in particular silica and high silica optical fibers find more and more applications. Owing to the possibility of shaping their internal structure and optical properties, devices using fiber optics exceed increasingly high limits. A good example here are optical fibers with shaped chromatic dispersion that have been successfully used in construction of new light sources as supercontinuum and fiber lasers.

There were elaborated technology of few standard and microstructure optical fibers with controlled chromatic dispersion in last year in Laboratory of Optical Fibers Technology UMCS.

For all-polarization-maintaining, stretched-pulse, mode locked, Tm-doped fiber laser was elaborated standard normal dispersion fiber with group velocity dispersion of 0.08 ps2⁄m. Fiber was fabricated by a modified chemical vapor deposition method. Its core was GeO_2-doped with the concentration of 36 mol%. Owing to the slight core ellipticity (major axis = 3.14 μm and minor axis = 2.7 μm), the fiber exhibit phase (B) and group (G) modal birefringence of $B = 8.3 \times 10^{-5}$ and $G = 1.69 \times 10^{-4}$ at 1950 nm, wavelength respectively. Fig. 1. presents SEM photos of cross section of fabricated fiber.

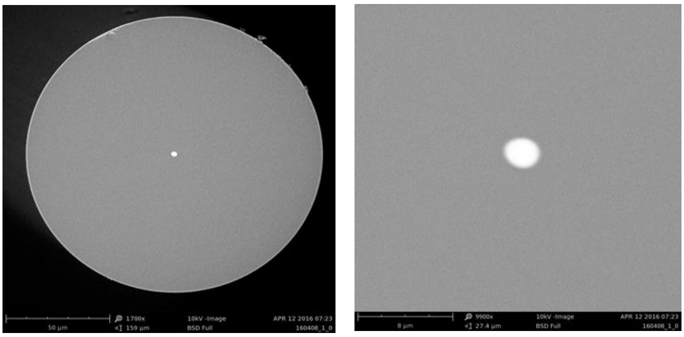

Fig. 1. SEM photos of fabricated classical fiber for Tm mode locked laser, core area (right).

For High-power frequency comb source tunable from 2.7 to 4.2 μm was elaborated first type microstructured highly nonlinear fiber HALF. The silica core with a 3.07μm diameter is surrounded by eight rings of air holes; the distance between the holes is equal to 2.47 μm, and the average diameter of the air holes is 1.84 μm. Figure 2 shows the chromatic dispersion curve of the HNLF, together with an image of the fiber cross-section taken with a scanning electron microscope (SEM).

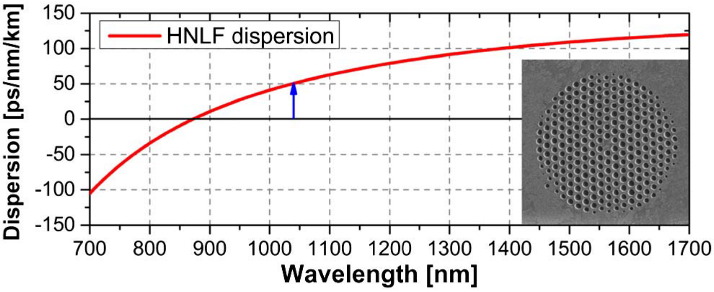

Fig. 2. Calculated dispersion of the first type HNLF with indicated pump wavelength (blue arrow). Inset: fiber cross-section SEM image.

For Generation of sub-100 fs pulses tunable from 1700 to 2100 nm from a compact frequency-shifted Er-fiber laser was elaborated second type of microstructured highly nonlinear fiber. The fiber preform was stacked from silica rods (cladding), and the germanium-doped rod fabricated by modified chemical vapor deposition method (core). The GeO_2 doping level was 18 mol%. Based on the scanning electron microscope (SEM) image of the fiber end facet (Fig. 3) geometrical parameters of the microstructure were estimated and are as follows: germanium-doped core diameter d = 4.05μm; diameter of the first air holes ring dr = 7.01μm; average diameter of the air holes in the first ring dh = 0.96μm.

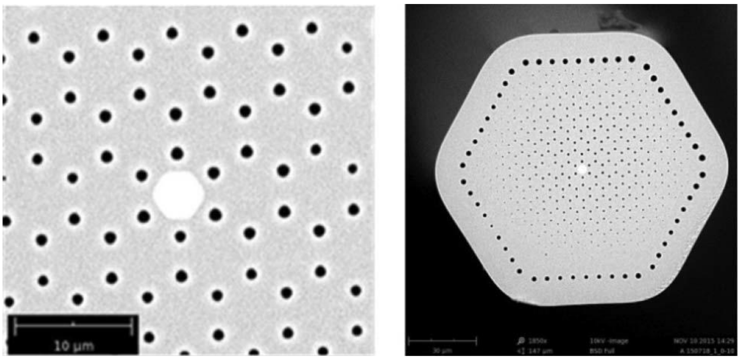

Fig. 3. SEM images of the fabricated second type HNLF.

THE ENVIRONMENTAL EFFECT OF ANTHROPOGENIC NANOMATERIALS

Bożena CZECH, Wiesława ĆWIKŁA-BUNDYRA,
Agnieszka MARCEWICZ-KUBA, Marcin KUŚMIERZ
DEPARTMENT OF ENVIRONMENTAL CHEMISTRY

There is a raising awareness that current consumption and reuse of goods is not environmental friendly and sustainable because a large variety of untreated wastes is introduced into environment. This requires the developing of new techniques for reuse and recycling of these materials in both an ecological and an economical way [1]. Among all of carbon based materials such as carbon fibres, fullerene, graphene and graphene oxide and carbon nanotubes (CNTs), the last ones have been successfully used in water purification and wastewater treatment [2]. CNTs are synthesized widely, but their cost of synthesis comparing to other mentioned carbon based material makes it hard to be used in water purification and catalysis application.

One of the regulatory factors in the environment is dissolved organic matter (DOM) [3]. Adsorption of DOM onto particles alters their surface charge and simultaneously changes their aggregation ability and deposition in water. DOM-coated CNT displays lower aggregation and deposition comparing to native CNTs [4]. Tannic acid (TA) is a well-known high-molecular-weight polyphenol with multiple adjacent hydroxyl groups found in different parts of plants [5]. On the other hand, naturally occurring water soluble organic matters in drinking water may act as the precursor of carcinogenic disinfection byproducts [6].

The effect of DOM sorption onto super hard carbon microtubes produced from cotton (at Deakin University, Geelong, Australia) was investigated as an alternative of CNTs. Both the extend of TA adsorption (kinetics and isotherms) and the stability of carbon microtubes (CTs) and CTs-TA solutions were established.

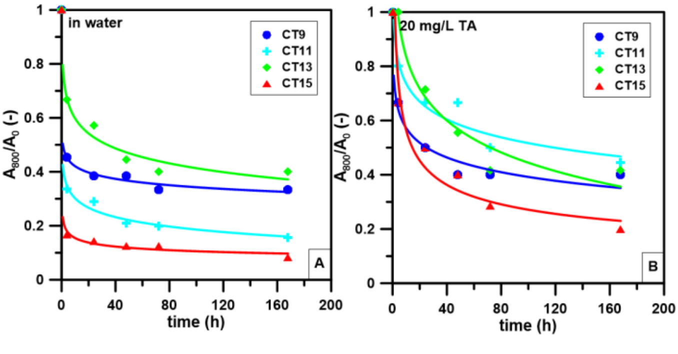

Fig. 1. The stability of CTs (2 mg·L^{-1}) in water and tannic acid solution (20 mg·L^{-1}).

The results presented in Fig. 1 indicate that in water almost all CTs sedimented quickly. The most significant changes in CTs stability were observed during first 24-48 hours (Fig. 1a). The greatest stability was revealed for CT9 and CT13, which was connected with surface charge and composition (the highest oxygen content) of CTs. Faster deposition observed using of CT11 and CT15 was the result of presence of large amount of surface –COOH groups on CTs.

Expectedly, TA changed the stability of CT and the time, when the stability was established (Fig. 1b). Generally, the nanotubes in the presence of TA formed stable suspensions. The greatest stability revealed for CT11 and CT13.

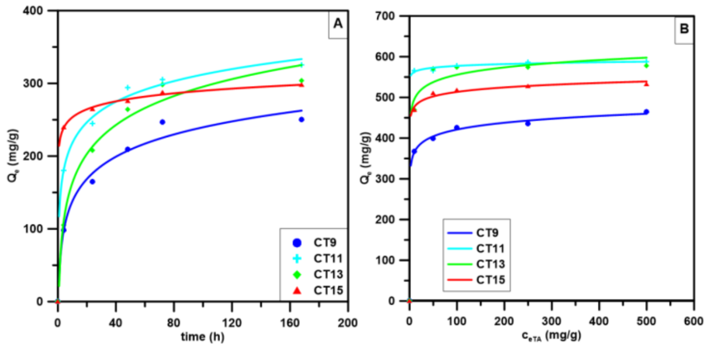

Fig. 2. The sorption of TA onto CTs (2 mg·L^{-1}): a) kinetics (10-500 mg·L^{-1}), b) isotherms (20 mg·L^{-1}).

The process of TA sorption was limited by chemical reaction of TA with CTs surface (a pseudo-second order kinetics). The good applicability of Langmuir model with simultaneously good fitting of other tested models (except Temkin) implied that monolayer sorption was the first step of TA adsorption onto CTs. The mechanism involved π-π interactions and hydrogen bonds between TA and CTs surface.

References:

[1] R. Arvidsson, B.A. Sandén, *J. Clean. Prod.*, **156** (2017) 253–261.
[2] B. Czech, W. Buda, *Environ. Res.*, **137** (2015) 176–184.
[3] T.B. Bittar, A. Stubbins, A.A.H. Vieira, K. Mopper, *Mar. Chem.*, **177** (2015) 205–217.
[4] D. Lin, B. Xing, *Environ. Sci. Technol.*, **42** (2008) 5917–5923.
[5] B. Czech, P. Oleszczuk, A. Wiącek, *Environ. Pollut.*, **200** (2015) 161–167.
[6] A. Phetrak, J. Lohwacharin, H. Sakai, M. Murakami, K. Oguma, S. Takizawa, *J. Environ. Sci.*, **26** (2014) 1294–1300.

ECOTOXICOLOGICAL AND CHEMICAL ASSESSMENT OF THE ENVIRONMENT SUBJECT TO ANTHROPOGENIC PRESSURE

Patryk OLESZCZUK, Bożena CZECH
DEPARTMENT OF ENVIRONMENTAL CHEMISTRY

The use of biochar in different applications related to fertilization and soil rehabilitation and remediation is becoming more and more common. Nevertheless, the content of organic contaminants in biochar, with polycyclic aromatic hydrocarbons (PAHs) being a significant group of such contaminants, can be a limitation for biochar application, in particular if it is used to improve soil properties [1,2]. Due to their mutagenic, cancerogenic and toxic properties, PAHs are considered to be contaminants that require special attention. This is particularly important in the case of fertilizer materials which, when applied to soils, can increase the content of these compounds in the soil. This may lead to the accumulation of PAHs in plants and subsequently to their incorporation into the human food chain. While there is intensive research on the effect of pyrolysis on the content and bioavailability of PAHs contained in biochar [2-5], in the literature there is a lack of information on the persistence and bioavailability of PAHs in biochar that undergoes aging processes under various conditions [6].

The aim of this study was to determine the effect of biochar aging on the content of polycyclic aromatic hydrocarbons (PAHs) (the total content – C_{tot}, and the freely dissolved – C_{free}) in biochar and its ecotoxicity. Two biochars (BCS and BCM) were aged for 420 days at different temperatures (-20^{o}C, 4^{o}C, 20^{o}C, 70^{o}C), at a variable temperature (-20/20^{o}C), in the presence of nutrients, and in the presence of inoculum and nutrients. After the aging process, C_{tot} and C_{free} PAHs were determined and an ecotoxicological analysis was performed, which involved tests with bacteria (*Vibrio fisheri*), invertebrates (*Folsomia candida*) and plants (*Lepidium sativum*). Aging significantly affected all the parameters tested. The range of changes in the studied parameters depended on the type of biochar and ageing conditions. For most of the aging methods, PAH content (C_{tot}, C_{free}) and toxicity were found to decrease. Aging in the presence of microorganisms and nutrients and in the presence of nutrients alone caused the greatest reduction in C_{tot} PAH content (a reduction from 30 to 100% relative to non-aged biochar), C_{free} PAH content (a reduction from 12 to 100%) (Fig. 1), root growth inhibition (a reduction from 73 to 90%), and luminescence inhibition (a reduction from 24 to 100%) (Fig. 2). For C_{free} PAHs and toxicity to *F. candida*, some aging methods caused their increase. The study also found a significant relationship between the changes in C_{tot} PAH content during aging and inhibition of root growth (BCS, BCM) and inhibition of *V. fisherii* luminescence (BCM). In no case was a significant correlation ($P \leq 0.05$) between C_{free} PAHs and the investigated toxicity parameters found.

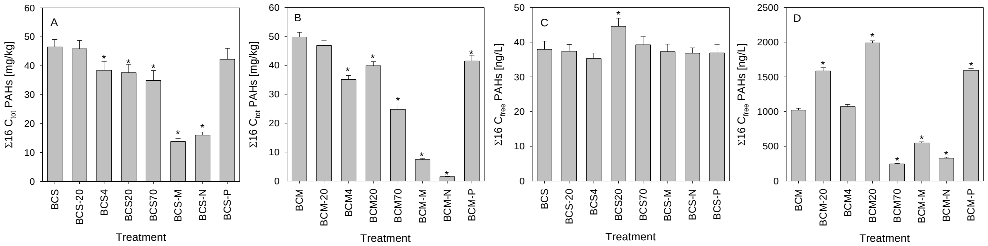

Fig. 1. C_{tot} (A, B) and C_{free} (C, D) content in aged biochars. A, C – biochar BCS, B, D – biochar BCM. * - statistical significant difference ($P\leq0.05$) comparing to fresh biochar.

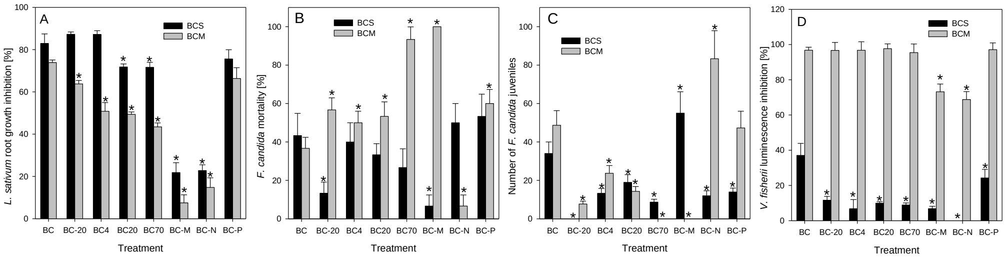

Fig. 2. Effect of fresh and aged biochars to root growth inhibition of *L. sativum* (A), *F. candida* mortality (B) and reproduction (C) and *V. fisheri* luminescence inhibition (D). * - statistical significant difference ($P\leq0.05$) comparing to fresh biochar.

The present study shows for the first time that, depending on the type of biochar and aging conditions, both the total PAH content and the content of freely dissolved PAHs change. In most cases, C_{tot} PAH content is observed to decrease, which is a positive trend. This confirms our previous observations in which a reduction in PAH content was found in biochar-amended soils. A decrease in PAH content was usually accompanied by a decrease in phytotoxicity of the biochars and in toxicity of their extracts. Under the aging conditions used in the present study, which are closest to environmental ones, the decrease in both toxicity and PAH content was highest.

References:

[1] P. Oleszczuk, I. Jośko, M. Kuśmierz, *J. Hazard. Mater.,* **260** (2013) 375–382.
[2] S.E. Hale, J. Lehmann, D. Rutherford, A.R. Zimmerman, R.T. Bachmann, V. Shitumbanuma, A. O'Toole, K.L. Sundqvist, H.P.H. Arp, G. Cornelissen, *Environ. Sci. Technol.,* **46** (2012) 2830–2838.
[3] A. Zielińska, P. Oleszczuk, *Biomass Bioenergy,* **75** (2015) 235–244.
[4] M. Stefaniuk, P. Oleszczuk, P. Bartmiński, *J. Hazard. Mater.,* **318** (2016) 417–424.
[5] A. Zielińska, P Oleszczuk, *Chemosphere,* **153** (2016) 68–74.
[6] M. Kołtowski, P. Oleszczuk, *Ecol. Eng.,* **75** (2015) 79–85.

HETEROGENEOUS CATALYSTS FOR PHOSPHORUS-CARBON BOND FORMATION

Elżbieta ŁASTAWIECKA,[1] Anna FLIS,[1] Wojciech GAC,[2]
Magdalena GRELUK,[2] Marek STANKEVIČ[1]
[1] DEPARTMENT OF ORGANIC CHEMISTRY
[2]DEPARTMENT OF CHEMICAL TECHNOLOGY

The development of new efficient methods of the synthesis of organic compounds is nowadays one of the main target in organic chemistry. At present, the most effective synthetic methods include catalytic transformations which are especially well suited for the synthesis of compounds which are usually hardly accessible using classical synthetic methods. Catalytic reactions usually proceed with high degree of chemo and regioselectivity which are achieved using catalytic systems where the central role is played by transition metal. Generally, transition metal-catalyzed reactions can be divided into those where the reaction proceed in completely homogeneous environment and those where the catalyst and the reaction constitute two immiscible phases. The latter is called heterogeneous catalysis. One of the advantages of heterogeneous catalysts is their simplicity, the ease of separation from the reaction mixture and potential recyclability.

Despite the obvious advantages, the use of heterogeneous catalysts in organophosphorus chemistry, and especially in phosphorus-carbon bond-forming reactions is barely known. The effective formation of phosphorus-carbon bond, and especially phosphorus-aryl bond, is one of the main targets in organophosphorus chemistry. This is due to the broad application of tertiary arylphosphines as reagents in organic synthesis as ligands in transition metal catalysis and as substrates for material chemistry. Therefore, it would be highly desirable to develop an effective synthetic method for the formation of phosphorus-carbon bond through coupling reaction between >P(O)H-type compounds and aryl halides in the presence of heterogeneous catalyst.

In the course of our research topic based on the development the new synthetic methodologies in organophosphorus chemistry we were interested in the coupling reaction between secondary phosphine oxides and aryl halides. One of the research problems as the application of heterogeneous catalysts for this reaction. In collaboration with the Department of Chemical Technology, Faculty of Chemistry, Marie Curie-Skłodowska University in Lublin the use of nickel doped on CeO_2 or Al_2O_3 as catalysts was envisaged.

First, a screen of the activity of a set of catalyst has been performed using a coupling reaction between diphenylphosphine oxide and 1-bromonaphthalene a a model reaction (Scheme 1).

Scheme 1

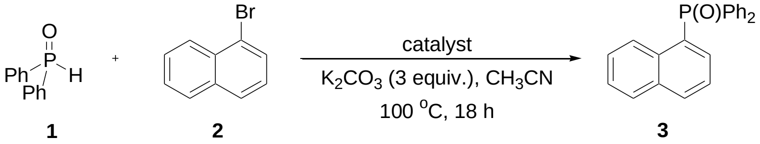

Ni10/Al_2O_3 (5%)	76%
Ni20/Al_2O_3 (5%)	100%
Ni30/Al_2O_3 (5%)	100%
Ni40/Al_2O_3 (5%)	100%
Ni10/CeO_2 (5%)	100%
Ni20/CeO_2 (5%)	90%
Ni30/CeO_2 (5%)	74%
Ni40/CeO_2 (5%)	39%

It appeared that the activity of the particular type of catalysts depended on few factors. For Ni doped on Al_2O_3 the metal loading had no particular influence on the outcome of the reaction. This can be explained by the properties of alumina which exhibited high degree of porosity which may affect metal distribution and crystallite size. For Ni doped on CeO_2 there was an evident decrease of the yield of the product with an increase of the amount of metal.

For one catalyst, Ni10/CeO_2 a set of coupling reactions between $Ph_2P(O)H$ and various aryl halides has been performed (Table 1).

Table 1

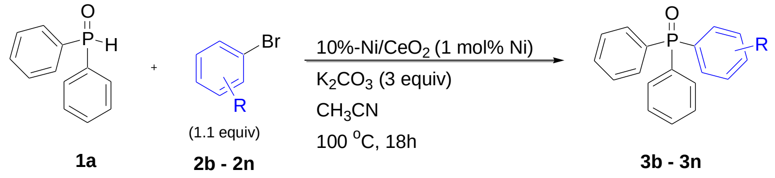

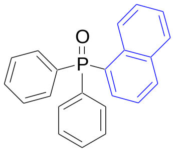

3a 86%

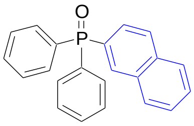

3b 73%^{b}

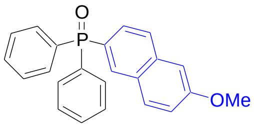

3c 71%^{b}

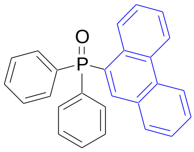

3d 34%^{b}

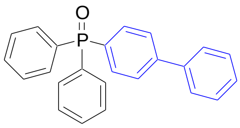

3e 41%^{b}

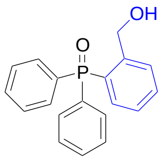

3f 75%^{b}

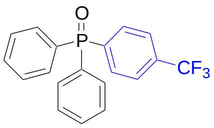

3g 47%

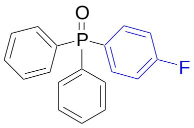

3h 64%^{c}

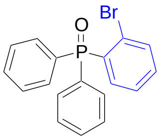

3i 0%

This project is still underway in our laboratory.

STUDY OF THE THERMODYNAMIC PROPERTIES AND STRUCTURE OF THE SELECTED SURFACE SYSTEMS

Małgorzata BORÓWKO, Paweł BRYK, Andrzej PATRYKIEJEW,
Wojciech RŻYSKO, Stefan SOKOŁOWSKI, Tomasz STASZEWSKI
DEPARTMENT FOR THE MODELLING OF
PHYSICO-CHEMICAL PROCESSES

THE EFFECTS OF GEOMETRIC NON-ADDITIVITY ON THE WETTING OF SYMMETRIC MIXTURES AT A WALL

The primary aim of this work has been to investigate how the geometric non-additivity affects the wetting behavior of symmetric mixtures which do not exhibit phase separation in the bulk. Our study throws some new light on the interplay between the wetting behavior of complex fluids at solid surfaces and the properties of bulk phases. From the earlier study of uniform three-dimensional symmetric mixtures [1,2], it follows that the geometric non-additivity determines the solid phase structure and leads to non-monotonous changes of the triple point temperature and of the critical point temperature of the vapor-liquid transition. Here, we have demonstrated that it also considerably influences the wetting behavior of symmetric mixtures.

We have considered the mixtures, with the components A and B interacting via the truncated (12,6) Lennard-Jones potential

$$u_{ij}(r) = \begin{cases} 4\varepsilon_{ij}\left[(\sigma_{ij}/r)^{12} - (\sigma_{ij}/r)^{6}\right], & r \le r_{\max} \\ 0 & r > r_{\max} \end{cases}$$

where r is the distance between a pair of the particles i and j. We have assumed that $\varepsilon_{AA} = \varepsilon_{BB} = \varepsilon$ is the unit of energy, and $\sigma_{AA} = \sigma_{BB} = \sigma$ is the unit of length. We have used the reduced temperature, $T^* = kT/\varepsilon$. The fluid-wall interaction potential has been represented by the following equation:

$$\upsilon(z) = \varepsilon_{gs}\left[\left(\frac{\sigma}{z}\right)^{9} - \left(\frac{\sigma}{z}\right)^{3}\right]$$

In the above, ε_{gs} is a measure of the fluid-wall interaction strength.

The model has been studied using the Monte Carlo simulation method in the grand canonical ensemble [3]. The quantities recorded included the average numbers of particles A (N_A) and B (N_B), and the density profiles for each component, $n_k(z)$. With the density profiles, one can calculate the surface excess densities of the components, $\rho_{k,ex}$ and the total excess density $\rho_{ex} = \rho_{1,ex} + \rho_{2,ex}$.

The strength of the interaction between the AA BB and AB pairs has been assumed to be same, and hence such mixtures do not exhibit phase separation.

It has been demonstrated that the wetting behavior strongly depends on the magnitude of the parameter $s=\sigma_{AB}/\sigma$, being the measure of the geometric non-additivity, on the strength of the fluid-wall interaction as well as on the structure and the stability of the bulk solid phases. The mixtures with $s<1$ being in contact with weakly adsorbing surfaces have been found to exhibit complete wetting only at the temperatures above the bulk triple points. The wetting has been found to be the first-order transition, preceded by the prewetting transition. For a given value of ε^*_{gs} the wetting temperature depends on the parameter *s*. The wetting temperature has been found to gradually decrease when ε^*_{gs} becomes larger, and reaches the bulk triple point temperature for a certain value of ε^*_{gs}. The mixtures with $s\leq 0.9$, have all been found to show the triple point wetting over certain ranges of ε^*_{gs}. The mixtures with $s\geq 1$, which form either the fcc crystals or the disordered glass-like solids in the bulk, have not shown the triple-point wetting. It is a direct consequence of the structures formed in the adsorbed films. The adsorbed films formed by the mixtures with $s>1$ have been found to show the formation of elongated clusters consisting of the like particles.

The figure below shows the changes of the wetting temperature versus *s*, obtained for different values of ε^*_{gs}. The open circles and open squares show the locations of the triple and critical points in bulk systems.

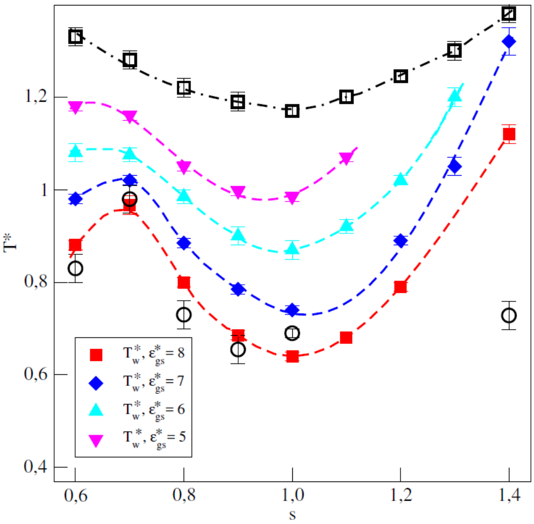

Concluding, we should note that for a given strength of the surface potential, the wetting temperature shown non-monotonous changes with *s*. This is demonstrated in the figure, which presents the changes of the wetting temperature versus *s*, for low values of ε^*_{gs}. The data presented in here confirm that the wetting temperatures of the mixtures with negative geometric non-additivity are correlated with the triple point temperatures, even when the wetting occurs only well above the bulk triple points. It is also shown that the wetting temperature is somehow correlated with the changes of the bulk critical temperature. In particular, the wetting temperature and the bulk critical temperature reach minimum values for $s\approx 1$.

References:

[1] A. Patrykiejew, *Phys. Rev. E*, **95** (2017) 012145.
[2] M.J. Vlot, J. Cornelis van Miltenburg, H.A.J. Oonk, J.P van der Eerden, *J. Chem. Phys.*, **107** (1997) 10102.
[3] A. Patrykiejew, *J. Stat. Mech.-Theory and Experiment*, (2017) 123208.

STUDY OF THE THERMODYNAMIC PROPERTIES AND STRUCTURE OF THE SELECTED SURFACE SYSTEMS

Małgorzata BORÓWKO, Paweł BRYK, Andrzej PATRYKIEJEW,
Wojciech RŻYSKO, Stefan SOKOŁOWSKI, Tomasz STASZEWSKI
DEPARTMENT FOR THE MODELLING OF
PHYSICO-CHEMICAL PROCESSES

MOLECULAR DYNAMIC STUDIES OF MIXTURES OF WATER AND ORGANIC COMPOUNDS IN BULK AND CONFINED SYSTEMS

The aim of our broad scientific project is to determine how miscibility of water with some organic compounds changes under confinement. The first step towards solving this problem is to study the bulk systems. In recently published work [1] we have employed isothermal-isobaric molecular dynamics simulations to examine a broad set of properties of the model water-1,2-dimethoxyethane (DME) mixture as a function of composition. The SPC-E and TIP4P-Ew water models [2,3] and the modified TraPPE model for DME [4] were applied. Our principal focus was to explore the trends of behavior of the structural properties in terms of the radial distribution functions, coordination numbers and number of hydrogen bonds between molecules of different species, and of conformations of DME molecules. Thermodynamic properties, such as density, molar volume, enthalpy of mixing and heat capacity at constant pressure have been examined. Finally, the self-diffusion coefficients of species and the dielectric constant of the system were calculated and analyzed. All the simulations were performed at room temperature and ambient pressure, 1 bar.

The principal conclusions of the present study can be summed up as follows. We explored the evolution of the microscopic structure in terms of the pair distribution functions together with the first coordination numbers of species. In this respect, the simulation results evidence that the structure of the subsystem of DME species is much more inert or much less sensitive to the composition, in comparison with the structure of an aqueous subsystem. The pair distribution functions for water species evidence that a heterogeneous density distribution at local scale can develop upon adding the DME molecules. However, we have not found that water clusters of significant size can be formed. The cross correlations seem to be not very strong as it follows from the corresponding coordination number, but mixing is well pronounced. Thus, the “associated” species involving water and DME molecules or their groups are formed in the system, with or without hydrogen bonds.

Statistical features of the hydrogen bonding in water and of water-organic co-solvent bonds do not show a peculiar behavior, in comparison to a qualitatively similar mixture of water with DMSO. On the other hand, the analyses of the most popular conformations and their fractions as function of mole fraction of DME at room temperature are in accordance with the recently reported results [5].

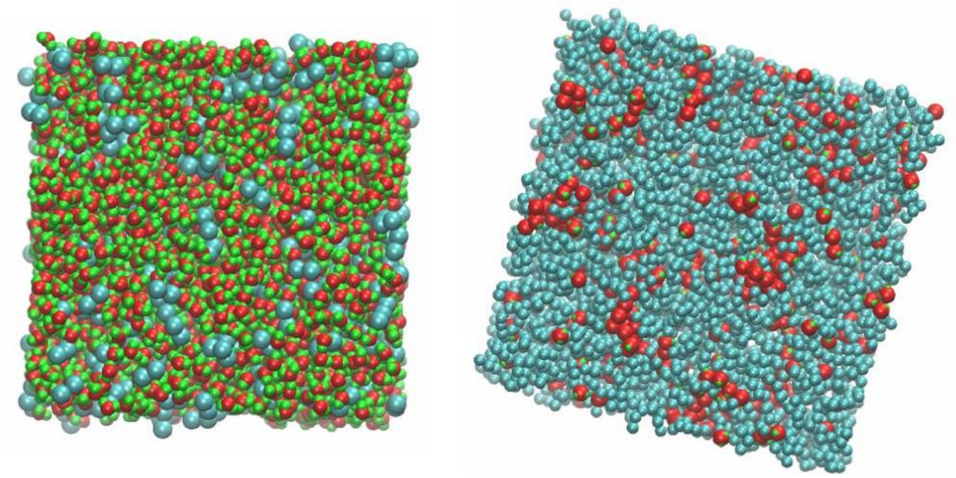

Fig.1. Visualization of the distribution of water and DME species in the simulation box for two values composition. Left panel is for $X_{DME} = 0.1$ whereas the right panel is at $X_{DME} = 0.8$. Only the carbon sites are shown for DME (cyan), water oxygens and hydrogens are given by red and green spheres, respectively

In order to provide an insight into the distribution of particles of each species, we present visualization in two panels of figure 1. From the left-hand panel we learn that the DME molecules are rather uniformly distributed in the medium with a predominant number of water molecules. The right-hand panel describes the situation at high DME fraction. The system is undoubtedly macroscopically homogeneous. However, the inspection of water molecules distribution leads to a conclusion that local heterogeneities are present, the presence of associates of a few water molecules is quite probable.

As we have mentioned above, our study is a first step toward systematic investigations of mixtures of water and DME at different thermodynamic states and different external conditions, using nonpolarizable models. The results of these studies will be presented in due course.

References:

[1] J. Gujt , H. Dominguez , S. Sokołowski and O. Pizio, *Condens. Matter Phys.*, **20** (2017) 33603.

[2] H.J.C. Berendsen, J.R. Grigera and T.P. Straatsma, *J. Phys. Chem.*, **91** (1987) 6269.

[3] H.W. Horn, W.C. Swope, J.W. Pitera, J.D. Madura, T.J. Dick, G.L. Hura, and T. Head-Gordon, *J. Chem. Phys.*, **120** (2004) 9665.

[4] D. Bedrov, M. Pekny and G.D. Smith, *J. Phys. Chem. B*, **102** (1998) 996.

[5] J. Fischer, D. Paschek, A. Geiger and G. Sadowski, *J. Phys. Chem. B*, **112** (2008) 2388.

SYNTHESIS AND CHARACTERIZATION OF POLYMER-AMINO-FUNCTIONALIZED SILICA COMPOSITES FOR THE SUSTAINED-RELEASE OF DICLOFENAC SODIUM

Agnieszka KIERYS, Andrzej SIENKIEWICZ, Patrycja KRASUCKA,
Wojciech STEFANIAK, Jacek GOWOREK
DEPARTMENT OF ADSORPTION

The development of controlled release administration of nonsteroidal anti-inflammatory drugs (NSAIDs) is very important since their long-time use causes gastrointestinal irritation and other side effects. Thus, efforts are constantly made to improve the NSAIDs delivery technology. One of interesting oral drug formulations is a multiparticulate system. Since such a system consists of a multiplicity of small discrete units referred as pellets, it is obvious that the functionality of the entire dose depends on the subunits exhibiting the desired characteristics [1]. The crosslinked polymers in the form of beads which are insoluble neither in the environment characterized by very low pH (e.g. stomach) nor in the neutral (e.g. intestine) or alkaline environment, do exhibit a notable potential in the formulation of oral multiparticulate drug release systems. However, in such polymers, a high initial delivery of the entrapped drug (especially in the case of water-soluble drugs) is observed immediately upon immersion into the released medium. To overcome problems connected with the so-called burst effect into the polymer-drug systems other ingredients are added. Among them, silica gel can be distinguished as an attractive material [2].

This study presents a highly promising strategy for producing an oral multiparticulate formulation of the sustained-release of diclofenac sodium (DS). It consists of pellets closed inside hard gelatin capsules. To produce pellets, the polymer Amberlite XAD7HP was selected as a drug carrier. The diclofenac sodium, a representative of the NSAIDs drugs was selected for this study. The amine-functionalized silica gel was selected as an encapsulating and/or coating agent since it had been previously presented that the 3-aminopropyl groups attached to the silica gel significantly alter the release of drugs [3]. Moreover, there are favourable reports concerning the cytotoxicity of this coating agent. The amine-functionalized silica gel was produced *in situ* within the pellets of the solid dispersion (Pel-D) through the transformation of a precursors mixture (i.e. tetraethoxysilane (TEOS) and (3-aminopropyl)triethoxysilane (APTES)) introduced into them by swelling method [4].

Although Pel-D themselves contains about 50 wt. % of DS, are still able to absorb the mixture of TEOS and APTES. The gelation of the precursors was initiated by the use of ammonia as a catalyst, which was supplied in the vapor phase and finally, ternary solid drug dispersions (TCD) was obtained. Introduction of silica species functionalized with 3-aminopropyl group into the polymer-drug pellets (Pel-D) results in the formation of non-porous samples. Moreover, the functionalization of Pel-D causes the appearance of the two diffraction bands centered at about 2Θ = 7° and 22° in the XRD patterns of TCD next to the reflexes indicating the presence of the drug (i.e. 2Θ = 6.6°, 8.5°, 11.2°, 12.6° and 15.2°). The first band is very characteristic for the amorphous silica species derived from the TEOS precursor whereas the origin of the second band is more difficult to explain especially in the case of materials of such a complex composition.

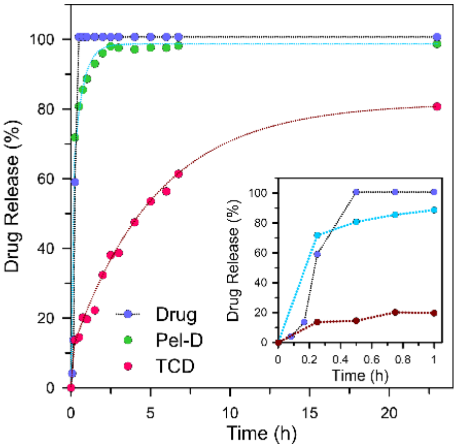

Fig. 1. Diclofenac sodium release kinetics from the subunits. The release was measured in buffer solution at 37 °C, pH=6.8. Inset, the drug release within first 1 h. In the figure, the lines are provided for convenience.

From the desorption curves (Fig. 1), it follows that pure DS dissolves very easily in the buffer solution (100 % within 30 minutes). Its dissolution rate decreases when it is placed in the Pel-D. However, Pel-D suffers from prominent burst release and controls the drug release rate only partially. The degree of burst release is successfully diminished for TCD and only 14 % of the drug is initially desorbed, with 56 % release in 6 h. Interestingly, TCD exhibits a lower efficiency of the drug desorption in comparison to Pel-D and no more than 82 % of the drug is released from it during 24 h. Nevertheless, the investigated TCD meets the pharmacopoeial requirements according to which 80 % of the active substance should be released from the solid dosage form [5]. Taking into account the complexity of the investigated system it is understandable that the incomplete release of DS from TCD is affected by a combination of several factors such as the specific host−guest interactions between DS and the carrier, the chemical character of the carrier and its internal structure as well as its possible erosion Moreover, from other obtained data (not presented here) it follows, that the amino-functionalized silica gel has been presented as a novel and effective agent which retards the DS release in the stomach environment and enables continuous, gradual and almost complete release in the neutral environment of the intestine during a 22-hour period. It can be concluded that TCD meets the requirements imposed for the sustained-release multiparticulate formulations.

References:

[1] C. Tuleu, C. Andrieux, P. Boy, J. C. Chaumeil, *Int. J. Pharm.*, **180** (1999) 123–131.

[2] P. Kortesuo, M. Ahola, S. Karlsson, I. Kangasniemi, A. Yli-Urpo, J. Kiesvaara, *Biomaterials*, **21** (2000) 193-198.

[3] N.H.N. Kamarudin, A.A. Jalil, S. Triwahyono, N.F.M. Salleh, A.H. Karim, R.R. Mukti, B.H. Hameed, A. Ahmad, *Micropor. Mesopor. Mater*, **180** (2013) 235-241.

[4] A. Kierys, A. Sienkiewicz, M. Grochowicz, R. Kasperek, *Mater. Sci. Eng. C*, (2017), https://doi.org/10.1016/j.msec.2017.12.020

[5] E. Pharmacopeia, European Pharmacopeia 8th ed., Council of Europe, Strasbourg, 2014, pp. 288.

SYNTHESIS, MODYFICATIONS AND STUDIES OF PROPERTIES OF MATERIALS WITH DIFFERENTIATED STRUCTURAL AND SURFACE CHARACTERISTICS WITH REGARD TO APPLICATIONS IN SORPTION PROCESSES

Anna DERYŁO-MARCZEWSKA, Małgorzata ZIENKIEWICZ-STRZAŁKA, Magdalena BŁACHNIO, Dariusz STERNIK, Agnieszka CHRZANOWSKA, Małgorzata SĘCZKOWSKA
DEPARTMENT OF PHYSICOCHEMISTRY OF SOLID SURFACE

The aim of the research was the synthesis and characterization of carbonaceous materials, metal-funcionalized mesoporous silicas and different classes of nanocomposites with polymers. The physicochemical properties of the synthesized materials were determined by using the following methods: diffraction (XRD, SAXS), spectroscopic (IR, XPS, XRF, UV-VIS) and transmission electron microscopy (TEM, SEM, EDX/TEM) techniques, low-temperature nitrogen adsorption/desorption measurements and thermal analysis. These studies were of importance from both theoretical and practical points of view. The kinetic and equilibrium adsorption measurements from aqueous systems of dyes, phenols and pesticides were performed.

One of the groups of synthesized materials were polymer/clay nanocomposites. There are several main types of methods of synthesis of polymer/layered silicate materials such as [1,2]: exfoliation-adsorption, in situ intercalative polymerization, melt intercalation and template synthesis. In this study the materials were obtained by mixing clay suspensions and chitosan solutions using the method presented in [3]. Chemically, chitosan is a linear polysacharide containing copolymers of D-glucosamine and and N-acetyl-D-glucosamine (acetylated units) linked by β- (1,4) glycosidic bonds.

The polymer modification leads to a decrease in the total porosity (specific surface area, the pore volume) of both minerals (bentonite and vermiculite). This process changes also a character of active sites and thermal stability. In the case of heating the pure aluminosilicates only two processes of dehydration and dehydroxylation occur. The first one takes place at temperatures up to 200˚C and is associated with the removal of physically adsorbed and interlayer water. At higher temperatures 400-900 ° C a dehydroxylation occurs [4]. In the case of composites in the range 150-700 ° C, additional inflections on TG curves (Fig.1) are associated with the defragmentation and oxidation of chitosan. The main gaseous components of chiosan decomposition determined by MS analysis are: H_2O, NO, C_2H_2O, $C_2H_4N^+$; $C_2H_4O_2$; CO_2; NO_2; C_3H_6O; C_2H_5NO; $C_5H_7^-$; C_4H_7O, $C_5H_6N^+$ [6].

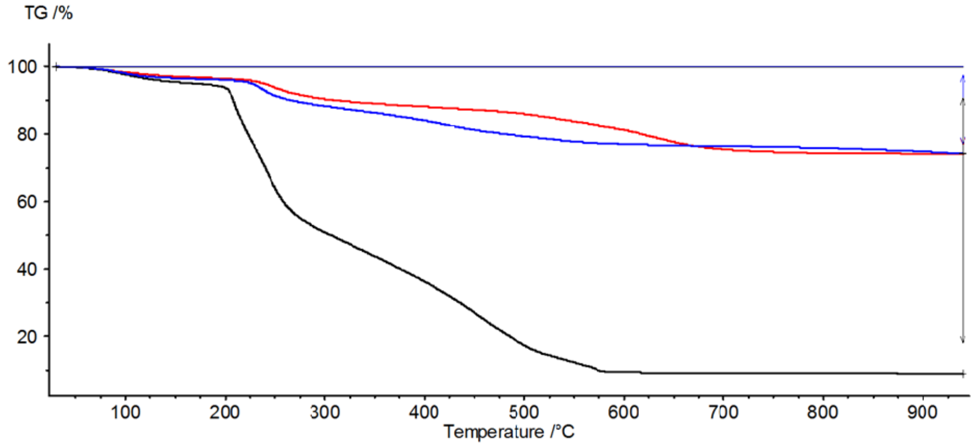

Fig. 1. TG curves of chitosan (black line), chitosan-bentonite (red line) and chitosan-vermiculite (blue line).

The obtained composites were characterized by inferior sorption properties towards cationic dyes. This confirms that the adsorption of cationic dyes on aluminosilicates mainly takes place according to the ion exchange mechanism.

References:

[1] Nanocomposites - New Trends and Developments. Editor, Farzad Ebrahimi. Publisher, InTech, 2012.

[2] M. Alexandre, P. Dubois, *Materials Science and Engineering*, **28** (2000) 1.

[3] I. Hamed, F. Őzogul , J.M. Regenstein, *Trends in Food Science & Technology*, **48** (2016) 40.

[4] E. Skwarek, O. Goncharuk, D. Sternik, W. Janusz, K. Gdula, V.M. Gun’ko, *Nanoscale Research Letters*, **12** (2017) 155.

[5] D. Sternik, A. Gładysz-Płaska, E. Grabias, M. Majdan, W. Knauer, *Journal of Thermal Analysis and Calorimetry*, **129** (2017) 1277

[6] T.M. Budnyak, E.S. Yanovska, D. Kołodyńska, D. Sternik, I.V. Pylypchuk, M.V. Ischenko, V.A. Tertykh, *Journal of Thermal Analysis and Calorimetry*, **125** (2016) 1335.

APPLICATION OF CHROMATOGRAPHIC METHODS IN THE STUDIES OF BIOLOGICALLY ACTIVE COMPOUNDS

Małgorzata JANICKA, Katarzyna STĘPNIK,
Irena MALINOWSKA, Marek STUDZIŃSKI
DEPARTMENT OF PLANAR CHROMATOGRAPHY

A group of 17 heterocyclic organic compounds belonging to triazinones was investigated using RP HPLC technique. These newly synthesized compounds are presently investigated as potential anticancer agents. Chromatography technique was used to predict their lipophilic and biological properties to be compared with parameters *in silico* evaluated from molecular structures. Two stationary phases: the IAM and ISRP columns imitating biological membranes were applied. As mobile phases there were used buffer-acetonitrile mixtures with acetonitrile concentration equal 0.3 and 0.4 v/v, while buffer pH value was equal to 7.4. Retention parameters log k were analyzed as lipophilicity descriptors of compounds and applied to predict their *in silico* biological descriptors relevant to optimal pharmacokinetics profile. The following pharmacokinetic descriptors: fraction unbounded in brain ($f_{u,brain}$), oral bioavailability (%*F*), intestinal permeability and absorption in jejunum (Caco-2 and $P_{e,\ jejunum}$), blood/brain concentration (log *BB*) and water-human serum albumin distribution (log P_{HSA}) were calculated by ACD/Percepta software from molecular structures of compounds. Moreover partition lipophilicity parameters (log *P*) were obtained from an internet software ALOGPS 2.1.

The quantitative retention activity relationships (QRARs) for tested compounds have been described by straight-line or parabolic equations (figures 1 and 2) with high statistical quality (R^2>0.8). Results of the PCA-based approach showed the similarities of the chromatographic partitioning parameters and properties relevant to pharmacokinetics (figure 3).

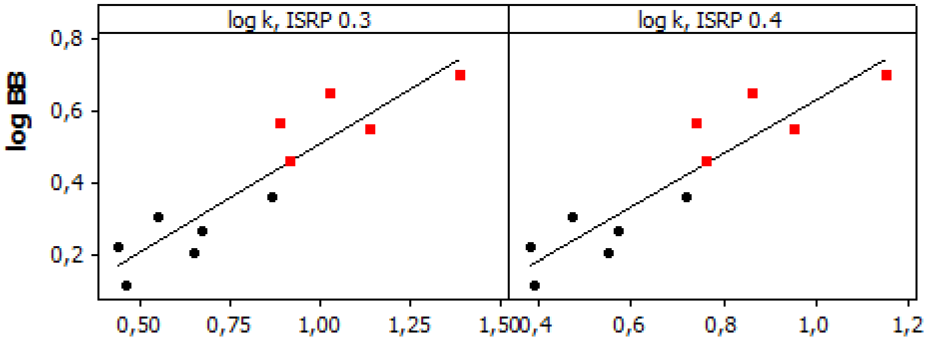

$$\log BB = 0.602\ (\pm 0.087)\ \log k_{ISRP,\ 0.3} - 0.091\ (\pm 0.076);\ s = 0.0822,\ R2 = 0.8407,\ F = 47.489,\ p = 0.000071$$
$$\log BB = 0.742\ (\pm 0.107)\ \log k_{ISRP,\ 0.4} - 0.107\ (\pm 0,077);\ s = 0.0818,\ R2 = 0.8424,\ F = 48.102,\ p = 0.000068.$$

Fig.1. log BB vs. log k relationships.

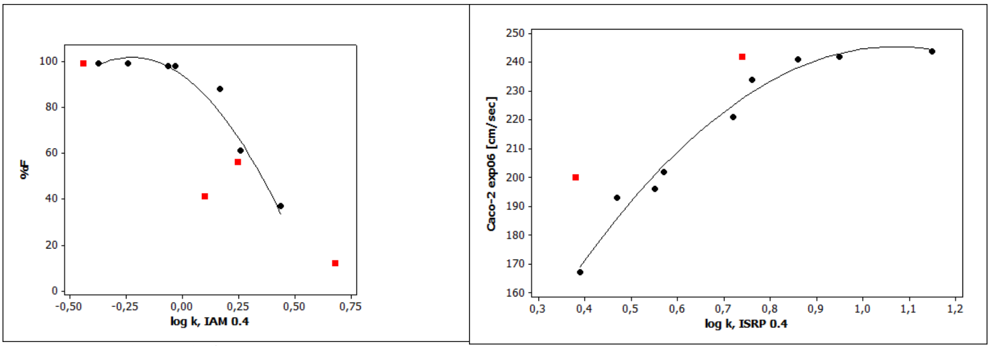

%F = -154.40 (±43.04) (log *k* IAM, 0.4)2 – 69.73 (±10.39) log *k* IAM, 0.4 + 93.81(±3.89);
s = 7.3519, R2 = 0.9359, F = 36.519, p = 0.001040
Caco-2 x 106 = -166.56 (±28.75) (log *k* ISRP, 0.4)2 + 356.05 (±44.17) log *k* ISRP, 0.4 + 55.24(±15.79);
s = 4.6106, R2 = 0.9786, F = 137.145, p = 0.000010

Fig.2. %F vs. log k and Caco-2 vs. log k relationships.

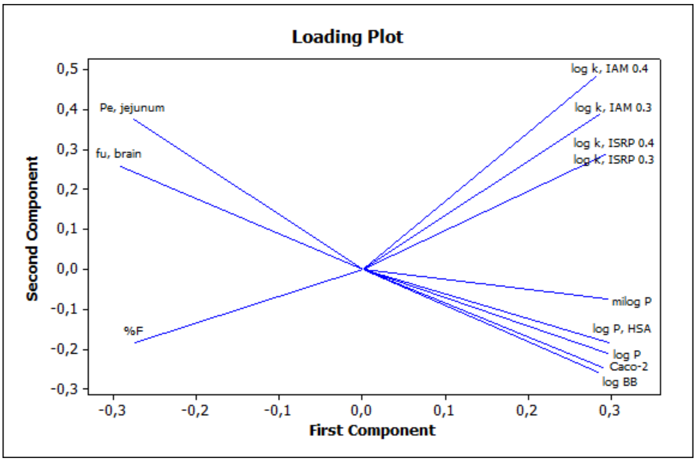

Fig.3. PCA analysis.

The application of IAM and ISRP columns for studying the lipophilic behaviour as well as predicting valuable pharmacokinetic descriptors allows for shortening the overall time required for HPLC measurements and simultaneously reducing costs of the performed analyses.

References:

[1] M. Sztanke, J. Rzymowska, M. Janicka, K. Sztanke, *Arabian Journal of Chemistry*, http://dx.doi.org/10.1016/j.arabjc.2016.12.02

SPECIAL PURPOSE SUBSIDY TO CONDUCT RESEARCH AIMED AT DEVELOPING YOUNG SCIENTISTS AND DOCTORAL STUDENTS

USE OF MODIFIED BIOCHARS IN THE ADSORPTION OF ORGANIC AND INORGANIC IMPURITIES

Justyna BĄK
DEPARTMENT OF INORGANIC CHEMISTRY

Owing to continuous technological innovations and growth in the number and diversity of electronic devices throughout the world, battery exploitation increases. Processing of spent batteries is very important not only regarding the treatment of hazardous wastes but also with recovery of valuable rare earth elements. The elements present in the batteries are heavy metals such as Ni(II), Cd(II), Fe(III) and rare earth elements La(III), Ce(III) and Nd(III) as well as others [1].

Sorption on the activated carbon or other carbonaceous sorbents is of considerable industrial importance because lanthanides are characterized by the possibility of separating lanthanides as well as non-clear solutions, a large recovery capacity even in dilute solutions and their insolubility in the analyzed solutions containing rare earth metals [2]. Additionally, combination of the features of biochar and zero valent iron allows separation of obtained sorbent after the sorption process of lanthanide ions. Taking into account the cognitive character of the process it is very interesting with respect to chemical separation, environmental purification and monitoring of aqueous solutions [3].

Biochar used in the studies was subjected to modification process through reduction of iron salts using sodium borohydride according to the equations:

$FeSO_4 + H_2O \rightarrow FeOHSO_4 + H^+$
$4Fe^{3+} + 3BH_4^- + 9H_2O \rightarrow 4Fe^0 + 3H_2BO_3^- + 12H^+ + 6H_2$

By the presence of zero valent iron on the biochar surface it assumes magnetic properties. Obtained sorbents at different molar ratio of $FeSO_4$ to $NaBH_4$ and mixing time of the suspenstion were denoted as MBC1, MBC2 and MBC3. The summary of equilibrium capacities for sorption of lanthanide La(III), Ce(III), Nd(III) ions for magnetic biochars were listed in Table 1.

Table 1. Summary of equilibrium capacities for sorption of lanthanide La(III), Ce(III), Nd(III) ions for MBC1, MBC2 and MBC3.

Ions	Concentrations [mg/L]	Magnetic biochars		
		MBC1	MBC2	MBC3
La(III)	50	9.69	10.19	10.28
	100	10.02	11.10	10.50
	150	10.31	11.41	11.41
	200	10.48	12.66	11.86
Ce(III)	50	9.98	9.71	9.12
	100	10.72	12.60	11.10
	150	11.31	13.82	12.15
	200	11.99	14.12	12.42
Nd(III)	50	10.68	10.35	10.13
	100	13.07	16.84	13.63
	150	14.24	17.49	13.81
	200	14.69	18.12	15.05

As follows from these data the amounts of adsorbed ions increase as the initial concentration of lanthanide ions solutions increase. Based on the above it can be stated that the series of affinity of lanthanide ions is as follows: Nd(III) > Ce(III) > La(III). The same investigations were carried out for methylene blue sorption on the magnetic biochars.

Magnetic biochars are an effective sorbents for removal of rare earth elements and dyes from aqueous solutions.

References:

[1] A. Fernandes, J. Carlos, A. Junqueira, B. Dutra, *Hydrometallurgy*, **133** (2013) 37.

[2] J. Kowalczyk, C. Mazanek, *Fizykochemiczne Problemy Mineralurgii*, **20** (1988) 229.

[3] I. Liatsou, I. Pashalidis, M. Oezaslan, C. Dosche, *Journal of Environmental Chemical Engineering*, **5** (2017) 4069.

STUDIES OF DYES, HEAVY METAL IONS AND PHENOLS SORPTION ON DIRRERENT TYPES OF ION EXCHANGERS AND SORBENTS FROM AQUEOUS SOLUTION AND WASTEWATERS

Anna WOŁOWICZ
DEPARTMENT OF INORGANIC CHEMISTRY

The main problems of world is the increasing amount of contaminants discharged into the environment as a result of intensive development of industry, exploitation of its goods and active human activity [1,2]. Particular attention should be paid to those branches of industries that consume significant amounts of water in technological processes and thus generate significant quantities of wastewaters containing harmful and toxic substances e.g. textile industry which consumes about 200 L of water/1 kg of textile and considerable quantities of chemical compounds [3]. As commonly known not only dyes but also heavy metal ions, phenol and its derivatives as well as the auxiliary substances such as salts, bases, acids, surfactants, reducers, oxidants are applied during the manufacturing process of the finished product [4]. Therefore, it is extremely important to remove such pollutants from waters and wastewaters using various physicochemical methods, among which, adsorption plays an important role [5].

The aim of this study was to compare removal efficiency of toxic heavy metal ions (Cr(VI), Ni(II), Co(II)) and metal-complex dyes (C.I. Acid Red 183 - AR183, C.I. Reactive Blue 21 - RB21, nickel(II) phthalocyanine-tetrasulfonic acid tetrasodium salt - NiPc-TSATSS from aqueous solutions using Lewatite VPOC 1065 and the Adsorbsia^{TM} As500 (TiO_2) (Table 1). The pH_{PZC} of both sorbents and the influence of the initial concentration on the sorption process were determined and maximum sorption capacity were obtained. For the most effective sorbent-sorbate system kinetic studies were carried out. Effects of hydrochloric acid concentration (for heavy metal ions systems) as well as auxiliaries such as sodium sulfate(VI), acetic acid, SDS (sodium dodecyl sulfate) (for the dyes containing systems) on sorbate removal was also taken into account. Moreover, possibility of phenol removal by Lewatit AF-5 and SIHA Aktivkohle GE sorbents was analysed.

Table 1. Characteristics of sorbents applied for metal-complex dyes and heavy metals removal.

Sorbent	Lewatit VPOC 1065	Adsorbsia™ As500
Functional group	primary amine, benzylamine	0.25 – 1.19 mm 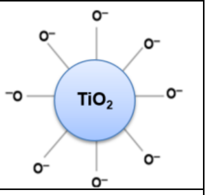
Matrix	crosslinked polystyrene	
Structure	macroporous	
Bead sizes Effective size	0.315 – 1.25 mm 0.47 - 0.57 mm	
Surface area BET	~ 50 m^2/g	200 m^2/g
Pore volume Pore diameter	0.27 cm^3/g 25 nm	0.4 cm^3/g -

The pH_{PZC} values of the sorbents were determined and equal to 5.63 for Adsorbsia^{TM} As500 and 2.45 for Lewatit VPOC 1065. The removal efficiency of the metal complex dyes (AR183, RB21, NiPc-TSATSS) and heavy metal ions such as chromium(VI), nickel(II), copper(II)) on the titanium dioxide Adsorbsia^{TM} As500 and the weakly basic anion exchanger Lewatite VPOC 1065 was compared. The highest sorption capacity (q_e = 816.1 mg/g) was found for AR183 and the selectivity series were as follows: Adsorbsia^{TM} As500: RB21 (59.2 mg/g) > AR183 (44.6 mg/g) > Ni(II) (42.8 mg/g) > NiPc – TSATSS (15.67 mg/g) > Cr(VI) (7.44 mg/g) >> Cu(II) (-); Lewatit VPOC1065: AR183 (816.1 mg/g) > Cr(VI) (67.25 mg/g) > RB21 (59.2 mg/g) > Ni (II) (44.88 mg/g) > NiPc – TSATSS (8.8 mg/g) >> Cu (II) (-). Lewatit VPOC 1065 gives much higher or slightly higher % removal of toxic substances than the titanium dioxide. Copper(II) sorption was not observed in the systems under discussion. In the acidic solutions functional groups of Lewatit VPOC 1065 are protonated therefore they can interact with anionic species e.g. dyes (sulphonic groups of dyes), the anionic chromium(VI) species results in high sorption capacities and in ion pair formation. Hydrophobic interactions π–π between aromatic rings of dyes and rings in the anion exchange resin structure and hydrogen bonds formation could be present. The mechanism of heavy metal ions sorption onto titanium dioxide is the surface complex formation (inner-sphere surface complexes forming) by the interactions of metal ions with the hydroxyl groups of titanium dioxide of amphoteric properties which are produced during the hydrolysis of oxide:

$$M^{2+} + (\equiv TiOH)_n \leftrightarrow (\equiv TiO^-)_{n-2}M + 2H^+ \qquad (1)$$

The q_t valeues (amount of toxic substances sorbed on Lewatit VPOC 1065) increases with the phases contact time and initial concentration increase. The reduction of Cr(VI) to Cr(III) was observed on WBA resin. The equilibration time was equal to 120 min (C_0 = 100 mg/L) and > 240 min for higher $C_{0.}$ The heavy metal ions removal efficiency was dependant on the solution acidity whereas the sorption capacity for AR183 insignificantly dropped with NaCl addition (5-50 g/L), increased with the increase of CH_3COOH concentration and slightly decreased with the increasing sodium dodecyl sulfate concentration. Phenol removal from aqueous solutions (1, 5, 10 mg/L) using carbonaceous sorbents was quantitative using Lewatit AF-5 and depended on phases contact time (equilibrium time = 30 min) whereas in the case of SIHA Aktivkohle GE about 28%, 85% and 92 % of phenol was removed.

Acknowledgements: The presented research was funded under the grant of the Minister of Science and Higher Education for the development of young scientists and PhD students, BS-M-03-002-17-C-03.

References:

[1] D.H.K. Reddy, S.-M. Lee, *Adv. Colloid Inter. Sci.*, **201–202** (2013) 68-93.

[2] F. Fu, Q. Wang, *Journal of Environmental Management*, **92** (2011) 407-418.

[3] M.A. Granato, T.M. Gaspar, A.F. Alves, A.A.U. de Souza, S.M.A.G.U. de Souza, *Environ. Technol.*, 2017, doi.org/10.1080/ 09593330.2017.1393017.

[4] J. Mielicki, Zarys chemicznej obróbki wyrobów włókienniczych, Warszawa: Wydawnictwo Naukowo-Techniczne, 1991.

[5] V.M. Vucurovic, R.N. Razmovski, M.N. Tekic, *J. Taiwan Inst. Chem. Eng.*, **43** (2012) 108–111.

SPECTROSCOPIC INVESTIGATIONS OF INTERACTIONS BETWEEN PORPHYRIN SYSTEMS AND SYNTHETIC DERIVATIVES OF XANTHINE

Agnieszka LIPKE
DEPARTMENT OF INORGANIC CHEMISTRY

The thio-caffeine derivatives were found to be highly potent cytoprotective agents, what predestines this class of compounds to act as effective antioxidants for preventing oxidative-stress induced diseases or artheriosclerosis [1]. Whereas water-soluble cationic porphyrins, the group of fluorescent macrocyclic compounds presenting the specific spectroscopic and redox properties, can play the role of sensing materials to detect different, especially biologically active substances, presented in aqueous environment [2].

To determine the binding interactions and ability to form the non-covalent systems, the association process between 5,10,15,20-tetrakis[4-(trimethylammonio)phenyl]-21H,23H-porphine tetra-p-tosylate (H_2TTMePP) and a series of five structurally diverse thio-caffeine analogues (Fig. 1) has been studied in ethanol and ethanol-water solution, analyzing its absorption and steady-state fluorescence spectra. The fluorescence lifetimes and the quantum yields of the porphyrin in the systems studied were established as well.

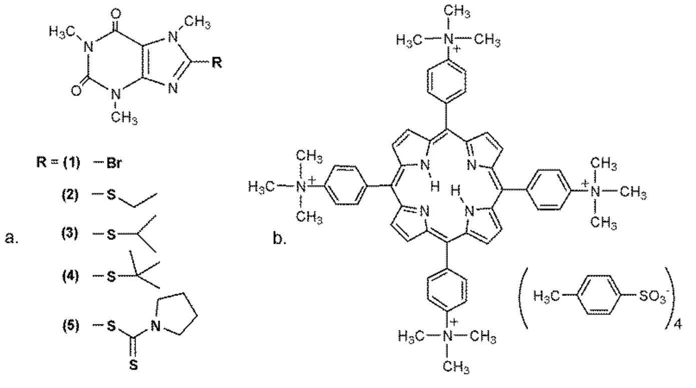

Fig.1. The molecular structures of (a) thio-caffeine derivatives ((1) 8-bromocaffeine, (2) 8-(ethylthio)caffeine, (3) 8-(isopropylthio)caffeine, (4) 8-(tertbutylthio)caffeine, (5) 8-[(pyrrolidin-1-ylcarbonothioyl)sulfanyl]caffeine) and (b) 5,10,15,20-tetrakis[4-(trimethylammonio)phenyl]-21*H*,23*H*-porphine tetra-*p*-tosylate (H_2TTMePP).

The fluorescence quenching effect observed during interactions of H_2TTMePP porphyrin with structurally diverse thio-caffeine compounds, as well as the order of binding and fluorescence quenching constants (of 10^5–10^3 mol^{-1}), and practically inalterable fluorescence lifetime of the porphyrin suggest the existence of the mechanism of static quenching due to the formation of non-covalent and nonfluorescent stacking complexes in all the systems studied. Additionally, the specific binding interactions, due to the changes in reaction environment polarity, can be noticed. The fluorophore fractional accessibility for the quencher was also observed in case of all the systems (Fig. 2). It appeared that thio-caffeine compounds quench the porphyrin fluorescence according to the spatial structure of thio-substituents in caffeine molecule. The most distinct decay of the porphyrin fluorescence intensity can be noticed in case of H_2TTMePP - 8-[(pyrrolidin-1ylcarbonothioyl)sulfanyl]caffeine system [3]. The obtained results can be potentially useful from scientific, therapeutic or environmental points of view, providing insight into the binding interactions of the water-soluble porphyrin with biologically active substances and into the pharmacology of thio-caffeine analogues.

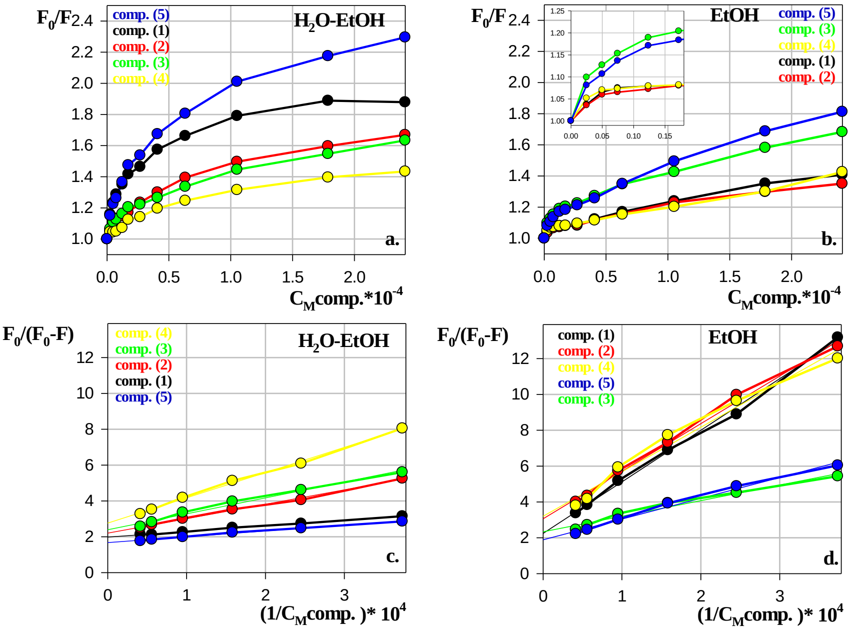

Fig.2. Stern–Volmer (a, b) and modified Stern-Volmer (c, d) plots for H_2TTMePP in water (a, c) and ethanol (b, d) during titration with particular thio-caffeine derivatives [3].

References:

[1] B. Jasiewicz, A. Sierakowska, N. Wandyszewska, B. Warżajtis, U. Rychlewska, R. Wawrzyniak, L. Mrówczyńska, *Bioorg. Med. Chem. Lett.*, **26** (2016) 3994.

[2] M. Makarska-Białokoz, *J. Fluoresc.*, **22** (2012) 1521.

[3] A. Lipke, M. Makarska-Białokoz, A. Sierakowska, B. Jasiewicz, *Spectrochim. Acta A Mol. Biomol. Spectrosc.*, **192** (2018) 304.

SCREEN-PRINTED CARBON ELECTRODES MODIFIED WITH METAL: PREPARATION, CHARACTERIZATION AND NEW APPLICATIONS

Katarzyna DOMAŃSKA
DEPARTMENT OF ANALYTICAL CHEMISTRY
AND INSTRUMENTAL ANALYSIS

In the performed experiments the commercially available integrated three-electrode screen-printed sensor with carbon electrode modified in situ during measurement with bismuth film was used for the determination of Tl(I) in natural water samples without long and complicated pretreatment. This type of electrode modification was chosen due to simplicity of performance and the eco-friendly character of the modifier. Additionally, the coating of carbon electrode surface with bismuth film significantly increased sensitivity of thallium analysis (Fig. 1). The effect of the working electrode surface covering with bismuth was confirmed after comparison of the images of a bare and in situ modified electrode surface obtained through optical and scanning electron microscopes.

Under optimized conditions very low limits of detection were reached, 8.47×10^{-10} and 6.71×10^{-12} mol L^{-1} for the deposition times of 60 s and 300 s, respectively. When compared with other voltammetric methods, the obtained limits of detection (LODs) are generally lower. The same order of magnitude of LOD was obtained in [1] work, but the distinguishing quality of the present procedure is the application of commercially available, miniaturized, and integrated three-electrode sensor, which is easily modified during rapid analysis and suitable for use in a portable analyzer. It should be mentioned that there are other methods that allow the determination of thallium on a higher or similar level of concentration, such as ICP-MS and AAS. The main disadvantage of these methods is the lack of possibility to perform the analysis outside the laboratory.

The newly developed procedure was applied for the determination of Tl(I) in certified reference materials: SPS SW-2 (surface water), SRM 1640a (natural water) and TMRAIN-04 (rain water). It should be mentioned that the influence of foreign metal ions and surfactants on the voltammetric signal of thallium in natural samples were minimized using 1×10^{-5} mol L^{-1} EDTA and Amberlite XAD-7 resin. Results obtained during water samples analyses prove that the use of integrated screen-printed carbon sensor with in situ plated bismuth film carbon working electrode allow to obtain precise and accurate results in water samples.

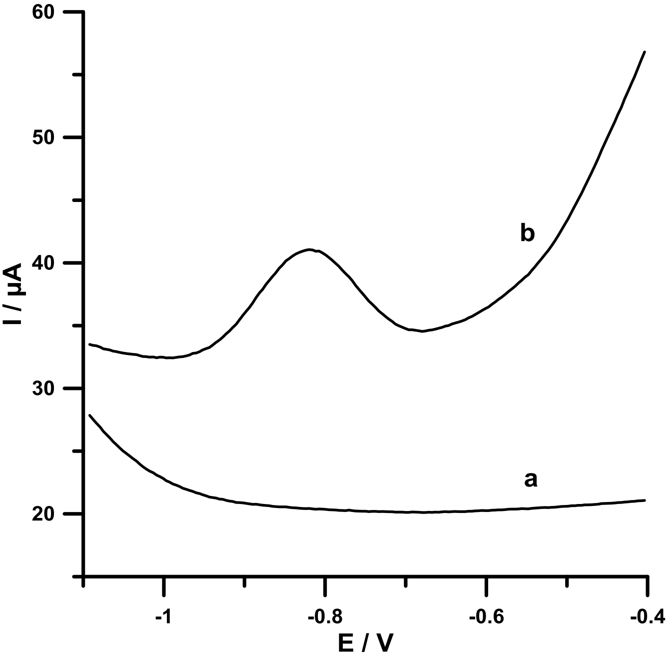

Fig. 1. Square wave voltammograms obtained at a) unmodified and b) coated with bismuth film screen-printed carbon electrode. Solution containing 2 × 10^{-7} mol L^{-1} Tl(I) and 0 (a) or 1 × 10^{-5} mol L^{-1} $Bi(NO_3)_3$ (b).

References:

[1] K. Węgiel, K. Jedlińska, B. Baś, *Journal of Hazardous Materials,* **310** (2016) 199.

VOLTAMMETRIC METHODS OF DETERMINATION OF TRACE CONCENTRATIONS OF SELECTED ELEMENTS USING VARIOUS WORKING ELECTRODES

Joanna WASĄG
DEPARTMENT OF ANALYTICAL CHEMISTRY
AND INSTRUMENTAL ANALYSIS

Stripping voltammetry is one of the most favorable techniques for the determination of heavy metal ions because of their low cost and high sensitivity. The unusually high sensitivities are based on the fact that the analyte is pre-concentrated on the working electrode before the potential scan is performed. The selection of a working electrode material is critical to experimental success. Ideally the electrode should provide a high signal-to-noise ratio over a wide potential range as well as a reproducible response and renewable surface. In this study a lowering of the detection limit of Ga(III) ions determination by stripping voltammetry with the use of a new type of mercury electrode has been proposed. Gallium is a chemical element that is relatively rare and it occurs in nature as gallium(III) compounds. The interest in the determination of gallium traces in the environment is connected with increasing applications of this element in the fields of electronics and medicine. Stripping voltammetry seems to be a powerful technique for trace gallium monitoring owing to its sensitivity together with relatively inexpensive instrumentation. Mercury electrodes are almost ideal for this purpose because they have good adsorptive properties, they are ideally polarizable, have the ideally smooth surface and have a broad negative potential window. That is why, in the above-mentioned voltammetric procedures of gallium determination, in the majority of cases mercury electrodes were used. However, because of the toxicity of mercury a renewable mercury film silver based electrode (Hg(Ag)FE) as a human-friendly construction was used in the proposed work. The possibility of its application for direct determinations in environmental water samples containing organic substances are additional advantages of the proposed idea.

During the optimization studies of the Ga(III) ions determination procedure, several complexing agents for adsorptive accumulation of gallium were employed such as solochrome violet, morin, pyrocatechol violet, chloranilic acid and cupferron. The result showed that the maximum peak current of gallium obtained using cupferron as a complexing agent. Cupferron forms stable complexes with many metals, so it is not surprising that it is widely used in adsorptive stripping voltammetry procedures for metal ultratrace determination. To obtain a low detection limit and good precision the adsorptive accumulation of the Ga(III)-cupferron complexes was chosen.

The Ga(III) determination procedure consists of the following steps:

The sample was pippeted to the voltammetric cell and the following reagents were added: 1 mL 1 mol L^{-1} acetic acid + 100 μL 1 × 10^{-2} mol L^{-1} cupferron. The sample was adjusted to 10 mL with water. The accumulation of the Ga(III)-cupferron complexes was carried out at -0.2 V for 30 s from the stirred solution. This process is the result of adsorption of the Ga(III)-cupferron complexes on the surface of Hg(Ag)FE and it is a non-faradaic process. After the equilibration time of 5 s, the differential pulse voltammogram was recorded, while the potential was scanned from -0.4 to -0.9 V, with the intensity of the obtained peak directly proportional to the concentration of Ga(III) in the sample. During this step, Ga(III) was reduced to the metallic state. The step potential, pulse amplitude and pulse time were 8mV, 100 mV and 2 ms, respectively. The measurements were carried out from undeaerated solutions. After each measurement a conditioning step was used to remove the target metals from working electrode before the next measurement.

The procedure optimization:

Introductory studies with Hg(Ag)FE in acetic-acetate solution containing Ga(III) and cupferron produced a reduction peak at the differential pulse voltammogram, so the optimization of experimental parameters in the determinations of gallium, such as pH and concentration, potential and time of accumulation was performed.

The study of the influence of the accumulation potential on the peak current of gallium was examined in the range from -0.6 to 0.2 V. The optimum deposition potentials were found to be -0.2 V. In the case of higher potential a decrease of the gallium peak height was observed. The influence of deposition time on Ga(III) peak current was studied in the range from 10 to 300 s. It was observed that analytical signal of gallium increased almost linearly with accumulation time prolonged to 60 s, in the case of longer accumulation times the peak current of gallium increased insignificantly. In order to shorten time of measurements further studies were performed at deposition time of 30 s.

The formation of the complexes, their stability, and the potentials of reduction are strongly dependent upon the pH value of the solution. Thus, the influence of the pH of the supporting electrolyte on the gallium voltammetric signal in the proposed procedure was examined. The measurement were performed for solutions containing following supporting electrolyte: 0.1 mol L^{-1} CH_3COOH (pH=2.88) and CH_3COOH/CH_3COONa in the range from 3.0 to 6.0 (CH_3COOH or NaOH was used to obtain the required medium). It was observed that the extreme signal was obtained in acetic acid and with the increase of pH the signal of gallium decrease.

The procedure of Ga(III) ions determination using Hg(Ag)FE as a working electrode and cupferron as a complexing agent requires further optimization. The studies of influence of foreign ions and environmental water samples of the Ga(III) determination will also be carried out.

HIGH RESOLUTION ATOMIC ABSORPTION SPECTROMETRY IN STUDIES OF CONCENTRATION AND DISTRIBUTION HETEROGENEITY OF TRACE AND ULTRATRACE ELEMENTS IN SOLID SAMPLES

Joanna DOBRZYŃSKA
DEPARTAMENT OF ANALYTICAL CHEMISTRY
AND INSTRUMENTAL ANALYSIS

High-Resolution Continuum Source Atomic Absorption Spectrometry (HR-CS AAS) due to application of the xenon short arc lamp, that is the source of radiation of high intensity in a wide spectral range, enable rapid sequential and simultaneous multi-element analysis. Using the high-resolution polichromator with CCD detector it is possible to obtain a highly resolved absorption spectrum, allowing not only for quantitative determination of analytes but also providing qualitative information about the sample. Because of the ability to tracking changes of absorption over the measurement time in a fairly wide wavelength range (0.4 nm) and high resolution of polichromator, not only determinations of metals based on atomic absorption lines but also determinations of non-metals using the selected molecular bands may be performed. The CCD detector enables the mathematical elimination of numerous spectral interferences related with the presence of complex matrix in analysed samples.

In the case of measurements carried out with atomic absorption spectrometers equipped with a line radiation source and a photomultiplier as a detector the determination of trace elements in samples containing oxides or hydroxides of aluminum, silicon and iron as matrix components is very difficult, because they are the main source of strong chemical and spectral interferences, which cannot be easily corrected using line source AAS devices.

In this work the results concerning the determination of palladium by HR-CS AAS in samples of aluminum-iron based catalysts are presented. In the case of palladium several atomic absorption lines can be used for analytical purposes. However the most intensive one at 244.791 nm is in the vicinity of the Fe line 244.771 and because of the huge content of iron in studied samples the Pd absorption signal cannot be measured at these two lines separately. Also Pd line at 247.642 cannot be applied, because it is too close to Fe line 247.666 and Ni line 247.688 nm. Additionally, for this two lines the Pd peak was not registered due to the presence of molecular background. In order to eliminate spectral interferences associated with the presence of nickel and iron atomic absorption as well as molecular bands the Pd 340.458 nm line was chosen for analytical purposes.

In order to establish the thermal stability of Pd in water solution, solution obtained by *aqua regia* digestion of aluminium-iron catalyst and slurry of the catalyst the pyrolysis and atomisation curves were prepared and presented in Fig.1 and 2. As can be seen in Fig.1, in the case of Pd contained in the water solution and in slurry of aluminium-iron catalyst prepared in water, the increase of pyrolysis temperature from 800 to 1600°C does not cause the decrease of Pd analytical signal.

In the case of the solution obtained by microwave mineralization of the catalyst in *aqua regia* the change of the pyrolysis temperature from 700 to 1600°C leads to gradual decrease of the Pd integrated absorbance from 0.18 to 0.11 s.

Due to the high thermal stability of Pd the analytical signal strongly depends on the atomisation temperature. It is worth to notice that at the temperature of 2100°C, in the case of Pd water solution and slurry, Pd analytical signal is not observed whereas for digested catalyst solution 0.06 s integrated absorbance was measured, which once again confirms that the presence of *aqua regia* cause the strong decrease of the thermal stability of palladium. Based on the relations presented in Fig.1 and 2 the temperatures of 800 and 2500°C were chosen for pyrolysis and atomisation, respectively.

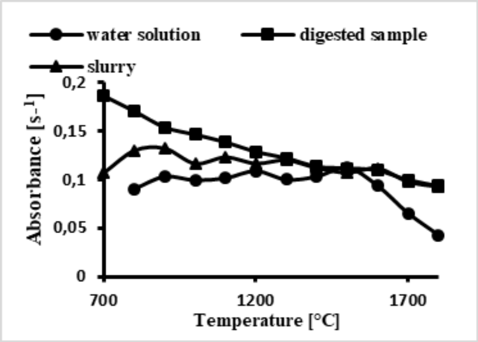

Fig.1. Pyrolysis curves for 4 ng of Pd contained in water solution, solution obtained by *aqua regia* digestion of aluminum-iron catalyst and catalyst slurry.

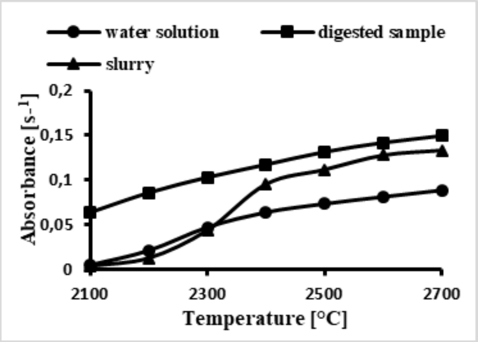

Fig.2. Atomization curves for 4 ng of Pd contained in water solution, solution obtained by aqua regia digestion of aluminum-iron catalyst and catalyst slurry.

Thus the differences in the thermal stability of Pd present in standard water solution and solution obtained by acidic digestion encourage to calibration with the use of standard addition method. Also in the case of slurries despite of thermal stability of analyte the standard addition method was necessary due to the complex unchanged matrix causing chemical interferences.

The limits of quantification obtained in the case of slurry sampling were equal to 3 µg/g for 0.5% slurry, whereas for classic approach (acidic digestion) 2 µg/g.

The concentrations of palladium determined in real industrial catalyst samples are presented in Table 1. As can be seen the values obtained by using classic analysis with the step of sample digestion and slurry sampling are in good agreement.

Table 1. The results of Pd determination in aluminum-iron catalysts.

Catalyst	Concentration [µg/g]	
	slurry	digested sample
I	7.54 ± 0.83	7.23 ± 0.05
II	17.32 ± 1.23	16.97 ± 0.65
III	15.87 ± 1.56	16.25 ± 1.22
IV	17.23 ± 1.89	18.38 ± 1.39

THE USE OF MICRO- AND NANOMATERIALS FOR THE CONSTRUCTION OF NEW ELECTRODES AND THEIR APPLICATION TO THE DEVELOPMENT OF HIGHLY SELECTIVE PROCEDURES FOR THE DETERMINATION OF TOXIC ELEMENTS BY THE STRIPPING VOLTAMMETRY METHOD

Mateusz Ochab
DEPARTMENT OF ANALYTICAL CHEMISTRY
AND INSTRUMENTAL ANALYSIS

Arsenic belongs to the elements with high prevalence in the Earth's crust occupying 20th place in terms of prevalence among elements. In nature, it occurs both in the form of inorganic compounds as well as organic compounds. The most frequent forms of arsenic that occur in the water samples are inorganic forms As(III) and As(V). The toxicity of these form of arsenic is different – As(III) is much more toxic than As(V). Therefore, speciation analysis of this element is much more required than the determination of total concentration of inorganic arsenic in water samples.

Stripping analysis allows for the direct determination of different forms of elements and it is characterized by a low detection limit. In addition, the apparatus required for the analysis is cheaper than in other analytical methods. Very important issue in the voltammetric method is the selection of the working electrode, wherein the material has an effect on the available range of potential and also to the limit of quantification. For the determination and speciation of arsenic, the gold electrodes are most often used [1,2]. They can be in the form of film electrodes of gold as well as microelectrodes. The disadvantage of gold electrodes, is the presence a large background, making it difficult to measure the signal and increases the limit of detection. For a carbon electrode: either with the glassy carbon, graphite or carbon nanomaterials is usually achieved lower levels of background, however, the arsenic signal is much lower compared to the gold electrodes. The aim of the project was to develop and practical application of the composite electrode made of carbon materials, and gold nanoparticles to determine arsenic speciation. As the electrode material, various carbonaceous materials containing gold were tested. Carbon black acetylene 100% compressed with the addition of 0.5 – 0.8 μm gold particles was used as the optimal electrode material. The obtained electrode is characterized by a low background value and a well-shaped current peak. This electrode is environmentally friendly mercury free electrode.

The standard procedure of measurement was performed in a following way. The 10 mL of the solution containing the analyzed sample, 0.1 mol L^{-1} acetate buffer and 3×10^{-5} mol L^{-1} EDTA was prepared. The deposition of As(III) at the Au/CB electrode was carried out at -0.8 V for 30 s from the stirred solution. Stirring was preformed using a magnetic stirring bar. After a rest period of 10 s a square wave voltammogram recorded at a frequency of 200 Hz, while the potential was changed from -0.75 to 0.3 V. The amplitude and the potential step were 25 and 5 mV, respectively. All measurements were carried out from undeaerated solutions.

Under the optimized conditions the calibration graph for As(III) with application of developed electrode was linear from 5×10^{-9} to 2×10^{-7} mol L^{-1} following deposition times of 30 s.

Voltammograms obtained for solutions containing increasing concentrations of As(III) are presented in Fig. 1. The detection limit for As(III) following the deposition times of 30 s, calculated as a 3 σ for a low concentration of As(III) was equal to 2.1×10^{-9} mol L^{-1}. The proposed procedure was used for As(III) determination in a Bystrzyca river water samples using the method of standard additions. Because the As(III) concentrations in water samples were below the detection limit, so recoveries of arsenic from the sample spiked with As(III) were studied. The voltammograms obtained in the course of studies of recoveries of As(III) from the river water sample are presented in Fig. 2. The obtained recoveries of As(III) were in the range from 96.9 to 104.7%. The above results show that the proposed procedure with the use of a developed composite electrode can be applied for the As(III) determination in natural water samples.

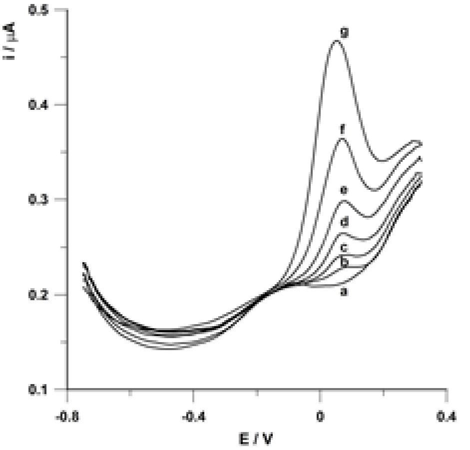

Fig. 1. Square wave voltammograms obtained for solutions containing low concentration of As(III): (a) 0; (b) 5; (c) 10; (d) 20; (e) 50;(f) 100; (d) 200 nmol L^{-1} As(III). Deposition at -0,8 V within 30 s

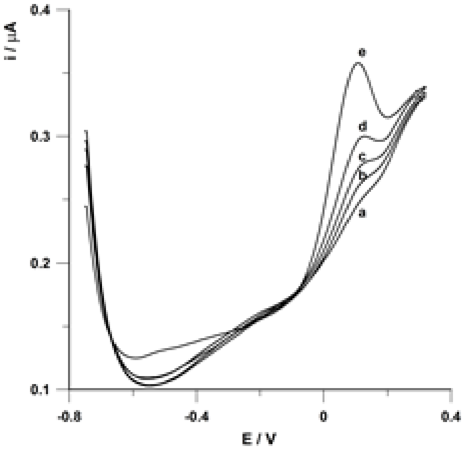

Fig. 2. Square wave voltammograms obtained in the course of studying As(III) recoveries from Bystrzyca river water sample: (a) river sample; (b) as (a) + 5 nmol L^{-1}; (c) as (a) + 10 nmol L^{-1}; (d) as (a) + 20 nmol L^{-1}; (d) as (a) + 50 nmol L^{-1} As(III). Deposition at 0,8 V within 180 s.

References:

[1] M. Korolczuk, M. Ochab, I. Rutyna, *Talanta*, **144** (2015) 517.

[2] G.M.S. Alves, J.M.C.S. Magalhaes, P. Salaunb, C.M.G. van der Berg, H.M.V.M. Soares, *Analytica Chemica Acta,* **703** (2011) 1.

NEW PROCEDURES FOR THE DETERMINATION OF SELECTED METAL IONS AND BIOLOGICALLY ACTIVE COMPOUNDS BY STRIPPING ANALYSIS WITH THE USE OF A NEW TYPE OFELECTRODES

Iwona GĘCA
DEPARTMENT OF ANALYTICAL CHEMISTRY
AND INSTRUMENTAL ANALYSIS

Because of a wide use of bismuth in such areas of human activity as: medicine, chemical industry, metallurgy, catalysis or cosmetology, living organisms are exposed to contact with this element. Due to this fact monitoring of bismuth content in environmental samples is required. For the determination of bismuth(III) in environmental samples, there are several frequently adopted analytical methods. Among them voltammetric methods are recognized as a powerful tool because of its sensitivity in connection with relatively inexpensive instrumentation.

The main aim of this work was to determine trace amounts of bismuth by anodic stripping voltammetry using a new type of electrodes to previously proposed double deposition and stripping step [1-3] and elimination of interfering ions effect. There were two working electrodes that differed significantly in their surface areas and built-in the voltammetric cell used in research: a gold film electrode plated ex situ on glassy carbon substrate as an electrode with large surface area and a gold film microelectrode plated ex situ on an ensemble of carbon fibers microelectrode as the second one. This kind of electrodes is environmentally friendly in comparison to the commonly used hanging mercury drop electrode. Bismuth was at first deposited at the electrode with a large surface area. As the deposition step at the first electrode was finished, the electrode was shifted at a short distance to the small one and the first stripping step was performed. Then the second deposition step was carried out using microelectrode ensemble. Taking into account the very small volume of space between the working electrodes, the concentration of Bi(III) between the electrodes was much higher as compared to that in the bulk solution. Due to the fact that the second deposition step was performed from solution with a much higher concentration of Bi(III), the detection limit was lowered.

This procedure was optimized by selection of various conditions, such as the supporting electrolyte, pH, accumulation potential and time. The additional purpose was a precise study of the influence of Cu(II) ions on the bismuth voltammetric peak current, because the presence of these ions causes the main interference effect in the case of bismuth determination due to the fact that anodic stripping signals of bismuth and copper are highly overlapped. The correctness of this procedure was tested by determination of Bi(III) in river water samples. The obtained results show that the proposed procedure can be applied to real water samples analysis and environmental monitoring for Bi(III) without the additional pre-concentration step.

Working electrodes were prepared as follows. The gold film was plated ex situ on glassy carbon substrate (Ø 12 mm) and on an ensemble of carbon fibers microelectrode by electrolytic deposition of gold from solution containing 2.5×10^{-4} mol L^{-1} Au(III), 0.025 mol L^{-1} HCl and 4 g L^{-1} urea. Gold deposition was carried out at the potential of -0.6 V for 180 s. V. Then the gold film was polarized at the potential of 0.2 V within 15 s for stripping impurities from the gold film. Working electrodes were polished and the gold films were plated daily before starting the measurements.

Determination of Bi(III) was performed in a following way. The sample was pippeted to the voltammetric cell and 7.5 mL of 1 mol L^{-1} acetate buffer (pH 4) was added. The sample was adjusted to the volume of 30 mL with water. Recommended procedure consists of the following steps: to obtain a low detection limit of Bi(III) determination before voltammetric stripping on microelectrode ensemble the Bi(III) ions was initially deposited on a gold film electrode (-0.35 V for 240 s). After that the large electrode was placed very near an microelectrode ensemble and the polarization of this electrode was stopped. During this step Bi(III) was stripped from the large electrode using air dissolved in the solution. Thus Bi(III) deposited on the large electrode went directly to the solution between the surface of a large electrode and microelectrode ensemble. Next deposition of Bi(III) on microelectrode ensemble was performed (-0.3 V for 120 s) from the non-stirred solution containing Bi(III) at a much higher concentration than that of the bulk solution. At the end the square wave voltammogram was recorded with the bismuth signal proportional to its concentration. After each measurement both working electrodes were cleaned electrochemically at the potential of +0.3 V for 15 s. All measurements were carried out without solution deoxygenation.

The procedure optimization

For Bi(III) determination by ASV using gold film electrodes acetate buffer $CH_3COOH + CH_3COONa$ (pH = 4.0) was used for these studies as a supporting electrolyte.

The accumulation potential at the first electrode was changed from -0.6 to +0.2 V while accumulation potential at the second electrode was -0.6 V. It was observed that the Bi(III) peak current attains the maximal value of deposition potential in the range from -0.4 to -0.1 V. Further measurements were carried out at deposition potential of -0.35 V.

The accumulation potential at the second electrode was changed from -0.6 to +0.2 V while accumulation potential at the first electrode was -0.35 V. It was observed that the Bi(III) signal attains the maximal value at deposition potential in the range from -0.3 to -0.1 V. For further studies deposition time of -0.3 V was chosen.

It was found that the calibration plot for Bi(III) with application of double deposition and stripping steps was linear from 2.5×10^{-9} to 2×10^{-8} mol L^{-1} following deposition times of 300 s at the first and second electrode, and obeyed the equation $y = 0.12x + 0.018$, where y and x are the peak current (nA) and Bi(III) concentration, respectively. The linear correlation coefficient r was 0.999. The estimated detection limit for Bi(III) following the deposition times of 300 s at the both working electrodes calculated as a 3 σ for a low concentration of Bi(III) was equal to 1.2×10^{-9} mol L^{-1}.

The main attention was paid on the Bi(III) determination in the presence of excess of Cu(II) as anodic stripping signals of these metals overlap and this fact makes the Bi(III) analytical signal difficult to interpret. The interference of Cu(II) ions on bismuth peak current was studied for a solution containing Bi(III) at concentration of 4×10^{-8} mol L^{-1}. The obtained results are presented in Fig. 1. The results show that in the presence of 3-fold excess of Cu(II) interference effect on Bi(III) signal was observed in the course of determination using one electrode, however, application of double deposition and stripping step leads to elimination of this interferences.

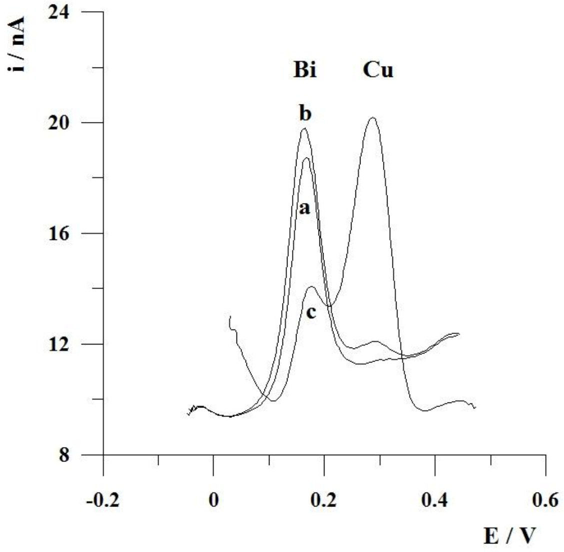

Fig. 1. The anodic stripping voltammograms obtained for supporting electrolyte containing: a) 4×10^{-8} mol L^{-1} Bi(III); b) as a) + 1.2×10^{-7} mol L^{-1} Cu(II) using double deposition and stripping steps at deposition time 300 and 120 s for the first and second electrode, respectively; c) as b) using traditional three electrode cell with microelectrode ensemble as a working electrode at deposition time 120 s.

References:

[1] I. Rutyna and M. Korolczuk, *Sensors and Actuators B*, **204** (2014) 136.
[2] I. Rutyna and M. Korolczuk, *Electroanalysis*, **26** (2014) 2639.
[3] M. Korolczuk, M. Grabarczyk and I. Rutyna, *Talanta*, **130** (2014) 342.

INFLUENCE OF PLASMA ACTIVATION ON SURFACE PROPERTIES OF POLYAMIDE

Diana RYMUSZKA, Konrad TERPIŁOWSKI, Lucyna HOŁYSZ
DEPARTMENT OF INTERFACIAL PHENOMENA

Polyamides are (PA) characterized by low hardness and high resistivity against striking. Most of the time they are white or cream-coloured but some of them are almost transparent or black. With the increasing amount of amide groups in the molecule, their melting point as well as hardness and inflexibility increase. Moreover, combinating of antifriction and electroisolate properties with resistance against corrosion and high mechanical durability allow its more extense application as constructive material (i.e.ventilators, bearings).

The aim of our study was investigation of plasma activation influence on surface properties of PA. For modification air plasma was used and PA plates were treated by plasma for 10, 30 and 60 seconds (PA-10, PA-30, PA-60). To determine the wettability of PA plates contact angles for two polar liquids: water, formamide and apolar diiodomethane were measured. The next step included surface free energy calculation using contact angle hysteresis (CAH) [1] and van Oss et al. [2,3] approaches. Surface topography changes were determined by interpretation of the images obtained from the optical profilometer and the values of roughness parameters.

Air plasma has significant influence on surface properties of PA which can be observed in wettability and surface free energy changes. Bare surface of PA is characterized by weak interactions with water but exposure to air plasma leads to the decrease of water contact angles measured on the modified surface. Such changes are also found in surface free energy mainly due to the increase of polar interaction.Air plasma modification of PA surface leads to decrease of contact angles regardless of a liquid used during measurements. The greatest decrease was observed for samples PA-30for polar liquids. Water contact angle values decreased from 82.9±1.4° to 15.0±0.7°, which is 82%. On the other hand, for formamide spreading on the surface was noticed. The greatest decrease for diiodomethane, around 64%, in comparison to the unmodified surface of PA was observed for PA-60.

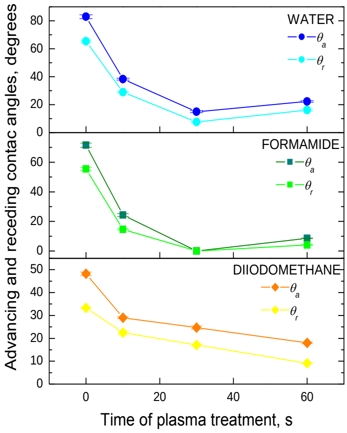

Fig. 1. Advancing (θ_a) and receding (θ_r) contact angles of water, formamide and diiodomethane measured on the unmodified and modified PA surface by air plasma for 10, 30 and 60 seconds.

The decrease of the contact angles measured on the modified PA surface is associated with the increasing surface free energy. The highest value of surface free energy was observed for PA-30 and PA-60 being much higher than the energy calculated for the unmodified surface. Increase of the surface free energy of modified by plasma PA is mainly caused by the increase of oxygen content introduced during the plasma process which resulted in creation of polar functional groups and increase of polar interactions. After plasma exposure the PA surface became hydrophilic. Analysis of the roughness parameters of PA suggests that exposure of PA to air plasma for 10 and 60 s leads to the decrease of surface roughness. On the other hand, modification by plasma for 30 s caused the increase of surface roughness.

References:
[1] E. Chibowski, *Adv. Colloid Interface Sci.*, **103** (2003) 149–172.
[2] C.J. van Oss, R.J. Good and M.K. Chaudhury, *J. Colloid Interface Sci.*, **111** (1986) 378–90.
[3] C.J. van Oss, R.J. Good and M.K. Chaudhury, *Langmuir,* **4** (1988) 884–91.

The research has been funded by the Ministry of Science and Higher Education for research and development, contributing to the progress of young researchers and doctoral students at the Faculty of Chemistry of the University–project titled *The influence of plasma activation on the surface properties of polyamide*, the time of the project: 2016, Faculty of Chemistry, Maria Sklodowska-Curie University.

INVESTIGATION OF QUERCETIN AND RUTIN INTERACTIONS WITH NONIONIC SURFACTANTS MICELLES

Anna TARABA
DEPARTMENT OF INTERFACIAL PHENOMENA

Flavonoids are an important element in the human diet. It is estimated that during the day, people should consume about 1g of flavonoid compounds. Despite intense research, the metabolism of flavonoids has not been fully understood. It is believed that almost half of the consumed flavonoids are absorbed unchanged. In the *in vivo* and *in vitro* studies flavonoids exhibit antioxidant, anti-inflammatory, antineoplastic, anti-atherogenic, antiaggregatory, spasmolytic, diuretic, detoxicating, anti-arrhythmic and antihypertensive effects and capillary vessel sealing [1,2].

Quercetin belongs to the best flavonoids tested so far, however, its solubility in aqueous solutions is small (0.17-7.7 μg/ml). It is similar with quercetin glycoside, rutin. Therefore much attention is paid to increasing the solubility and the mechanism of transport of these compounds by using for example: microemulsions, nanoparticles, complexes with cyclodextrins or encapsulation using liposomes. It is worth emphasizing that up to now the basic method used for isolation of biologically active substances from raw plant materials is extraction performed under various conditions (hot, cold, assisted by microwave or ultrasonic field, supercritical conditions, etc.). A relatively new method, is the process in which surface active compounds (surfactants) are used for the extraction of active ingredients of plant origin at high concentration. The available literature data mainly concern the study of antioxidant properties of quercetin as well as rutin. Moreover, they are based on random analysis and unjustified thermodynamic selection of experimental conditions [3,4,5].

The aim of the project was to examine the interactions of quercetin and routine with micelles of selected nonionic surfactants. These interactions were determined by testing flavonoids in the aqueous and alcoholic environment without and with surfactants using measurements of surface tension, both flavonoid solutions and surfactants as well as spectrophotometric and spectrofluorimetric measurements.

Taking into consideration the results solubilization of quercetin molecules by Tween 80 micelles is much higher than that by Triton X-114 which is evident among others, from the shape and size of Tween 80 micelles and the influence of quercetin molecules on the water structure around the surfactant chains. Considering the values of the partition coefficient of surfactant-flavonoid and the fixed flavonoid-alcohol bond for the studied systems, it can be concluded that in practical applications, for example in the extraction process, mixtures with the best efficiency should be characterized:

- Tween 80 + Quercetin + propanol
- Triton X-114 + Routine + ethanol.

References:

[1] W. Vermerris, R. Nicholson, *„Phenolic compound biochemistry”*, Springer, 2006.
[2] M. Majewska, H. Czeczot, *Terapia i leki*, **65** (2009) 369.
[3] W. Wiczkowski, MK. Piskuła, *Pol. J. Food Nutr. Sci*., **13** (2004) 101.
[4] P.C.H. Hollman, M.B. Katan, *Food Chem. Toxicol.*, **37** (1999) 937.
[5] C. Manach, A. Scalbert, C. Morand, *Am. J. Clin. Nutr*., **79** (2004) 727.

SOLUBILIZATION OF ALKYL NAPHTHYL ETHERS IN MICELLES OF ANIONIC SURFACTANTS

Andrzej LEWANDOWSKI
DEPARTMENT OF INTERFACIAL PHENOMENA

Solubilization may be defined as the spontaneous dissolving of a substance by reversible interactions with the micelles of a surfactant in a solvent to form a thermodynamically stable isotropic solution with reduced thermodynamic activity of the solubilized material [1]. The significant increase of solubility due to micellar solubilization resulted in many applications of this phenomenon in diverse areas, including pharmaceuticals, detergency, cosmetics, agricultural products, surfactant-based separations, analytical chemistry, emulsion polymerization and micellar catalysis [1,2]. For example, solubilization in surfactant micelles allows to easily incorporate perfumes into detergent products to yield transparent solutions. However, reduction of thermodynamic activity of perfume raw materials due to solubilization in micelles, significantly affects their volatilization from surfactant solutions. This in turn may result in alteration of the olfactory profile and performance of perfume added to detergent product [3]. Due to interesting olfactory profile, low cost and high chemical stability, alkyl naphthyl ethers find broad use in functional perfumery, especially in soap perfumes [4]. However, data on their interactions with surfactant micelles are very limited [5,6]. The aim of this study was to quantitatively investigate partitioning of alkyl naphthyl ethers between water and micelles formed by sodium lauryl sulfate (SLS) and sodium lauryl poly(oxyethylene)$_2$ sulfate (SLE2S) by optical spectroscopy. These anionic surfactants were chosen due to their widespread use in consumer products [7].

The maximum of a red-edge band of 2-ethoxynaphthalene UV absorption spectrum in water, 0.1M SLS solution and 0.1M SLE2S solution was found at 325.6 nm, 327.6 nm and 328.0 nm, respectively. Similarly, the absorbance ratio at 329.4 nm and 325.6 nm reaches higher value for SLE2S than SLS micelles (Fig. 1.). Both observations implies that stabilization of the molecule in the ground state decreases due to solubilization in SLS micelles and, to a higher extent, in SLE2S micelles. This implies lower polarity of solubilization site and/or weaker hydrogen bonding between water and solute molecules, when solubilized in SLE2S micelles than in SLS micelles [8,9]. Most probably, 2-ethoxynaphthalene molecules are solubilized at the hydrocarbon chain/oxyethylene chain boundary in SLE2S micelles and at hydrocarbon chain/sulfate group boundary in SLS micelles. The differences in solubilization site are reflected in the values of micelle-water partition coefficients, which were determined by fitting experimental values of absorbance ratio $A_{329.4\text{ nm}}/A_{325.6\text{ nm}}$ in the pre- and postmicellar region of surfactant concentrations (Fig. 1) to a mathematical model based on the APN model [10]. The value of micelle-water partition coefficient for SLS micelles was found to be higher (K_{ml} = 890±130 $dm^3 \cdot mol^{-1}$) than for SLE2S micelles (K_{ml} = 594±26 $dm^3 \cdot mol^{-1}$).

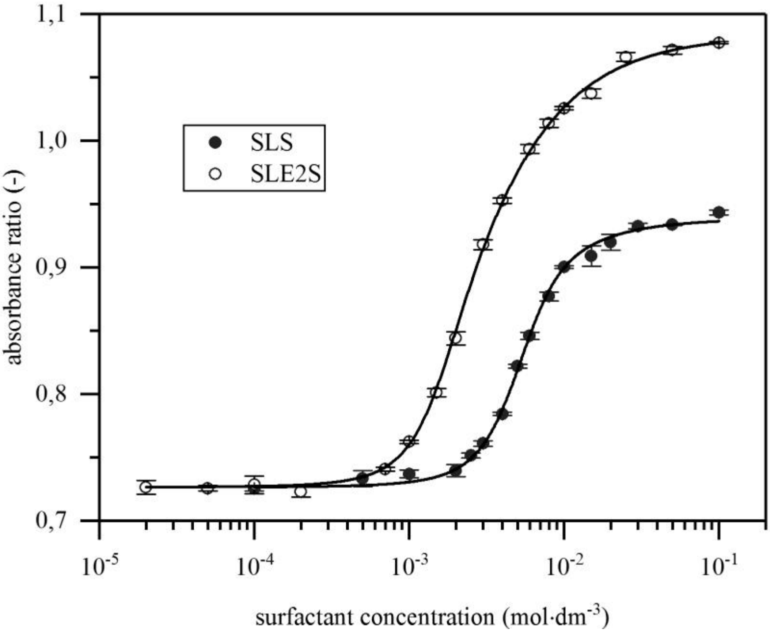

Fig. 1. The effect of surfactant concentration on the absorbance ratio $A_{329.4\ nm}/A_{325.6\ nm}$ of aqueous solution ($5 \cdot 10^{-5}$ $mol \cdot dm^{-3}$) of 2-ethoxynaphthalene at 313K. Solid lines are best fits to APN model for monomer and micellar concentrations in surfactant solutions [10].

References:

[1] M.J. Rosen and J.T. Kunjappu, *Surfactants and Interfacial Phenomena*, 4th ed., Wiley, Hoboken, 2012.
[2] S.D. Christian and J.F. Scamehorn (ed), *Solubilization in Surfactant Aggregates*, Marcel Dekker, New York, 1995.
[3] J.N. Labows, J.C. Brahms and R.H. Cagan, in: M.M. Rieger and L.D. Rhein (ed.) *Surfactants in Cosmetics*, 2nd ed., Marcel Dekker, New York, 1997, 605-619.
[4] H. Surburg and J. Panten, *Common Fragrance and Flavor Materials*, 6th ed., Wiley-VCH, Weinheim, 2016.
[5] E. Abuin and E. Lissi, *J. Colloid Interface Sci.*, **112** (1986) 178.
[6] A. Srivastava and K. Ismail, *J. Mol. Liquids*, **195** (2014) 105.
[7] M.J. Schwuger, in: M.J. Rosen (ed.) *Structure/Performance Relationships in Surfactants*, ACS, Washington, 1984, 3-26.
[8] B.-Z. Magnes, N.V. Strashnikova and E. Pines, *Isr. J. Chem.*, **39** (1999) 361.
[9] K.M Solntsev, D. Huppert and N. Agmon, *J. Phys. Chem. A*, **102** (1998) 9599.
[10] W. Al-Soufi, L. Piñeiro and M. Novo, *J. Colloid Interface Sci.*, **370** (2012) 102.

APPLI CATION OF CHROMATOGRAPHIC AND SPECTROPHOTOMETRIC MEASUREMENTS IN RELIABLE ESTIMATION OF ANTIOXIDANT POWER OF COLORED SUBSTANCES

Małgorzata OLSZOWY
DEPARTMENT OF CHROMATOGRAPHIC METHODS

Antioxidant activity is defined as the ability of given compounds or mixtures to reduce pro-oxidants or reactive species, including free radicals. Among methods which are used for determination of antioxidant activity, two colorimetric methods, DPPH and ABTS (employing 2,2'-diphenylpicrylhydrazyl and 2,2'-azinobis (3-ethylbeznothiazoline-6-sulfonic acid) diammonium salt) seem to be the most popular [1]. In both methods the antioxidant activity of an examined antioxidant is determined in terms of absorbance changes of colored radicals: DPPH·or ABTS$^+$ [2,3]. The reduction degree of colored radical during its reaction with antioxidant is measured at 515-517 nm in the case of the DPPH method and at 734-744 in the ABTS assay. As results from the literature [4], the mentioned methods should not be applied for the estimation of antioxidant properties of substances which themselves (or their oxidation products formed during neutralization of radicals) absorb in the range of the monitored wave length.
The presence of such compounds in the measuring system falsifies the changes of absorbance resulting from the concentration decrease of the colored radical and makes the estimation of the real antioxidant activity of the examined compounds impossible.

Table 1. IC$_{50}$ values [mg ml^{-1}] for examined antioxidants estimated by: analyzing DPPH radical and ABTS cation radical concentration changes in the measuring system chromatographically, and monitoring the absorbance changes of the measuring system spectrophotometrically (n=3).

Anti-oxidant	**DPPH method**			**ABTS method**		
	HPLC	**Spectrophotometric**	**ε** (dm^{3}mol^{-1}cm^{-1}) at 516 nm	**HPLC**	**Spectrophotometric**	**ε** (dm^{3}mol^{-1}cm^{-1}) at 744 nm
BHA	0.15±0.01	0.15±0.01	0	0.12±0.01	0.13±0.00	0
BHT	0.46±0.02	0.47±0.02	0	0.29±0.01	0.29±0.01	0
Trolox	0.09±0.01	0.09±0.01	0	0.12±0.01	0.12±0.00	0
quercetin	0.07±0.00	0.07±0.00	0	0.06±0.00	0.06±0.00	0
cyanidin	0.14±0.01	0.16±0.01	2.97E+04	0.07±0.00	0.07±0.00	0
alizarin	0.78±0.02	2.03±0.10	7.74E+02	0.26±0.01	0.26±0.01	0
E132	4.75±0.34	-*	3.66E+02	0.39±0.01	0.38±0.02	0
thymol blue	1.03±0.05	-*	3.23E+03	0.51±0.02	0.52±0.02	0
E155	0.98±0.05	-*	1.29E+04	4.84±0.24	4.93±0.20	0

All measurements were carried out by using 2940 μl of DPPH radical (or ABTS radical) and 60 μl of antioxidant solution; *The value was not determined

Table 1 shows the antioxidant properties of chosen colored antioxidants, estimated by the DPPH and ABTS methods. The antioxidant activities (expressed as IC_{50} values) established by these two spectrophotometric methods are compared with those determined by HPLC.

As results from the data, the IC_{50} values estimated spectrophotometrically and chromatographically in both applied method are almost the same for antioxidants which do not absorb 516 nm ($\varepsilon=0$ at 516 nm is observed for BHA, BHT, Trolox and quercetin) and 744 nm wavelengths ($\varepsilon=0$ at 744 nm is observed for all examined antioxidants). For cyanidin and alizarin spectrophotometrically estimated IC_{50} values in DPPH method are greater than those calculated from the chromatographic measurement and for three examined compounds: E132, thymol blue and E155 could not determine the IC_{50} values spectrophotometrically. These data (see Table 1 column 3) can be explained by analyzing the extinction of 516 nm wavelength by these antioxidants (see Table 1) and their residue in the measuring systems after the reactions with the DPPH radicals (see Table 2).

Table 2. Chromatographically determined % of residue antioxidant after its reaction with the DPPH radical.

Concentration (mg ml^{-1})	**% of remaining antioxidant**				
	cyanidin	**alizarin**	**E132**	**thymol blue**	**E155**
0.05	0.00	-*	-	-	-
0.10	2.67	-	1.23	14.81	1.93
0.15	5.87	-	-	-	-
0.25	21.44	7.17	36.81	28.62	19.96
0.50	-	14.07	41.01	38.01	43.73
1.00	-	21.50	44.68	50.69	64.19
1.50	-	24.24	-	-	-
2.00	-	47.35	67.07	75.85	82.63
5.00	-	-	69.52	-	-

As results from the presented data:

– ABTS and DPPH is adequate for measuring antioxidant characteristics when the spectrum of examined antioxidant or real biological system does not coincide with the wavelength used to monitor colored radical depletion;

– if the examined antioxidant absorbs the wavelength used to monitor radical concentration changes, the difference between true and spectrophotometrically estimated IC_{50} values depends not only on its extinction coefficient of the monitored wavelength but also on its residue concentration in the measuring system;

– it is possible to apply spectrophotometric measurements for the estimation of the antioxidant properties of compounds absorbing the monitored wavelength provided that the examined antioxidant, reacting with colored radicals, undergoes total depletion and that the reaction products allow to monitor the neutralization reaction of DPPH or ABTS radicals.

References:

[1] K. Mishra, H. Ojha, N. K. Chaudhury, *Food Chemistry*, **130** (2012) 1036.

[2] R. L. Prior, X. Wu, K. Schaich, *Journal of Agricultural and Food Chemistry*, **53** (2005) 4290.

[3] A. Floegel, D-O Kim, S-J. Chung, S.I. Koo, O. K. Chun OK, *Journal of Food Composition and Analysis*, **24** (2011) 1043.

[4] M. B. Arnao, *Trends in Food Science and Technology*, **11** (2000) 419.

STUDY OF THE INFLUENCE OF PHENOLICS EXTRACTION CONDITIONS ON THE RESULT OF THEIR ANALYSIS IN PLANT MATERIAL

Marta GIL
DEPARTAMENT OF CHROMATOGRAPHIC METHODS

Phenolic compounds are a group of substances represented in the realm of plants with a very diverse structure and properties, taking into account extremely valuable pro-health and healing properties. Unfortunately, these compounds are not synthesized by the human body. Their only source is food, especially green plants, fruits and seeds.

Among the phenolic compounds phenolic acids deserve special attention, and especially caffeoylquinic acids (CQAs). Nowadays much is known about CQAs pro-health properties, including anti-cancer activity. Yet, the supposition that they may be helpful in fighting obesity and modify glucose-6-phosphatase involved in glucose metabolism have led to a revival of research on CQAs properties and their natural occurrence. For the same reasons, increased demand for these compounds of many industries has been seen. The consequence of this phenomenon is the need to develop new, more effective ways of obtaining these compounds from plant material.

Given the increased consumer interest in natural products rich in chlorogenic acids, more efficient extraction methods, leading to obtain extracts with enhanced CQAs content, are being sought. In this point, it is worth to add that it is not so easy since these compounds easily degrade/transform to others, the more that in most cases the long-lasting high-temperature extraction methods are applied, such as Soxhlet extraction. The alternative technique to Soxhlet extraction is pressurised liquid extraction (PLE). The technique has proven to be an equivalent or superior alternative for the extraction of different analytes from various matrices. In PLE, compounds are extracted with a solvent at temperatures exceeding the boiling temperature of the solvent under the atmospheric pressure. At present there are available also other enhanced extraction techniques, such as ultrasound-assisted solvent extraction (UASE) and microwave-assisted solvent extraction (MASE), which allow for the full recovery of the components of interest from the sample matrix in a short time.

The report presents the results of research work on the influence of phenolics extraction conditions on the evaluation of their actual content in plants. The results obtained using MASE and UASE are compared to those revealed by matrix solid phase dispersion (MSPD). The last method has gained recognition as a simple and cheap sample preparation procedure involving simultaneous disruption and extraction of various solid and semi-solid materials, in which both sorbent and sea sand can be used as a dispersing agent. The great advantage of the MSPD technique is that it could be perform with high efficiency in low temperatures, what is very beneficial for the isolation of unstable analytes such as 5-caffeoylquinic acid (5-CQA), in particular 1,3-dicaffeoylquinic acid (1,3-diCQA), which is easily disintegrated during the extraction process.

Effect of MASE and UASE techniques on degradation of 5-CQA and 1,3-diCQA in simulated extraction conditions and during their actual extraction from the chosen plant (*Cynara scolymus*) is presented on Fig. 1. Chromatograms of methanolic standard solutions of 5-CQA and 1,3-diCQA are shown in the upper part of the figure. Chromatograms obtained for the solutions subjected to MASE, UASE and MSPD to simulate their extraction process are presented in its lower part. Chromatograms of *Cynara scolymus* extracts obtained under the same MASE, UASE and MSPD conditions are presented in the right part of the figure.

Comparison of the chromatograms obtained for standard solutions, non-subjected and subjected simulated extractions, shows that both examined compounds easily degrade/transform to other phenolic acids under high-temperature processes. The destructive character is especially seen for MASE conditions. MSPD, as it was supposed, does not lead to destruction of the compounds.

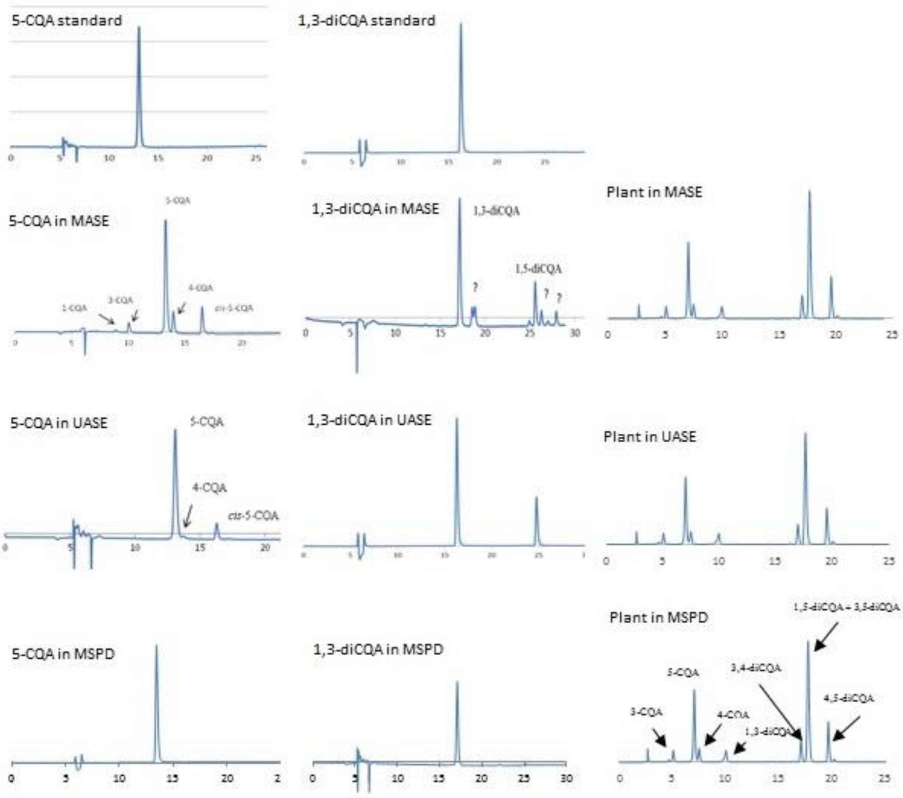

Fig. 1. Effect of extraction technique on degradation of 5-CQA and 1,3-diCQA in the standard solution and during their extraction from *Cynara scolymus*.

Comparison of the chromatograms of *Cynara scolymus* extracts, obtained under MASE and UASE, discloses that the majority of 5-CQA and 1,3-diCQA degradation products revealed during their simulated extraction is also present it the plant extracts. The change of the extraction technique does not modify the quantitative and qualitative extracts composition. These compositions are analogous to those obtained applying MSPD, the technique which is not destructive for phenolics. Concluding, the proved degradation of 5-CQA and 1,3-diCQA during their simulated MASE and UASE extraction is not confirmed during their actual isolation from the plant material.

DESIGNING OF FORMULA OF NANOSTRUCTURAL OXIDE CATALYSTS BY USE OF PRECUSORS OF HYDROTALCITE TYPE FOR HYDROGEN PRODUCTION

Magdalena GRELUK
DEPARTMENT OF CHEMICAL TECHNOLOGY

Hydrogen is very attractive for use in proton exchange membrane (PEM) fuel cells as a readily available gas, a renewable energy source, a hazard-free, environmentally-friendly and efficient fuel. Among the possible methods of hydrogen production (reforming of hydrocarbons, electrolysis, photolytic and biological conversion), steam reforming of ethanol (SRE) seems to be very attractive. Ethanol has the advantage over other conventional substrates such as natural gas, gasoline or liquefied petroleum gas (LPG) that it is readily available, easy to obtain from biomass, CO_2-neutral (bio-ethanol) and safe to handle [1-3].

The key technology in the process of catalytic SRE is to find suitable catalyst for maximization of the hydrogen yields and minimization of the production of carbon deposition and carbon monoxide. Cobalt-based catalysts have become one of the most promising groups of SRE catalysts because they have comparable activity with noble metals for C─C bond cleavage in the medium temperature range, but considerably lower prices. The primary disadvantages of cobalt catalysts, such as sintering or deactivation owing to coke formation, can be limited by selection of a suitable support.

The aim of this work was to study the catalytic properties of the cobalt catalyst under steam reforming of ethanol conditions.

The reaction of ethanol conversion with water was carried out under atmospheric pressure in a fixed-bed continuous-flow quartz reactor over the catalyst (0.1 g; 0.15-0.3 mm) reduced in situ with hydrogen at 400°C for 1 hour, prior to the reaction. The aqueous solution of ethanol (H_2O/ethanol=12/1) was supplied to an evaporator (150°C) and the reactant vapours, without diluting with any inert gas, and were fed to the reactor at a flow rate of 100 mL×min-1. The catalytic performance was tested in the temperature range of 390-480°C. The analysis of the reaction mixture and the reaction products (all in gas phase) were carried out on-line by means of two gas chromatographs. One of them, Bruker 450-GC was equipped with two columns, the first filled with a porous polymer Poropak Q (for all organics, CO_2 and H_2O vapor) and the other one—capilary column CP-Molsieve 5 Å (for CH4 and CO analysis). Hellium was used as a carrier gas and a TCD detector was employed. The hydrogen concentration was analyzed by the second gas chromatograph, Bruker 430-GC, using a Molsieve 5 Å, argon as a carrier gas and a TCD detector. Steam reforming of ethanol ($EtOH/H_2O$ =1/12) over catalyst showed that the temperature of 540°C was the most advantageous for this process. The catalyst indicated the high SRE process selectivity to two most desirable products of reaction, hydrogen and carbon dioxide and amounts of carbon monoxide, methane and acetaldehyde formed in side reactions were much smaller.

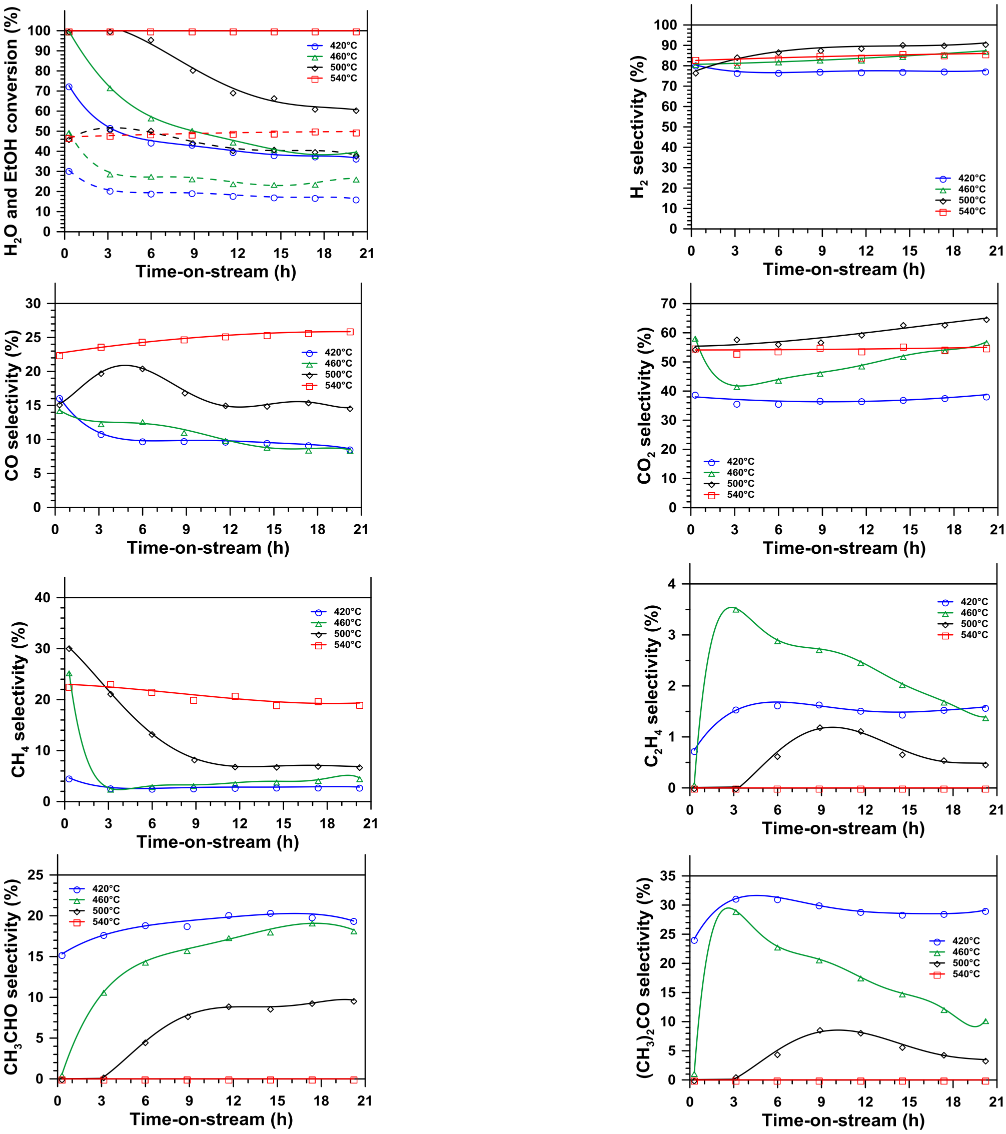

Fig. 1. Effect of the reaction temperature on ethanol and water conversion and selectivity to products over A catalyst under SRE conditions.

References:

[1] S. Jampa, K. Wangkawee, S. Tantisriyanurak, J. Chanpradit, A.M. Jamieson, T. Chaisuwan, A. Luengnaruemitchai, S. Wongkasemjit, *Int. J. Hydrog. Energy*, **42** (2017) 5537-5548.

[2] S. Turczyniak, D. Teschner, A. Machocki, S. Zafeiratos, *J. Catal.*, **340** (2016) 321-330.

[3] R. Espinal, E. Taboada, E. Molins, R.J. Chimentao, F. Medina, J. Llorca, *Top. Catal.*, **56** (2013) 1660-1671.

OPTIMIZATION OF CHEMISORPTION ON THE CATALYSTS FOR STEAM REFORMING OF ETHANOL

Grzegorz SŁOWIK
DEPARTMENT OF CHEMICAL TECHNOLOGY

In the steam reforming of ethanol (SRE) besides operating conditions, the use of suitable catalyst plays a crucial role in achieving selective, efficient and economically profitable process. The commonly used in the SRE heterogeneous catalysts are cobalt-based ones, usually highly dispersed on inorganic oxide supports, which show a high activity and stability, relatively low cost and a high selectivity for the most desirable reaction products (H_2 and CO_2). Among supports of the active phase, ceria was used very often in various catalytic systems.

The catalytic properties of catalysts depend on their key parameters, such as crystallites size, structure and morphology. Dispersion and the average size of the metallic active phase are one of the most important parameters characterizing the heterogeneous catalysts, which are essential for the activity, selectivity and stability of catalytic processes. The catalytic activity of a supported catalysts depends on the degree of dispersion of the metallic active phase and its active surface area, and it usually increases with increasing dispersion of metal and decreasing its crystallites size. On the other hand, the crystallites shape and their size distribution are important for mechanism of catalytic reaction, which dependents on the crystal faces exposed at the surface. The crystallites size of metallic active phase are usually determined by hydrogen chemisorption, X-ray diffraction (XRD) or TEM (Transmission Electron Microscopy), but sometimes different results are found from various methods for the same catalyst.

From three methods (hydrogen chemisorption, TEM and XRD) used for crystallites size determination, only TEM shows distinct advantages for the direct measurement of crystallites size in comparison with other methods, because the metal active phase crystallites can be quite clearly distinguished from the catalyst support and directly measured [1].

The aim of studies provided in the project is (i) determination on the basis of the results obtained with different methods (hydrogen chemisorption, TEM and XRD), the optimum temperature hydrogen chemisorption and evaluation of the proper use of data for the total or strong chemisorption to determine the average crystallite size of cobalt active phase, which should be consistent with the results of microscopic examination. Another objective is also to (ii) determine the effect of addition of the potassium promoter to the cobalt catalyst on the optimum temperature hydrogen chemisorption, appropriate to determine the average crystallite size of the active phase.

Cobalt catalysts with CeO_2 support, unpromoted and promoted with potassium were prepared by an impregnation method. Reduced catalysts were subjected to hydrogen chemisorption at different temperatures in the range of 313-453 K. Studies have shown that calculated Co crystallites size depends on the temperature of chemisorption. Comparison of the average size of the cobalt-based crystallites measured by TEM, hydrogen chemisorption and XRD methods proved that the good agreement between values obtained from total chemisorption and TEM data is possible (Fig. 1 and Table 1). The total hydrogen uptake on the potassium-free catalyst, measured at 383 K, leads to the estimation of the size of crystallites compatible with the values measured by the most objective, microscopic method. When potassium is present in the catalyst, the optimum of hydrogen chemisorption temperature is higher by c.a. 30 K, i.e. 413 K.

The average size of cobalt-based crystallites estimated from XRD data is congruous with that measured by the TEM method only in the case when among crystallites there are no very small ones [1].

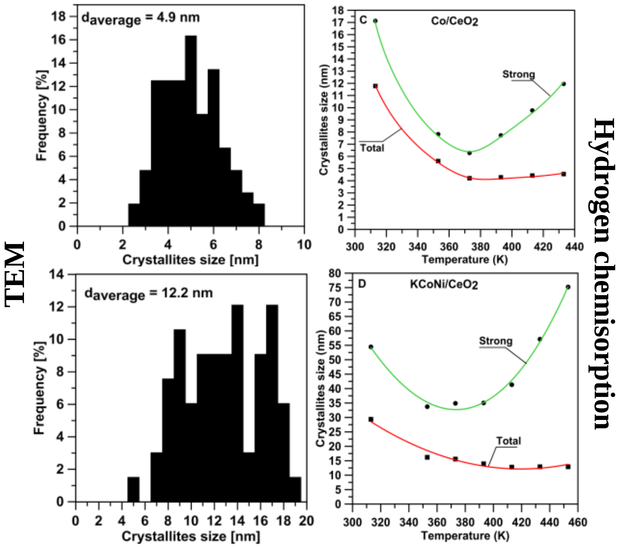

Fig. 1. TEM and hydrogen chemisorption measurements of cobalt crystallites size.

Table 1. Comparison of the average size of crystallites determined by TEM, XRD and hydrogen chemisorption for reduced (at 673 K) Co/CeO$_2$ and KCo/CeO$_2$ catalysts.

Catalyst	TEM [nm]	XRD [nm]	Hydrogen Chemisorption [nm]
	Reduced	Reduced	
Co/CeO$_2$	4.9 ± 0.3	7.8 ± 0.4	4.1 ± 0.3*
KCo/CeO$_2$	12.2 ± 0.7	15.2 ± 0.8	12.5 ± 0.3**

Measured at *383K/ **413K

References:

[1] G. Słowik, A. Gawryszuk-Rżysko, M. Greluk, A. Machocki, *Catal. Lett.*, **146** (2016) 2173–2184.

STUDY OF THE MECHANISM OF OXIDATION OF SOOT FROM DIESEL EXHAUST GASES ON THE SURFACE OF THE COBALT CATALYST WITH USE OF STABLE ISOTOPES OF OXYGEN

Marek ROTKO
DEPARTMENT OF CHEMICAL TECHNOLOGY

The removing (oxidation) of soot from diesel exhaust gases is a very important issue due to the negative impact of this type of pollution on human health and climate of our planet. Diesel soot is carcinogenic and contributes to the greenhouse effect. Therefore, many countries have introduced limits on the emission of soot and still are exacerbated. In order to decrease the content of soot in the engine exhaust, a diesel particulate filter (DPF) is widely mounted in vehicles. For the proper functioning of such filters, a regeneration step is required. One of the most promising ways of the diesel particulate filter regeneration is employed of catalytic substances, which allow to remove (oxidize) soot in the exhaust gas temperature. For this purpose, catalysts, which demonstrate high activity and selectivity to carbon dioxide and high resistance to operating conditions, are proposed. One of them is Co_3O_4, whose catalytic properties are connected with the mobility of oxygen on the surface and in the bulk. Therefore, the main aim of this study was the analysis of these properties with use of stable isotopes of oxygen ($^{16}O_2$ and $^{18}O_2$).

The cobalt catalyst was prepared from an aqueous solution of cobalt acetate by the precipitation method. The catalyst precursor was calcined at 400^{o}C by 2 h. Its basic physicochemical parameters were determined by the N_2 adsorption/desorption experiment and X-ray diffraction spectroscopy (Table 1). The activity of the cobalt catalyst was measured in the “tight contact” using model soot (Printex U) and the reaction mixture containing 10 vol.% of O_2. The main study with use of stable isotopes of oxygen was carried out at 327^{o}C. At the beginning of the experiment, the reaction mixture contained 10 vol% of $^{16}O_2$, after the switch – 10 vol% of $^{18}O_2$. The results of this switch for the pure cobalt catalyst and mixed with soot were analyzed by a mass spectrometer. Moreover, also the temperature-programmed exchange experiment was performed from 150^{o}C to 550^{o}C with ramp rates of 10^{o}C/min. During this experiment, the mixture containing 5 vol% of $^{18}O_2$ and inert gases (He and Kr) was dosed into the reactor with the catalyst bed.

Table 1. The basic physicochemical parameters determined for the cobalt catalyst.

Total BET surface area (m^2/g)	Mean pore size [nm]	Total pore volume (cm^3/g)	Content of Co_3O_4 (%)	Mean size of crystallites (nm)
44.5	19.71	0.222	100	20

The process of soot oxidation on the cobalt catalyst begins at about 285°C, and the maximum rate is observed at about 395°C, whilst the process of oxidation of soot without employing a catalyst needs much higher temperature (Fig. 1).

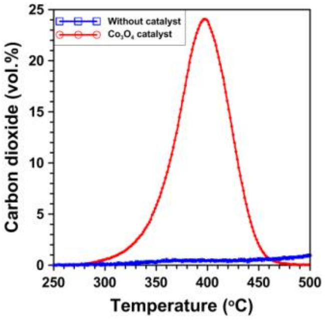

Fig. 1. Concentration of CO_2 in the post-reaction mixture during soot oxidation.

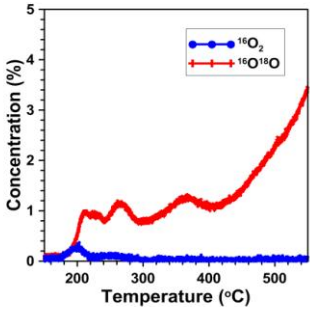

Fig. 2. Effects of temperature-programmed exchange experiment with use of $^{18}O_2$.

The process of oxygen exchange between the gas phase and the catalyst lattice begins at about 180°C, but its rate is low until to 400°C (Fig. 2). After exceeding 400°C, the fast increase of $^{16}O^{18}O$ concentration is observed.

The results of the switch between $^{16}O_2$ and $^{18}O_2$ for the catalyst mixed with soot (Fig. 3) demonstrate that oxygen from the catalyst lattice undergoes not only the exchange with oxygen from the gas phase, but also takes part in the process of soot oxidation. After the switch, the long delay between Ar and $C^{16}O_2$ is observed and also the significant amounts of $C^{16}O^{18}O$ are appeared. Moreover, the amounts of oxygen from the catalyst lattice, which undergo the exchange, are much lower than those involved in the process of soot oxidation. The curves showing concentration of $^{16}O_2$ and $^{16}O^{18}O$ much faster aim to the zero value than those showing concentration of $C^{16}O_2$ and $C^{16}O^{18}O$.

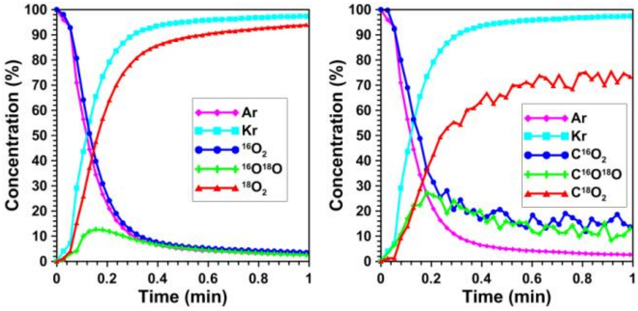

Fig. 3. Results of the switch between $^{16}O_2$ and $^{18}O_2$ for the catalyst mixed with soot.

The amounts of oxygen from the catalyst lattice, which undergo the exchange with oxygen from the gas phase, determined for the pure catalyst (Fig. 4) are comparable with the amounts of oxygen from the catalyst lattice, which undergo the exchange during soot oxidation (Fig. 3). It means that this significant part of oxygen from the catalyst lattice is unavailable for the process of soot oxidation and the change of this state of affairs would probably affect positively on the catalytic capability of the cobalt catalyst.

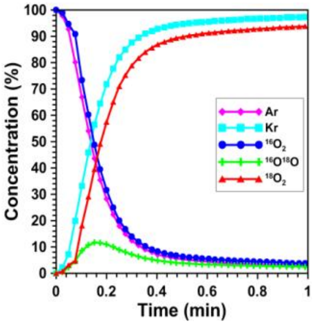

Fig. 4. Results of the switch between $^{16}O_2$ and $^{18}O_2$ for the pure catalyst.

SIMULTANEOUS STUDIES OF CATALYSTS ACTIVITY AND COKING RATE IN THE REACTION OF HYDROCARBONS CONVERSION WITH APPLICATION OF TAPERED ELEMENT OSCILLATING MICROBALANCE

Marcin CICHY
DEPARTMENT OF CHEMICAL TECHNOLOGY

Very often catalytic chemical reactions involving hydrocarbons (e.g. methane reforming with carbon dioxide) are accompanied by undesired processes leading to deactivation of the catalyst. One of its main factors is the deposition of a carbon deposit on the catalyst surface, which in turn leads to a decrease in its activity. Therefore, it is important to conduct research on the resistance of catalytic systems to coking.

Despite the large popularity of gravimetric methods (TGA) for the evaluation of resistance to coking, there are objections to it, caused by incomplete contact of the reaction mixture (part of the stream flows past the weighting pan) with the catalyst sample, as well as different hydrodynamic conditions. The objections also concern the lack of assessment of the effects of carbon deposit formation on catalyst activity. The appearance in the Department of Chemical Technology the possibility of using TEOM microbalance (Tapered Element Oscillating Microbalance), allowing simultaneous investigation of catalyst activity and coke deposition rate, prompted the work to characterize a number of catalytic systems in terms of their resistance to coking. The TEOM microbalance use the change in oscillation frequency of the tapered element to determine mass changes. The use of an oscillating scale eliminates the problem of the sample washing by the reaction gas stream and allows the determination of the amount of the coke deposited on the catalyst continuously during the reaction. The gases leaving the catalyst bed cannot be directly directed to the analytical system, because the oscillating element must vibrate freely. Therefore, a washing gas is used which flows out of the oscillating element and directs the reaction products to the Varian CP-4900 microchromatograph (Micro-GC) to analyze the composition of the reaction mixture.

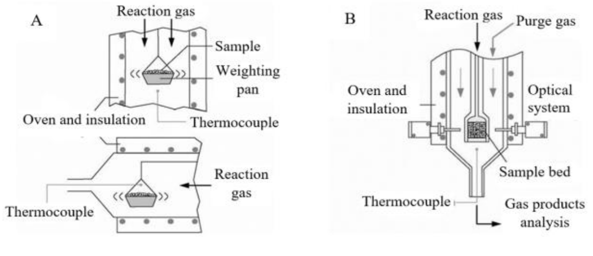

Fig. 1. Comparison of traditional TGA reactor (A) and TEOM microbalance (B).

Thanks to the such reaction and analytical system design, it is possible to obtain not only information about the mass change of catalysts, and thus the amount of coke deposited, but also the full process characteristics, primarily conversion of raw materials and selectivity to individual gas products. Comparison of traditional TGA analytical system and TEOM microbalance essentials presents Fig 1.

Studies made during realization of this project were in fact attempts to compare activity and coking resistance results obtained independently by TPSR (Temperature-Programmed Surface Reaction) method (coking) and gradientless reactor (catalysts activity) and simultaneously by TEOM technique. Studies were conducted with use of commercially available Ni/α-Al_2O_3 catalyst modified with different amounts of rhenium in methane with carbon dioxide reforming reaction. Catalysts containing up to 4 wt. % of Re were tested at temperatures of 550 and 600 ^{o}C.

Fig. 2. presents activity and resistance to coking measurements obtained independently, while Fig. 3. shows TEOM results. It must be noted that coking initiation temperature curve (Fig. 2) has opposite course that coking rate curve (Fig. 3) [1].

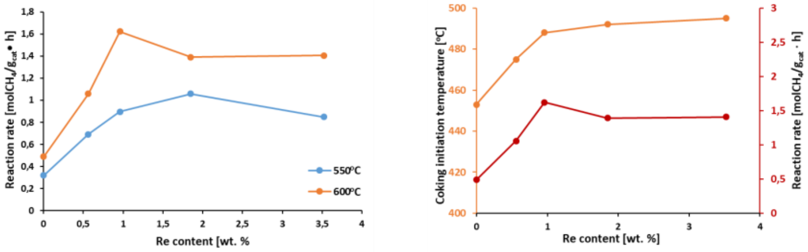

Fig 2. Reaction rate (gradientless reactor) and coking initiation temperature (TPSR) as function of Re content in studied catalysts.

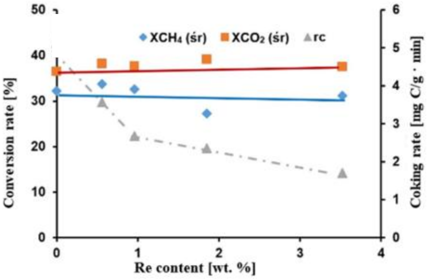

Fig. 3. Both conversion rate and coking rate obtained simultaneously by TEOM microbalance.

Obtained results were very consistent (both activity and resistance to coking) regardless of the measurement methods used (simultaneously or independently) and were presented during LX Annual Congress of the Polish Chemical Society in Wroclaw.

References:

[1] T. Borowiecki, W. Grzegorczyk, A. Gołębiowski, *Catal. Lett.*, **79** (2002) 119 – 124

PREPARATION AND CATALYTIC CHARACTERISTICS OF ACTIVE NANOMATERIALS FOR STEAM REFORMING OF ETHANOL

Magdalena GRELUK
DEPARTMENT OF CHEMICAL TECHNOLOGY

Cobalt catalysts belong to the most active ones in the ethanol steam reforming reaction. Despite the extensive studies of supported cobalt catalysts in the SRE, only a few reports discussed the application of manganese oxides as modifiers or supports of cobalt catalysts in this reaction. Numerous methods have been proposed in the literature for synthesis of Co-Mn oxides, used for development of batteries, magnetic materials and catalysts, including precipitation, sol-gel, thermal decomposition, solid state reactions. This raport discusses chief aspects of the structural and surface changes of cryptomelane-based cobalt-manganese catalysts applied in the SRE reaction. Cryptomelane-type manganese oxides contain regular one-dimensional channels composed from the double chains of edge shared MnO_6 octahedral units, joined by the corners. The potassium ions located in the 2×2 channels, which influence the stability of the manganese oxide framework, can be replaced by other ionic species. This may induce distortion of manganese oxide structure, and simultaneously changes of the redox and catalytic properties.

The aim of this work was to study the physicochemical properties of the supported cobalt catalyst.

Unmodified and cobalt-modified manganese oxides were obtained by the redox precipitation method. Unmodified manganese oxide was prepared by using aqueous solution of potassium permanganate ($KMnO_4$), obtained by the dissolution of salt in in of distilled water and the solution of manganese acetate ($Mn(CH_3COO)_2 \cdot 4H_2O$), by dissolution in distilled water. The first solution was introduced dropwise while vigorous stirring to the second solution mixed with acetic acid solution (CH_3COOH). The reaction mixture was refluxed at 50 °C while stirring for 24 hours. The obtained black material was filtered, washed with distilled water, dried overnight at 80 ºC, and next calcined at 350 °C for 3 hours. Similar procedures were used to synthesize cobalt-manganese catalyst, adding potassium permanganate solution to the solution obtained by the dissolution of manganese acetate and cobalt acetate ($Co(CH_3COO)_2 \cdot 4H_2O$) in distilled water, mixed with the acetic acid solution.

The content of cobalt in the catalyst was determined by the application of X-ray fluorescence method. Structural and surface properties of the samples after calcination and reduction were evaluated from the nitrogen adsorption/desorption isotherms recorded at -196 ºC using ASAP analyzer. Transmission electron microscopic studies (TEM) were performed by the application of the high-resolution electron microscope.

Physicochemical properties of catalysts are presented in Table 1.

Table 1. Physicochemical properties of A catalyst.

	A
Cobalt content (wt.%)	17.5
S_{BET} (m^2/g)	133
Pore volume (mL/g)	0.26
Average pore diameter (nm)	9.1

TEM and STEM-EDS images recorded after reduction of the samples (Figures 1 and 2) confirm migration and transformation of dispersed manganese, cobalt and potassium elements into the larger ensembles. Co-MnOx sample after reduction contains regular manganese oxide particles of the size ranging from about 40 to 100 nm. Almost spherical cobalt metallic nanoparticles of the size ranging from about 10 to 30 nm are located on the surface of MnO particles.

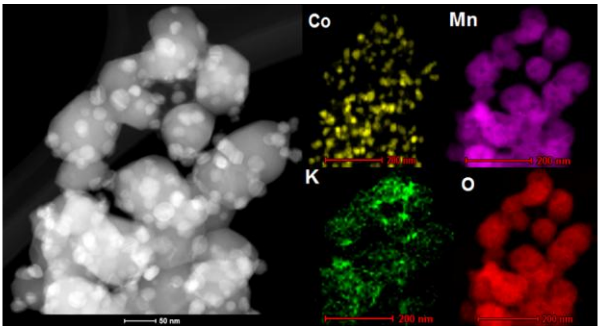

Fig. 1. STEM-EDS images of A catalyst after reduction.

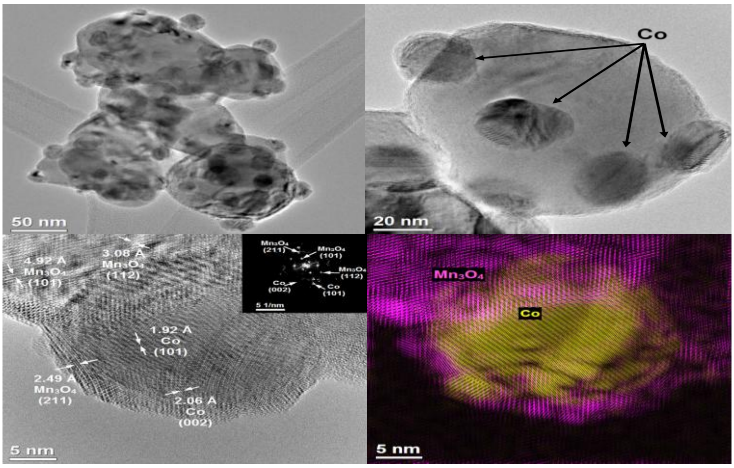

Fig. 2. HR-TEM with FFT images of particles of A catalyst after reduction.

STUDY OF THE MECHANISM OF SOOT OXIDATION FROM EXHAUST GASES OF DIESEL ENGINES ON THE SURFACE OF CATALYTICALLY ACTIVE NANOMATERIALS WITH USE OF STABLE ISOTOPES OF OXYGEN

Marek ROTKO
DEPARTMENT OF CHEMICAL TECHNOLOGY

One of the promising catalytic materials for the process of soot oxidation is the cobalt-cerium catalyst, which demonstrates high activity and selectivity to carbon dioxide and good resistance to operating conditions. Its catalytic properties are strongly connected with the mobility of oxygen on the surface and in the bulk. Therefore, the main aim of this study was the analysis of these properties with use of stable isotopes of oxygen ($^{16}O_2$ and $^{18}O_2$). Additionally, for comparison purposes, the similar analysis was also conducted for the cerium catalyst.

The cerium catalyst and the cobalt-cerium catalyst were prepared from an aqueous solution of cerium acetate and from the mixture containing proper amounts of cobalt acetate and cerium acetate by the precipitation method. The catalyst precursors were calcined at 400^{o}C by 2 h. Its basic physicochemical parameters were determined by the N_2 adsorption/desorption experiment and X-ray diffraction spectroscopy (Table 1), while the content of metals was determined by X-ray fluorescence spectroscopy (XRF). The catalytic activity was measured in the “tight contact” using model soot (Printex U) and the reaction mixture containing 10% of O_2. The temperature-programmed exchange experiment was performed from 150^{o}C to 750^{o}C with ramp rates of 10^{o}C/min. The non-steady state isotopic transient kinetic analysis (N-SSITKA) was carried out at 331^{o}C and 363^{o}C for the cobalt-cerium catalyst and the cerium catalyst, respectively. At the beginning of this experiment, the reaction mixture contained 10% of $^{16}O_2$, after the switch – 10% of $^{18}O_2$.

Table 1. The basic physicochemical parameters determined for the studied catalysts.

Catalyst	Content of metals	Total BET surface area	Content of crystalline phases
Co-Ce	21% of Co 55% of Ce	77 m^2/g	29% of Co_3O_4 71% of CeO_2
Ce	80% of Ce	112 m^2/g	100% of CeO_2

The oxidation of soot on the surface of the cobalt-cerium catalyst begins at lower temperature than on the surface of the cerium catalyst (Fig. 1). Similarly, the maximum of the formation of carbon dioxide on the cobalt-cerium catalyst is located at lower temperature than on the cerium catalyst. The cobalt-cerium catalyst is much more active than the cerium catalyst.

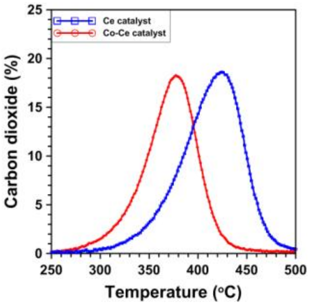

Fig. 1. Concentration of CO_2 in the post-reaction mixture during soot oxidation.

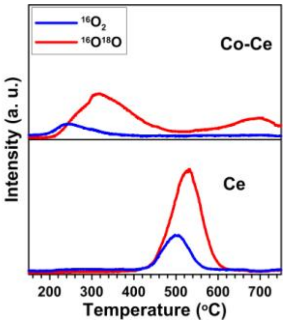

Fig. 2. Effects of temperature-programmed exchange experiment with use of $^{18}O_2$.

The process of oxygen exchange between the gas phase and the crystal lattice of the cobalt-cerium catalyst begins at much lower temperature than for the cerium catalyst (Fig. 2). The significance amounts of exchanged oxygen molecules for the cobalt-cerium catalyst are already observed at about 240°C, while for the cerium catalyst at much higher temperature (460°C).

The results of the switch between $^{16}O_2$ and $^{18}O_2$ for both catalysts (Fig. 3 and 4) demonstrate that oxygen from the crystal lattice takes part in the process of soot oxidation. After the switch, the long delay between Ar and $C^{16}O_2$ is observed and also the significant amounts of $C^{16}O^{18}O$ are appeared. In the case of the cerium catalyst oxygen from its crystal lattice plays probably main role in soot oxidation, while for the cobalt-cerium catalyst its importance is smaller (signal of $C^{16}O_2$ for Co-Ce much faster disappears than for Ce). In addition, these studies confirm that oxygen from crystal lattice of both catalysts can also undergo the exchange with oxygen from the gas phase. However, for the cerium catalyst this exchange is vanishingly small compared to the cobalt-cerium catalyst.

The obtained results demonstrate that oxygen from the crystal lattice of studied catalysts takes part in soot oxidation, which suggests that this process proceeds, at least partially, according to the Mars-van Krevelen mechanism.

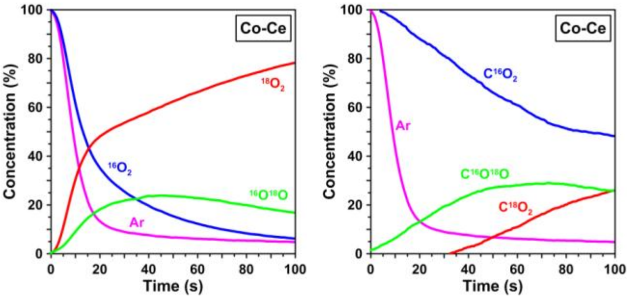

Fig. 3. Results of the switch between $^{16}O_2$ and $^{18}O_2$ for the cobalt-cerium catalyst at 331°C.

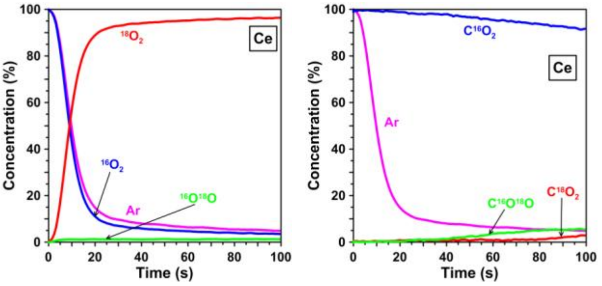

Fig. 4. Results of the switch between $^{16}O_2$ and $^{18}O_2$ for the cerium catalyst at 363°C.

SYNTHESIS AND PROPERTIES OF COORDINATION POLYMERS OBTAINED ON THE BASIS OF d- AND f-ELECTRON METAL IONS AND SULPHUR-CONTAINING CARBOXYLATE LIGANDS

Justyna SIENKIEWICZ-GROMIUK
DEPARTMENT OF GENERAL AND COORDINATION CHEMISTRY

Design and synthesis metal-organic coordination polymers through coordination or noncovalent bonds have attracted much attention due to their particular topologies and some potential applications, such as catalysis, adsorption, magnetism, photochemistry and NLO materials. The selection of suitable ligand with certain features, such as flexibility, versatile binding modes and the ability to form hydrogen bonds is crucial to the construction of polymeric complexes [1]. The universal involvement of carboxylic compounds (containing not only the oxygen donor atoms but also the other types of donors present in the organic unit, such as sulphur and/or nitrogen) as building bricks for the construction of stable supramolecular networks with transition as well as lanthanide metal ions due to their ability to create extended systems of various non-covalent forces including coordination bonding, hydrogen bonding, aromatic–aromatic π–π stacking interactions and also the electrostatic and charge-transfer interactions [2].

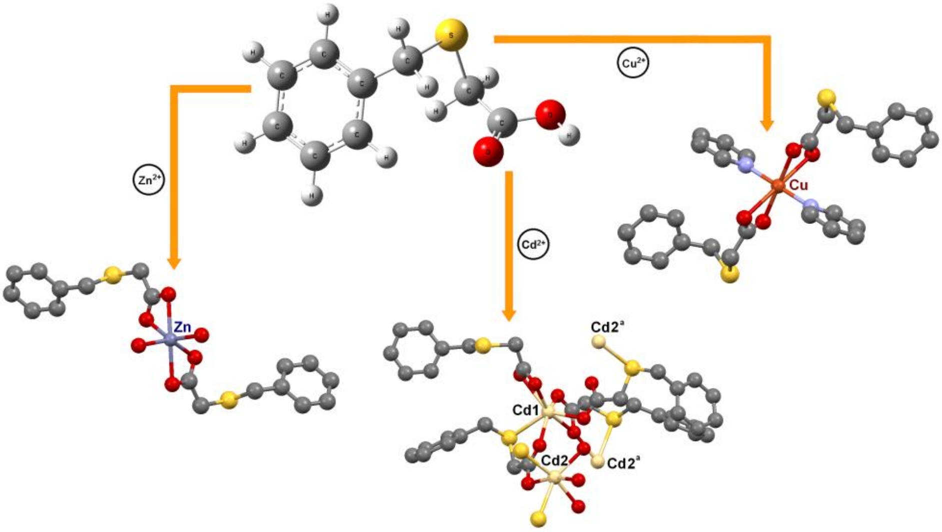

Fig.1. Coordination environments of Zn(II), Cd(II) and Cu(II) ions in the obtained (benzylthio)acetate complexes.

The (benzylthio)acetic acid is a mono-carboxylate ligand, which possesses flexibility owing to the presence of $–CH_2–S–CH_2–$ group between the phenyl ring and carboxyl moiety. The molecule of selected ligand contains three potential binding sites, namely two acidic ″hard″ oxygen donor atoms and one basic/alkaline ″soft″ sulphur donor atom which can create coordination bonds with metal ions not only through oxygen atoms but also with the share of the sulphur atom [2, 3]. Thus, these versatile coordination fashions (Fig. 1) are visible in the obtained structures of the zinc(II), cadmium(II) and cooper(II) complexes [4, 5].

The main stage of research was to find the efficient method of synthesis of the complexes in question, that is way the classic precipitation method as well as the solvothermal method were used to prepare these compounds. During the syntheses some parameters of the process were changed, such as: the type of starting substrates (chlorides, nitrates, acetates of metal ions), pH value, the temperature value, the time of contact or the type of solvent (water, alcohols, DMF, DMSO). Among the syntheses carried out so far, the use of the conventional wet method allowed to obtain the compounds in the form of hydrated precipitates. The (benzylthio)acetates of selected transition metal ions, like Cd(II), Co(II), Ni(II), Cu(II) and Zn(II) were obtained as monohydrates with the metal:ligand ratio of 1:2 and the general formula of $M(C_8H_9S(COO^-)\cdot H_2O$. The results of infrared spectroscopy for the Ni(II) compound as a representative of this group of complexes clearly confirm the occurrence of a full coordination process. Thus, in the spectrum of Ni(II) the bands derived from the deprotonated carboxylate (COO^-) groups are visible at 1578 cm^{-1} (asymmetric stretches) and 1392 cm^{-1} (symmetric vibrations mode), respectively. In a high energy region in the registered IR spectrum, the broadened band located at 3452 cm^{-1} is associated with the stretching vibrations of hydroxyl group derived from water molecules. In the case of recorded IR spectrum of lanthanide(III) series, the full deprotonation is also noticeable. For example, in the IR profile of Ce(III) compound the most intense bands situated at 1541 and 1387 cm^{-1} are associated with the stretching vibrations of COO^- groups. The registered curve of thermal decomposition shows that hydrated Ni(II) complex heated in air loses the water molecule between 30−118 ºC (calculated mass loss: 4,09%; found mass loss: 3,61%). The anhydrous compound is stable up to about 230 ºC and during further heating it finally decomposes to NiO (calculated mass of residue: 17,01%; found residue mass: 17,61%). Unfortunately, it has not been possible so far to obtain the desired and monocrystalline forms of synthesized complexes which would be suitable for structural studies.

References:

[1] R.Yan-Wei and D. Li-Long, *J. Struct. Chem.*, **46** (2005) 352.
[2] J. Sienkiewicz-Gromiuk, *Spectrochim. Acta A*, **189** (2018) 116.
[3] J. Sienkiewicz-Gromiuk, B. Tarasiuk and L. Mazur, *J. Mol. Struct.*, **1110** (2016) 65.
[4] W.-H. Chan, T.C.W. Mak, W.-H. Yip, G. Smith, E.J. O'Reilly and C.H.L. Kennard, *Polyhedron*, **6** (1987) 881.
[5] W.-H. Chan, T.C.W. Mak, G. Smith, E.J. O'Reilly and C.H.L. Kennard, *Polyhedron*, **4** (1985) 1443.

SYNYHESIS OF POROUS MICROSPHERES FUNCTIONALIZED WITH LINEAR POLYMERIC CHAINS AND THEIR APPLICATION AS HPLC COLUMN PACKINGS

Marta GROCHOWICZ
DEPARTMENT OF POLYMER CHEMISTRY

Despite the advantages of the columns packed with modified silica and their widespread applications, some chromatographic determinations can be performed using only the polymeric columns. Polymeric column packings in the form of microspheres are mainly porous copolymers of styrene with divinylbenzene. However, experiences from use as HPLC column packings and as sorbents in the solid state extraction technique (SPE) indicate an excessively hydrophobic nature of such materials. This results in a limited range of their applications in the analysis of organic compounds. Therefore, there are ongoing efforts to produce polymeric microspheres of a less hydrophobic character than the ST-DVB material. Functional groups can be introduced into the structure of crosslinked polymers in two ways. The first involves the synthesis of microspheres from polar monomers. The second one involves surface modification of microspheres via grafting methods. In general, two different approaches can be mentioned, the ‘grafting to’ and the ‘grafting from’ approach. In the ‘grafting to’ technique a reactive terminal group on a functional polymer chain reacts with the activated surface of microspheres. As a polymerization method for obtaining polymeric chains, reversible addition-fragmentation polymerization is often used. The dithioester moiety of a RAFT agent serves two purposes. Initially, the dithioester moiety functions as a RAFT agent for obtaining polymer chains of predetermined molecular weight carrying RAFT end groups; subsequently these dithioester functionalities can be employed as a reactive heterodienophile in heteroatomic Diels Alder cycloaddition reaction (HDA) with a functionalized diene.

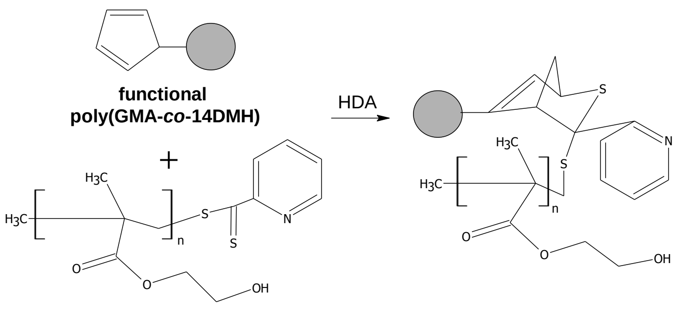

Scheme 1. The modification reaction of microspheres.

The aim of the project was the functionalization of the surface of copolymeric microspheres. Primary porous microspheres were obtained from glycidyl methacrylate (GMA) and 1,4-dimethacryloyloxybenzene (1,4DMH) with the use of seed swelling polymerization. Linear polymeric chains of poly(2-hydroxyethyl methacrylate) were obtained via RAFT polymerization. The HDA reaction was performed according to Scheme 1. The morphology of the obtained material was confirmed by SEM method (Fig.1). To evaluate the chromatographic properties of the new porous packing the Smith method was applied. The exemplary chromatograms of separation of alkyl aryl ketones and N-alkylanilines are presented in Fig 2. The conducted research show that microspheres of poly(GMA-co-14DMH) grafted with poly(HEMA) can be applied as column packings for the reversed phase HPLC.

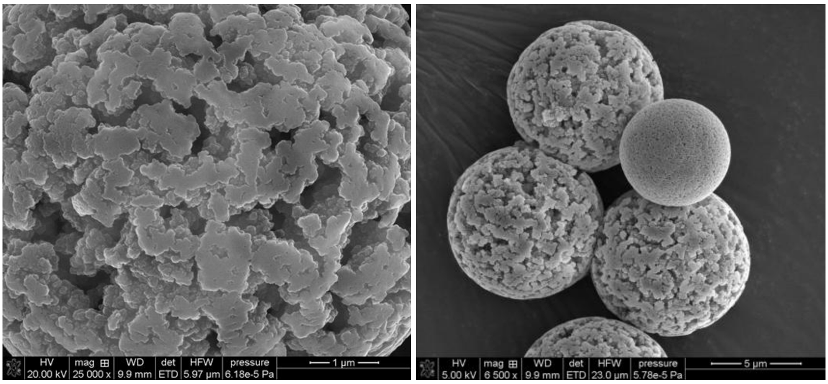

Fig. 1. SEM images of poly(GMA-co-14DMH) grafted with RAFT-poly(HEMA)

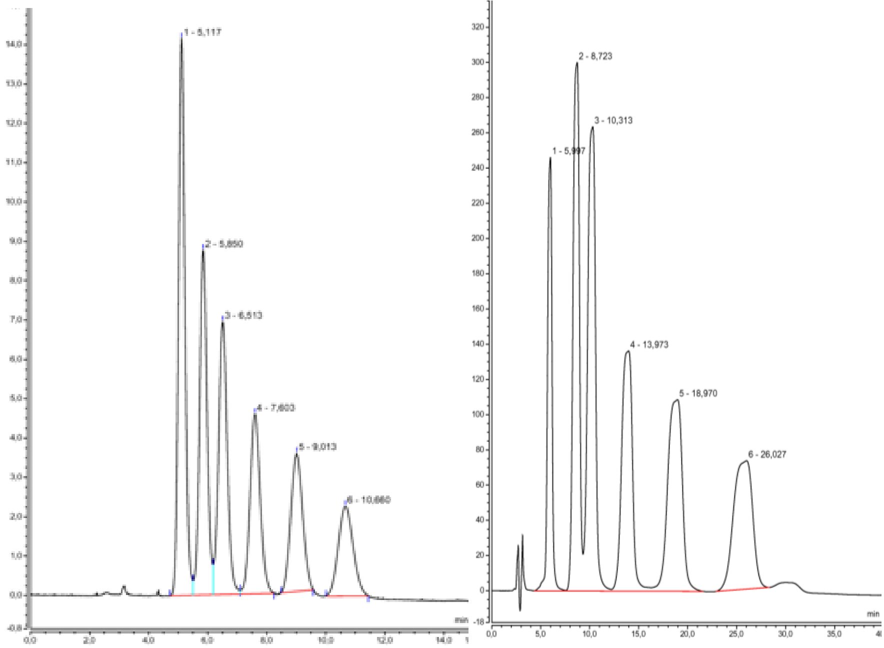

Fig. 2. Chromatograms of alkyl aryl ketones (left) and N-alkylanilines (right). Conditions: column 100 × 4.6 mm id; ACN concentration 50%; mobile phase ACN/buffer; 1mL/min; UV detector 254 nm. (1) acetophenone, (2) propiophenone, (3) butyrophenone, (4) valerophenone, (5) hexanophenone, (6) heptanophenone; (1) aniline, (2) N-methylaniline, (3) N-ethylaniline, (4) N-propylaniline, (5) N-butylaniline, (6) N-pentylaniline.

COPPER FRACTIONATION IN SOIL CONTAMINATED WITH DIFFERENT COPPER FORMS

Izabela JOŚKO
DEPARTMENT OF ENVIRONMENTAL CHEMISTRY

The recent years have seen a dynamic development in nanotechnology, manifested in the increasing number of scientific publications and new research centres specialising in the study of nanomaterials. Along with the academic advances in the field of nanotechnologies, nanotechnology products have been already put in use in different industries. Due to their nano size (100 nm), nanomaterials exhibit higher efficiency, hence their popularity. The diameter of a nanoscale particle determines a larger specific surface area, leading to a greater reactivity of nanomaterials and a number of other more desirable properties (including electrical, mechanical, optical, and magnetic properties) compared to their more sizeable counterparts. While promising many benefits, the development of nanotechnologies and a growing number of such products remains ecologically ambiguous, as the environmental risk and the impact of nanomaterials on living organisms is an open question [1, 2]. The exploitation of nano-products releases ingredients such as nanoparticles into various components of the environment, including the soil [3]. Due to the importance of the soil in both environmental and economic terms, it is crucial to assess potential implications arising from the presence of nanomaterials in the soil [4].

The aim of this study was to determine the copper fractionation in soil (sandy clay loam) with different moisture level (30, 50, 80% of water holding capacity, WHC). In the study, the different Cu forms were added to soil: nanoparticles (nano-Cu, nano-CuO), microparticles (bulk-CuO) and metal salt ($CuCl_2$). The mentioned materials (as powder) were applied to soil at dose of 10 mg kg^{-1}, then the samples were carefully mixed and incubated for 1 day. The soil samples without Cu supplement were the control samples. Directly after the end of incubation, the samples were dried and subjected to multistage sequential analysis, which allows distinguishing 5 metal fractions (exchangeable (F1), carbonate (F2), bound to iron and manganese oxides (F3), organic (F4) and residual (F5)). Table 1 shows the concentration of Cu fraction in control samples.

Table 1. The concentration of copper fractionated in control soil.

The soil moisture	Cu concentration [mg kg^{-1}]					
	F1	F2	F3	F4	F5	Total concentration
30%	1.07	0.27	12.91	9.08	16.67	21.2±1.5
50%	3.08	1.09	9.97	7.69	8.67	21.9±2.1
80%	1.03	0.45	12.06	0.55	11.91	22.3±2.4

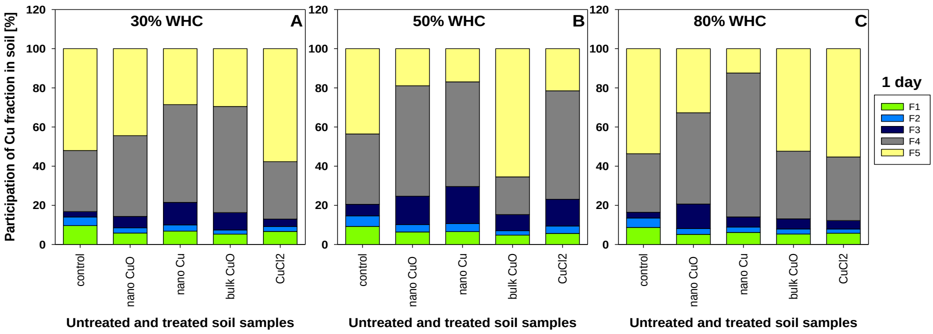

Fig. 1. The Cu fractionation in untreated and treated soil with different Cu forms under various humidity conditions.

The participation of Cu fractionated in soil was dependent on the used Cu form as well as the moisture level (Fig. 1). The percentage of F3, F4, F5 fractions, which the sum was over 80%, was subjected to the greatest changes. The participation of F1 was found to range from 4.4. to 9.6%, whereas the fraction F2 was below 5 %. Regardless of the soil moisture level, the percentage of F3 was higher in treated soils (especially with nano-CuO/nano-Cu) than in control samples. The participation of F4 in Cu distribution was between 19.3 and 64.4%. The highest percentage of this fraction was observed in soil with bulk-CuO (30% of WHC), nano-CuO (50% of WHC) and nano-Cu (80% of WHC). In most of cases, the participation of F5 fraction was the highest among the all fractions. Additionally, the percentage of F5 was lower in the treated soils in comparison with control samples. The study provided the differences in Cu fractionation in soil under different humidity conditions treated with various Cu forms. The obtained results confirm high affinity of Cu to bind Fe and Mn oxides and organic matter fractions (less labile Cu forms).

References:

[1] I. Jośko, P. Oleszczuk, B. Futa, *Geoderma,.,* **232–234** (2014) 528–537.
[2] I. Jośko, P. Oleszczuk, *Chemosphere*, **92** (2013) 91–99.
[3] B. Pan, B. Xing, *Eur. J. Soil Sci.*, **63** (2012) 437–456.
[4] P. Wang, N.W. Menzies, E. Lombi, B.A. McKenna, B. Johannessen, C.J. Glover, P. Kappen, P.M. Kopittke, *Environ. Sci. Technol.*, **47** (2013) 13822–13830.
[5] J.L. Gardea-Torresdey, C.M. Rico, J.C. White, *Environ. Sci. Technol.*, **48** (2014) 2526–2540.

POROUS POLYMERS AS AN ENVIRONMENT FOR HYDROLYSIS AND CONDENSATION OF INORGANIC OXIDE PRECURSORS

Agnieszka KIERYS, Piotr BOROWSKI, Radosław ZALESKI,
Andrzej SIENKIEWICZ, Jacek GOWOREK
DEPARTMENT OF ADSORPTION

Porous resins produced by the suspension polymerization exist primarily in the form of spherical beads which are insoluble both in organic and inorganic solvents but they swell in them to a certain extent [1]. Individual polymer bead possesses very complex internal structure which may be considered as a continuous pore network set within a continuous polymer phase of a specific chemical character. The pore network which consists of interconnected free volumes of different size may be regarded as a specific microreactor where different chemical reactions can take place. Indeed, polymer-supported reactions gained considerable interest, especially in the context of organic combinatorial syntheses [2]. However, it has previously been shown that porous polymers may be regarded as a system in which precursors of inorganic oxides (e.g. silica [3, 4]) can undergo the process of transformation which involves hydrolysis and condensation. Although, these processes conventionally takes place in aqueous solutions of desired pH, they can also occur when catalysts are provided in the vapour phase of the desired composition [5].

The present paper describes the synthesis of polymer-silica composites by *in situ* transformation of silica precursor (i.e. ethyltriethoxysilane, ETEOS) within the porous polymer support in the presence of the vapor mixture of water and ammonia (B) or water and hydrochloric acid (A). The Amberlite XAD7HP (XAD7) resin has simultaneously served as the specific microenvironment for gelation of organoalkoxysilane precursor and the polymer support. The properties of final products have been presented.

The dry XAD7 beads rapidly swell in the liquid ETEOS which leads to the increase of their size. The swelling process irreversibly changes the internal structure/ arrangement of the XAD7 since from the Positron Annihilation Lifetime Spectroscopy (PALS) measurements it follow that the pore size distribution (PSD) of the material obtained by introduction and evacuation of ETEOS differs significantly from the PSD of the initial XAD7.

Exposure of the XAD7 saturated with ETEOS to catalyst vapors initiates and accelerates the precursor transformation, which in turn, leads to *in situ* formation of the polysilsesquioxane (PSQ) network composed of a repeated C_2H_5–$SiO_{1.5}$ unit within the polymer support. The XRD patterns of composites indicate not only the successful development of PSQ network within XAD7 but also the existence of the differences between acid and base set PSQ on the molecular level.

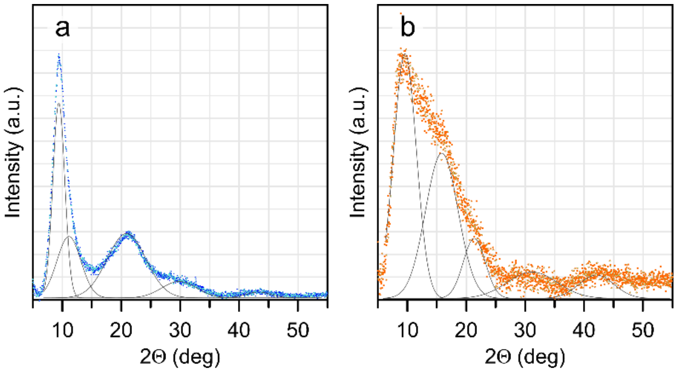

Fig. 1. X-ray diffraction patterns of the AC (a) and BC (b) composites.

The presence of distinct diffraction peaks at $2\theta_1 \approx 9°$ and $2\theta_2 \approx 21°$ of acid set composite (AC) (Fig.1a) clearly indicates the existence of the ladder-like structure in the macromolecular network of PSQ [6]. Base set composite (BC) exhibits slightly different diffraction patterns (Fig.1b) since only one diffraction peak at $2\theta_1 \approx 9°$ associated with PSQ is clearly visible in X-ray patterns whereas the second peak, located roughly between 19° and 23°, is revealed only after deconvolution. Thus, it may be assumed that the base set PSQ network is formed of a lower amount of the stacked ladder-like structures than acid set PSQ.

From the ^{29}Si NMR supported by calculations of the chemical shifts of silicon atoms it may be assumed that PSQ network formed under acidic conditions is composed of the long ladder-like structures whereas small three- and four-membered rings seem to dominate in the PSQ network formed in the presence of base catalyst. Moreover, the polymer-PSQ composites differ significantly in respect to the parameters characterizing their porosity. The AC sample exhibits very low specific surface area and total pore volume (S_{BET} and V_p for AC is 17 m^2/g and 0.1 cm^3/g, respectively) in comparison to XAD7 (S_{BET} = 460 m^2/g and V_p = 0.6 cm^3/g) and the BC sample (S_{BET} = 230 m^2/g and V_p = 0.7 cm^3/g). Interestingly, the storage of composites affects their porosity. Both S_{BET} and Vp increase by over 200 % for AC, while these parameters decrease by ca. 18 % and 5 %, respectively, for BC.

To sum up, the presented vapour phase synthesis route gives opportunity to obtain polymer-polysilsesquioxane composites. The architecture of the PSQ network formed in the spatially limited system of polymer pores strongly depends on the type of the applied catalyst vapors.

References:

[1] D.C. Wu, F. Xu, B. Sun, R.W. Fu, H.K. He and K. Matyjaszewski, *Chem. Rev.*, **112** (2012) 3959-4015.
[2] P. Hodge, *Chem. Soc. Rev.*, **26** (1997) 417-424.
[3] A. Kierys, M. Dziadosz, J. Goworek, *J. Colloid Interf. Sci.*, **349** (2010) 361-365.
[4] A. Kierys, R. Zaleski, W. Buda, S. Pikus, M. Dziadosz, J. Goworek, *Colloid Polym. Sci.*, **291** (2013) 1463-1470.
[5] I. Halasz, A. Kierys, J. Goworek, *J. Colloid Interface Sci.*, **441** (2015) 65-70.
[6] M. Handke, W. Jastrzebski, A. Kowalewska, W. Mozgawa, *J. Mol. Struct.*, **924** (2009) 248-253.

SYNTHESIS OF SANDWICH-TYPE COMPOSITES FOR SELECTIVE AND REVERSIBLE MACROMOLECULES ADSORPTION

Andrzej SIENKIEWICZ, Agnieszka KIERYS, Jacek GOWOREK
DEPARTMENT OF ADSORPTION

The ability of Amberlite resin XAD7 HP to swell in the tetramethyl orthosilicate - TMOS, (3-(2-Aminoethylamino)propyl]trimethoxysilane) - APTS, followed by hydrolysis and condensation of both silica precursors within polymer matrix, by conditioning of the swollen Amberlite in HCl vapours was exploited to synthesise sandwich-type composites [1, 2]. The polymer continuous phase in which hydrophilic silica domains located along hydrocarbon chains can be considered as an organic-inorganic-organic sandwich-type composite. Detailed synthesis procedure was described in previous report. Obtained materials were named MTM, M00, M05 and M10 which corresponds to the APTS:TMOS molar ratio – 0:1, 1:0, 1:5 and 1:10 respectively. In the presented research adsorption of the azo dye (i.e. cochineal red - E124) on the composites, pure XAD7HP and silica gel Si 40 has been investigated. Reversible adsorption form aqueous solutions water-soluble colourants is of great importance for the environment. The azo dyes contribute significantly to the overall pollution of aquatic systems, mostly due to theirs reduction products [3]. Many ways has been developed to deal with such pollution [4]. However the adsorption of the azo dye seems like the ‘cleanest way’ to reduce its concentration in the environment.

The static adsorption experiment was conducted at 30°C in air tight closed vessels. During the experiment 100 mg of materials under study were in contact (for at least 20 h) with 25 ml of adsorbate aqueous solution. The detection of the azo dye was done on the UV-Vis spectrometer at 507 nm. The Lambert-Beer law has been confirmed for E124 in water solution in the range of molar concentration from $9 \times 10^{-7}\ mol/dm^3$ to $2 \times 10^{-4}\ mol/dm^3$. Subsequently adsorbent with bonded adsorbate were filtered and dehydrated at 80°C for 2h in vacuum drier. Next, the azo dye was separately released to the aqueous solution of desired pH (neutral, acidic: pH=3, basic: pH=10). The pH of solutions was adjusted by addition of small amounts of 1M HCl and 1M NaOH and their values were confirmed by the pH measurement performed on Elmetron CX-401 multifunctionmeter. To obtain more information about synthesized materials the lowtemperature nitrogen adsorption-desorption was used to estimate the specific surface area (S_{BET}) and the total pore volume (V_p). Additionally atomic force and scanning electron microscopies (AFM, SEM) were used to gain knowledge about sample morphology.

The adsorption properties of synthesized materials are very interesting. Despite the fact that the low temperature nitrogen adsorption-desorption experiment reveals that the specific surface area of all materials under study diminishes quite rapidly in a following order XAD7 HP, MTM, M10, M05, M00 from 469 m^2/g for polymer to 0 m^2/g for M00, the M00 composite exhibits large value of the E124 adsorption (n_s = 46.0 mg/g). In comparison with the composites parent polymer

XAD7 HP has quite small adsorption capacity of this dye. Its maximum adsorption is at level of 0.1 mg/g while composite MTM (without amino groups) has it at 1.0 mg/g. The adsorption capacity of M10 (composite with amino groups) is at 10.0 mg/g (Fig. 1. a).

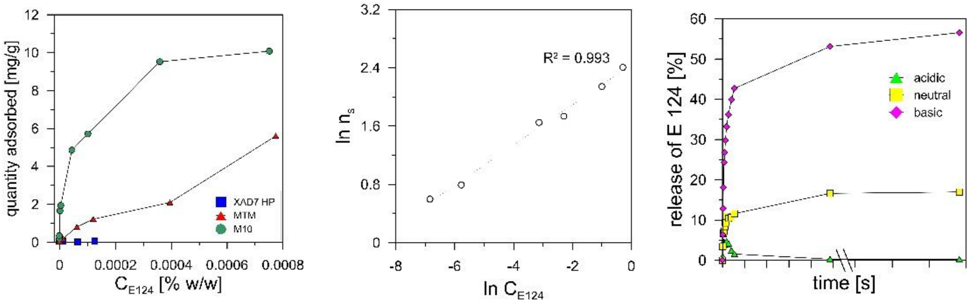

a) b) c)

Fig. 1. The dye adsorption isotherm for three materials XAD7 HP, MTM and (a), the linear adsorption Freundlich adsorption isotherm for M10 composite (b). The desorption of the azo dye from MTM material at different pH values – each tick on x scale represents 2×10^4 seconds (c).

Moreover points on the adsorption isotherm for composites MTM, M10, M05 and M00 fit quite well (R^2 for all is higher than 0.9 – see Fig. 1. b) the Freundlich adsorption model. Furthermore, desorption of the azo dye depends on the pH of the solution (Fig. 1c). The adsorption process is not fully reversible. Composites desorb in basic environment up to 60% (for MTM) of the introduced dye. Since cochineal red is an azo dye which in water exists in form of anion it is no surprise that presence of amino groups (which in solution can be protonated and gain positive charge) significantly increases sorption capacity of composites. However it is very interesting that composite MTM (S_{BET} = 270 m^2/g) which is composed of silica domains scattered within polymer matrix has ten times higher sorption capacity than parent XAD7 HP. Probably azo dye interacts with both positively charged silica surface via $-SO_3^-$ and with polymer matrix via its aromatic rings. On the other hand adsorption of E 124 on XAD7 HP is a fully reversible process.

As a conclusion it can be stated that newly synthesized composites have a great potential to become materials for anionic azo dyes removal from aqueous solution.

References:

[1] A. Kierys, M. Dziadosz, J. Goworek, *J Colloid Interf Sci*, **349** (2010) 361-5.

[2] I. Halasz, A. Kierys, J. Goworek, *J Colloid Interf. Sci.*, **441** (2015) 65-70.

[3] N. Sugaya, Y. Sato, M. Takahashi, K. Sakurai, T. Kawakami, *Yakugaku Zasshi*, **137** (2017) 95-109.

[4] K. Siddique, M. Rizwan, M. J. Shahid, S. Ali, R. Ahmad, H. Rizvi, Textile Wastewater Treatment Options: A Critical Review, *Enhancing Cleanup of Environmental Pollutants, Vol 2: Non-Biological Approaches*, (2017) 183-207.

TEMPERATURE-DEPENDENT MODIFICATION OF POLYMER MATRIX BY INORGANIC OXIDES
(CONTINUATION)

Patrycja KRASUCKA, Jacek GOWOREK, Agnieszka KIERYS
DEPARTMENT OF ADSORPTION

In the recent years spherically shaped polymer- silica composites were obtained by swelling method [1]. It appears that cross-linked polymers like moderately polar Amberlite XAD7HP (Rohm and Haas co.) easily swell in the silica precursor tetraethoxysilane (TEOS). Initially combination of polymer and silica component was conducted at room temperature. However, mixing of polymer and silica component is evidently dependent on temperature. Therefore, it is essential to test how the temperature of TEOS and polymer mixing followed by silica gelation influences porosity of the composite product.

Previously, polymer-silica composites at 150°C (which is glass transition temperature Tg for XAD7HP) were synthesized. Our preliminary experiments of mixing of TEOS above Tg temperature indicates that both components are perfectly mixed and homogeneous phase of the composite is formed. In high temperature TEOS is homogeneously absorbed within polymer beads which are in rubbery state. The porosity parameters of obtained materials are high and comparable to those for the pure polymer or the composite prepared at room temperature. After calcination of polymer component the remaining silica gel exhibits two times larger specific surface area and relatively high pore volume as compared to materials prepared at room temperature. It is worth to mention that after combustion of the organic component, pure silica gel preserves the spherical form of the initial beads [2]. The aim of the present investigations was to verify how to elevated temperature influences condensation of silica species dispersed within polymer particle.

Table 1. Parameters characterizing the porosity of received samples obtained from nitrogen adsorption/desorption isotherms at 77 K: S_{BET} – the specific surface area, V_p – the total pore volume, $D_{PSD1,2}$ – the pore diameter at the peak of PSD.

Sample	**S_{BET} [m^2/g]**	**V_p [cm^3/g]**	**$D_{PSD\,1;2}$ [nm]**
Poly	458	0.56	3.8; 9.4
Poly-SiRT	388	0.27	3.8
SiO_2-RT	889	1.30	7.6
Poly-SiET	460	0.30	3.8
SiO_2-ET	805	1.33	9.3; 19.1

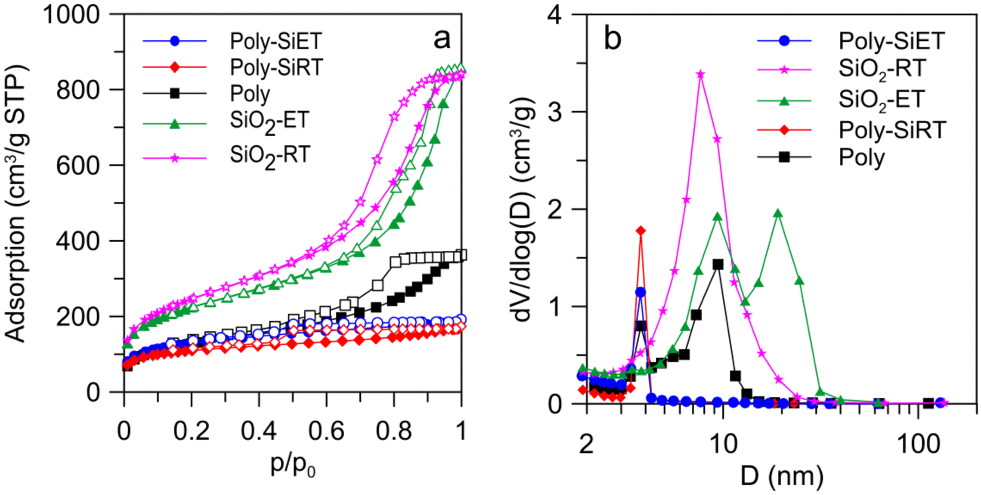

Fig. 1 Adsorption (full point)/desorption (open point) isotherms – (a) and PSDs – (b) of all investigated samples.

Table 1 shows porosity parameters derived from nitrogen adsorption data and Figure 1 presents adsorption/desorption isotherms and PSDs for pure polymer (Poly), composites and silicas prepared at room temperature (Poly-SiRT/ SiO_2-RT) and those prepared at 80^{o}C (Poly-SiET/ SiO_2-ET).

The applied elevated temperature c.a. 80^{o}C influences hydrolysis and condensation of TEOS and consequently influences the pore system of the products. Specific surface area of composite prepared at 80^{o}C is about 20% higher than those prepared at room temperature. Higher temperature caused softening of polymer matrix what facilitates penetration of polymer skeleton by TEOS molecules, and accelerates its transformation compared to RT. On the other hand silica derivate after calcination of composites prepared at room temperature shows higher specific surface area and narrower, uniform PSD comparing to SiO_2-ET sample. Slower transformation of silane at RT enables the formation of silica with high structural homogeneity and porosity. As a conclusion one can state that mixing of polymer with silica precursor as well as condensation of silica species at elevated temperatures makes possible tailoring of pore structure of polymer-silica composite and/or silica gel.

References:

[1] A. Kierys, M. Dziadosz, J. Goworek, *Colloid Interf. Sci.*, **349** (2010) 361–365.

[2] P. Krasucka, R. Zaleski, K. Skrzypiec, J. Goworek, *Micropor. Mesopor. Mat.*, **237** (2017) 210-221.

SELECTIVE ADSORPTION OF BIOLOGICALLY ACTIVE COMPOUNDS ON CARBON-CHITOSAN AND SILICA-CHITOSAN COMPOSITES

Małgorzata ZIENKIEWICZ-STRZAŁKA
DEPARTMENT OF PHYSICOCHEMISTRY OF SOLID SURFACE

The polymeric nanocomposites as qualitatively new and advanced functional materials with great application perspectives become an important stage in actual research. These perspectives refer to preparation of nanocomposites as barriers for gases, solvents and chemicals [1-3], energy storage systems and sensors [3, 4], materials with low flammability and coatings. The polymeric materials modified by inorganic nanoparticles as nanostructured fillers are of great importance. This is a good way for getting materials with specific catalytic and electrochemical properties [5, 6], as an intelligent therapeutic agents [7], systems for bioimaging [8], optically effective additives, materials with magnetic properties and finally a whole world of materials with antibacterial properties.

The chitosan/silica (CS/silica) nanocomposites in the form of polymer nanofibers have been prepared and characterized. The aim of presented work was creating the materials with good quality, by simple, low-cost and repetitive manner and apply them for adsorption of biologically active compounds represented by at least two different types of substances: inorganic colloidal silver nanoparticles as well as organic sterol (cholesterol) molecules. CS/silica nanocomposite materials were synthesized by electrospinning technique for obtaining highly porous 3D nanofiber scaffold thus creating a material suitable for membrane applications. The physicochemical characterization of nanofibers by using the most important analytical techniques as well as their applicability in the characterization of this type of nanocomposites were discussed. They were characterized using small angle X-ray scattering (SAXS), X-ray diffraction (XRD) and atomic force microscopy (AFM). The morphology of composites, size of nanoparticles and their crystallinity, as well as chitosan fibers characteristics were illustrated by electron microscopy techniques (SEM and TEM). The general observations resulting from the work are as follows. The obtained XRD profiles suggests that chitosan creating nanofibres is not completely crystallized. The nanofibers form a two-phase system in which, apart from crystalline areas characterized by a spatial arrangement of macromolecules, also some amorphous regions typical for semi-crystalline systems can be visible. The visible crystallinity is the effect of the structure stabilization and stiffening of crystalline domains by hydrogen bonds and electrostatic interactions between N-acetyl groups. Typically, two characteristic crystalline peaks at 10° and 20° of 2θ with comparable crystallinity related to crystal I and crystal II in chitosan structure [10] and minor other reflections at higher 2θ values should be distinguished for chitosan (Fig.1A). The changes of crystallinity degree are visible depending on various types of silica phase added to the chitosan phase. The additional phase in the composite structure which can be responsible for improvement of mechanical properties and stability of chitosan composites may be easily interpreted by SAXS measurements. The same measurement guarantees obtaining information about the metallic phase by determining the size of electron nonuniformity (Fig. 1B).

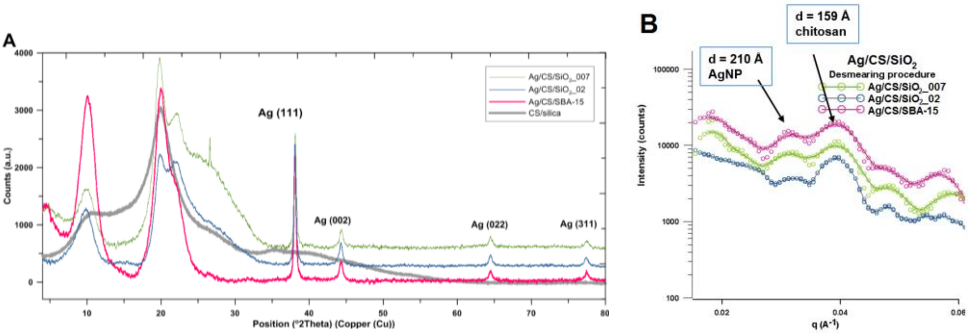

Fig. 1. A) X-ray powder diffraction pattern of the Ag/CS/silica nanofibers; B) Experimental SAXS profile as a line collimation data after desmearing for investigated samples. **Note:** The desmearing routines in EasySAXS use a matrix inversion technique based on the Cholesky decomposition.

The chitosan nanocomposites exhibit adsorption capacity due to the presence of functional groups in their structure. They play an important role in the interaction with biomolecules (proteins, sterols, metallic ions and metallic nanoparticles). Possible interactions can be assigned as coordination, creating hydrogen bonding and chemical bonding between biomolecules and biopolymer chain. The adsorption capacity depend on properties of chitosan phase (DA, molecular weight), experimental conditions (pH, ionic strength) as well as properties of adsorbate (type and characteristics). The lipid and sterol adsorption mechanism is not elucidated completely. It was observed the cholesterol-lowering effect by investigated nanofibres. The concentration changes was evaluated by HPLC technique. One of the probable mechanisms indicates that cationic nature of chitosan (NH_3^+ groups) leaggds to strong interaction with molecules having an opposite charge. The cholesterol-lowering effect by chitosan nanofibers composites is the important issue in the field of humans and animals field of science.

References:

[1] Y.C. Ke, P. Stroeve, Background on Polymer-Layered Silicate and Silica Nanocomposites, Polymer-Layered Silicate and Silica Nanocomposites, 1st Edition, Elsevier, Amsterdam, (2005).
[2] S.S. Ray, M. Okamato, *Prog. Polym. Sci.*, **28** (2003) 1539.
[3] Suryani, Y.-L. Liu, *Journal of Membrane Science*, **332** (2009) 121-128.
[4] S. Chuang, S.L. Hsu, Y. Liu, *Journal of Membrane Science*, **305** (2007) 353–363.

[5] J. Macanas, J. Parrondo, M. Munoz, S. Alegret, *Phys. Stat. Sol.*, **204** (2007) 1699-705.

[6] S. Ahmad, S.A. Agnihotry, S. Ahmad, *J. Appl. Polymer. Sci.*, **107** (2008) 3042–3048.

[7] D.E. Owens, J.K. Eby, Y. Jian, N.A. Peppas, *J. Biomed. Mater. Res.*, **3** (2009) 692–695.

[8] J.H. Kim, K. Park, H.Y. Nam, S. Lee, K. Kim, I.C. Kwon, *Progress in Polymer Science*, **32** (2007) 1031-1053.

[9] J. Kumirska, M. Czerwicka, *J. Mar. Drugs*, **8** (2010) 1567-1636.

[10] E.S. Abdou, K.S.A. Nagy, M.Z. Elsabee, *Bioresour Technol.*, **99** (2008) 1359–1367.